



**Lucianno Augusto Coddato Antunes e Defaveri**

## **Nonlinear Brownian Machines**

### **Tese de Doutorado**

Thesis presented to the Programa de Pós-graduação em Física of PUC-Rio in partial fulfillment of the requirements for the degree of Doutor em Física.

Advisor : Prof. Welles Antonio Martinez Morgado  
Co-advisor: Prof. Sílvio Manuel Duarte Queirós

Rio de Janeiro  
April 2018



## **Lucianno Augusto Coddato Antunes e Defaveri**

### **Nonlinear Brownian Machines**

Thesis presented to the Programa de Pós-Graduação em Física of PUC-Rio in partial fulfillment of the requirements for the degree of Doutor em Ciências – Física. Approved by the undersigned Examination Committee.

**Prof. Welles Antonio Martinez Morgado**

Advisor

Departamento de Física – PUC-Rio

**Prof. Sílvio Manuel Duarte Queirós**

Co-Advisor

CBPF

**Prof. Marcelo Lobato Martins**

UFV

**Prof. Daniel Adrian Stariolo**

UFF

**Prof. Luca Roberto Augusto Moriconi**

UFRJ

**Profa. Celia Beatriz Anteneodo de Porto**

Departamento de Física – PUC-Rio

**Thiago Barbosa dos Santos Guerreiro**

Departamento de Física – PUC-Rio

**Prof. Márcio da Silveira Carvalho**

Vice Dean of Graduate Studies

Centro Técnico Científico – PUC-Rio

Rio de Janeiro, April 13<sup>rd</sup>, 2018.

All rights reserved.

### **Lucianno Augusto Coddato Antunes e Defaveri**

Received the title of Bachelor of Science degree in Physics from the Pontifícia Universidade Católica do Rio de Janeiro in 2012. Majored in physics by the Centro Brasileiro de Pesquisas Físicas (Rio de Janeiro, Brazil) in 2014.

#### Bibliographic data

Defaveri, Lucianno Augusto Coddato Antunes

Nonlinear Brownian Machines / Lucianno Augusto Coddato Antunes e Defaveri; advisor: Welles Antonio Martinez Morgado; co-advisor: Sílvio Manuel Duarte Queirós. – Rio de Janeiro: PUC-Rio, Departamento de Física, 2018.

v., 105 f: il. color. ; 30 cm

Tese (doutorado) - Pontifícia Universidade Católica do Rio de Janeiro, Departamento de Física.

Inclui bibliografia

1. Física Estatística – Teses. 2. Física de Não Equilíbrio – Teses. 3. Física Estatística;. 4. Motores Térmicos;. 5. Termodinâmica;. 6. Física de Não Equilíbrio;. I. Morgado, Welles Antonio Martinez. II. Queirós, Sílvio Manuel Duarte. III. Pontifícia Universidade Católica do Rio de Janeiro. Departamento de Física. IV. Título.

CDD: 530

## Acknowledgments

Firstly I would like to thank my advisor Welles Antonio Martinez Morgado for his support and guidance, not only in the past four years but throughout my entire trajectory in physics, essentially from day one.

I would like to thank my co-advisor Sílvio Manuel Duarte Queirós for his dedication and for all the patience required to work with me.

I would like to thank my family for all of their support which, undoubtedly, is the main reason I managed to thread this far.

I would like to thank my friends and colleagues Eduardo Colombo, Michael Cândido, Carlos Olivares, João Ribeiro, Julio Nicolini and Julio Ribeiro, for all the riveting conversations and for the unending stream of unwanted, undesired and most of all unsolicited pieces of advise.

I would like to thank the administrative staff of the physics department, Gizelda Dias da Silva, Eduardo da Silva Rodrigues, Marcia Arjona, Juliana Pecis and Julinho (Malvino Garcia) for all their assistance.

Finally, I would like to thank the funding agencies CAPES and CNPq, for the financial support that made this research viable.

## Abstract

Defaveri, Lucianno Augusto Coddato Antunes; Morgado, Welles Antonio Martinez (Advisor); Queiróz, Sílvio Manuel Duarte (Co-Advisor). **Nonlinear Brownian Machines**. Rio de Janeiro, 2018. 105p. Tese de doutorado – Departamento de Física, Pontifícia Universidade Católica do Rio de Janeiro.

In the recent decade we have seen great interest in the physics of single particle microscopic engines. Not only we have seen advances in the theoretical understanding of how such systems behave but also, thanks to the advanced level of microscopic manipulations, we are capable of reproducing these systems in experimental situations. The literature is quite large when considering machines where a single particle is subjected to a harmonic potential where we can control the stiffness and in contact with a heat bath of controllable temperature. Motivated by these outstanding results, we have decided to investigate an alternative mechanism to studying machines. We propose and investigate a setup where a single particle with an internal nonlinear potential in contact with a heat bath of temperature  $T$  that we can control, then we introduce an external quadratic potential centered in a position  $L$  which will break the internal symmetry and create a direction where the particle can fluctuate to with greater ease. We can use this symmetry breaking to convert heat into work. Starting with a nonlinear correction to a predominantly linear internal potential, we use perturbation theory to solve the Langevin equation of the system up to the first order in  $k_4$  and obtain the expected work and absorbed heat. We then relax the restriction of a small nonlinear by imposing that the cycle periods are so large that, at least to some extent, the system can be considered in equilibrium with the heat bath. Using classical statistical mechanics we obtain results for a wider range of nonlinearities. Since the key component of our machines is the asymmetry, we extend the internal potential to the more general but not always analytical form  $V_i(x) \propto |x|^\alpha$  which we label  $\alpha$ -type potential. Using primarily numerical techniques investigate its properties and outputs for different values of  $\alpha$ . Lastly we study the Carnot cycle by replacing the adiabatical branches with isentropic ones, investigating the relationship between  $\alpha$  and the isentropic trajectories. All results are compared with numerical simulations.

## Keywords

Statistical Physics; Thermal Engines; Thermodynamics; Nonequilibrium Physics;

## Resumo

Defaveri, Luciano Augusto Coddato Antunes; Morgado, Welles Antonio Martinez; Queiróz, Sílvio Manuel Duarte. **Máquinas Brownianas Não Lineares**. Rio de Janeiro, 2018. 105p. Tese de Doutorado – Departamento de Física, Pontifícia Universidade Católica do Rio de Janeiro.

Na última década temos visto grande interesse na física de motores microscópicos de uma partícula. Não só temos visto grandes avanços na descrição teórica de como esses sistemas se comportam como também, graças aos avanços na área de manipulação microscópica, somos capazes de reproduzir esses sistemas experimentalmente. A literatura é vasta quando consideramos máquinas onde uma partícula é sujeita a um potencial harmônico onde podemos controlar sua rigidez e em contato com um banho térmico de temperatura controlável. Motivados por esses resultados fascinantes, decidimos investigar um mecanismo alternativo para o estudo de máquinas. Propomos e investigamos uma configuração onde uma única partícula com potencial interno não linear em contato com um banho térmico de temperatura  $T$  que controlamos, em seguida introduzimos um potencial quadrático externo centrado em uma posição  $L$  que quebrará a simetria criando uma direção onde a partícula pode flutuar com maior facilidade. Podemos usar essa quebra de simetria para converter calor em trabalho. Começando com uma correção não linear ao potencial interno predominantemente linear, usamos a teoria de perturbação para resolver a equação de Langevin do sistema até a primeira ordem da não linearidade  $k_4$  e obtemos o trabalho esperado e o calor absorvido. Então relaxamos a restrição de pequena não linearidade impondo que o período de cada ciclo seja tão grande que, ao menos parcialmente, o sistema possa ser considerado em equilíbrio com o banho térmico. Usando mecânica estatística clássica obtemos resultados para um alcance maior das não linearidades. Uma vez que a componente central de nossas máquinas é a assimetria, extendemos o potencial interno para o mais geral, embora nem sempre analítico  $V_i(x) \propto |x|^\alpha$ , que chamamos de potencial tipo- $\alpha$ . Usando principalmente técnicas numéricas investigamos as propriedades e resultados para diferentes valores de  $\alpha$ . Por fim estudamos o ciclo de Carnot substituindo os ramos adiabáticos com isentrópicos, investigando o relacionamento entre  $\alpha$  e as trajetórias isentrópicas. Todos os resultados são comparados com simulações numéricas.

## Palavras-chave

Física Estatística; Motores Térmicos; Termodinâmica; Física de Não Equilíbrio;

## Table of contents

1	Introduction	14
2	Perturbative Approach	18
2.1	The Model	18
2.1.1	Step and elliptical cycles	20
2.1.2	Work Calculations	22
2.1.3	Heat calculations	23
2.2	The Role of Non-Linearities	26
2.3	Perturbative Approach	30
2.4	Work Output	35
2.4.1	Zeroth order	35
2.4.2	First Order	36
2.5	Heat Exchanges	37
2.6	Final Remarks	39
3	The Quasi-Static Regime	40
3.1	Equilibrium Distribution	40
3.2	Small Nonlinearity Approximation ( $k_4 \rightarrow 0$ )	42
3.2.1	Large Nonlinearity Approximation ( $k_4 \rightarrow \infty$ )	45
3.3	Convergence Issue	47
3.4	Numerical Approach	50
3.5	Numerical Results	52
3.6	Final Remarks	54
4	Generalized Nonlinear Machines	59
4.1	The $\alpha$ -type Potential	59
4.2	The Role of $\alpha$ in the asymmetry	60
4.3	Numerical Approach	62
4.4	Numerical Results	65
4.5	Adiabaticity versus isentropy	67
4.6	$\alpha$ -type Isentropy	71
4.7	Final Remarks	78
5	Final Remarks	80
5.1	What have we done?	80
5.2	What have we learned?	81
5.3	Where can we go from here?	82
A	Stratonovich Calculus	84
B	General Calculations	87
B.1	Time Average of a Single Function	87
B.2	Broken Time Averages	88
B.3	An Illustrative Example	89

C	Useful Laplace Transforms	<b>92</b>
C.1	Laplace Transform of $x^3(t)$	92
C.2	Correlation with Time-Dependent Temperature	92
C.3	Laplace Transform of the Temperature	93
D	Isentropic Process Derivation	<b>94</b>
D.1	Interpreting the result	96
D.2	Examples	96
	Bibliography	<b>99</b>

## List of figures

- Figure 2.1 An analogous mechanical representation of our Brownian machine. 19
- Figure 2.2 Figure on top represents a step cycle (a) and the elliptical cycle is represented on the bottom (b). For the step cycle, compression phase ( $L_m + \Delta L/2 \rightarrow L_m - \Delta L/2$ ) is performed (labelled 1) in contact with the hot source ( $T_H$ ), at the end there we instantaneously switch (labelled 2) with the cold source ( $T_C$ ) following by an expansion ( $L_m - \Delta L/2 \rightarrow L_m + \Delta L/2$ , labelled 3). At the end we instantaneously switch back to the hot source (labelled 4). For the elliptical cycle, both  $T$  and  $L$  change continuously with the BP absorbing heat while  $T$  increases (labelled 1) and rejecting heat when  $T$  decreases (labelled 2). 21
- Figure 2.3 We present here the ensemble averages obtained through numerical simulations of equation 2-14. The parameters used were  $\gamma = \omega = m = 1$ . 25
- Figure 2.4 We present here the ensemble averages obtained through numerical simulations of equation 2-14 with the elliptical temperature. The parameters used where  $\gamma = \omega = m = 1$ . The solid line represents the result for the linear case 2-22. 27
- Figure 2.5 Visual representation of a dynamical equation. In the linear case, on top, the answer consists on the sum of the two individual entries contributions while for the nonlinear system, bottom, the answer consists in a non-trivial combination of the two. 28
- Figure 2.6 A simple representation of two stages of a machine. With the high temperature  $T_H$ , we move the piston in the direction of the pressure from the particles. With the lower temperature  $T_C$ , because the pressure on the piston is now lower, we require less work to push it back to its original position, thus having a net gain of work at the end of the cycle. 29
- Figure 2.7 The figure on the top represents (a) the effective potential  $V(x) = \frac{k_2}{2}x^2 + \frac{k_L}{2}(x - L)^2$  and on the bottom (b) represents the probability distribution of the particle at different temperatures. The solid black line represents  $\langle x \rangle$ , which does not change with the temperature. We have considered  $k_2 = 1$  and  $k_L = 1$ . 31  
 2.7(a) 31  
 2.7(b) 31
- Figure 2.8 The figure on the top (a) represents the effective potential  $V(x) = \frac{k_2}{2}x^2 + \frac{k_4}{4}x^4 + \frac{k_L}{2}(x - L)^2$  and on the bottom (b) represents the probability distribution of the particle at different temperatures. The solid black line represents  $\langle x \rangle$ , which increases with the temperature. We have considered  $k_2 = 1$ ,  $k_L = 1$  and  $k_4 = 1$ . 32  
 2.8(a) 32

2.8(b)

32

Figure 2.9 The step cycle is represented where we have highlighted the same displacement  $L$  but for different temperatures in order to compare compression with expansion phases. The power output for the fixed value of  $L$  is  $P_W = -k_L(\langle x \rangle_{T_H} - \langle x \rangle_{T_C})\dot{L}$ , which is negative since  $\langle x \rangle_{T_H} > \langle x \rangle_{T_C}$ .

33

Figure 3.1 Here we represent a cycle from the perspective of the conjugated variables, the top figure (a) represents the plot of temperature versus entropy ( $T \times S$ ) while the bottom figure (b) represents the plot of  $F_L \times L_m$  which is equivalent to the  $p \times V$  plot of an ideal gas. Following 3-10, the work output is the area between the two lines. The red line represents the step cycle while the blue dotted line represents the elliptical cycle. Both cases have  $L_m$ ,  $\Delta L$ ,  $T_m$  and  $\Delta T$ .

43

3.1(a)

43

3.1(b)

43

Figure 3.2 Nonlinear potentials that remain symmetric.

44

Figure 3.3 The red points represent the absolute values of the expansion constants, on the top (a) we represent the approximation for small nonlinearities, the figure on the bottom (b) for large nonlinearities. For small nonlinearities the values grow so rapidly that by the tenth term we already have values up to  $10^{12}$ , for large nonlinearities the growth is much more tamed, but still very clear. The auxiliary blue line highlights how the growth is exponential in both cases. The values used are  $\Delta T = \Delta L = m = k_2 = k_L = 1$  and  $L_m = T_m = 1.5$ .

48

3.3(a)

48

3.3(b)

48

Figure 3.4 The solid (black) line represents the numerical integration of equation 3-6, using our analytical expansions for the step cycle. The dotted lines, blue and violet depict expansions of equation 3-6 for small values of  $k_4$  while the dot-dashed lines, orange and red, depict expansions for large values of  $k_4$ . For both cases we display the first and tenth orders to illustrate how there is no conversion radius. The values used are  $\Delta T = \Delta L = m = k_2 = k_L = 1$  and  $L_m = T_m = 3/2$ .

49

Figure 3.5 The solid black line represents the numerical integration of equation 3-6 while the dashed red line represents the absolutely convergent expansion for  $N = 2$  and the dotted blue line for  $N = 4$ . The values used are  $\Delta T = \Delta L = m = k_2 = k_L = 1$  and  $L_m = T_m = 3/2$ .

50

- Figure 3.6 Average work performed by the machine  $-\mathcal{W} \times k_4$  with  $m = k_2 = k_L = \gamma = 1$ ,  $L_m = 3/2$ ,  $\Delta L = 1$  and  $\Omega = \pi/100$ . The solid blue line corresponds to the step cycle with  $T_H = 2$  and  $T_C = 1$ , whereas the green dotdashed line depicts the analytical results assuming the local equilibrium approach which yields maximum at  $k_4 = 1.47$ . The red dashed line corresponds to the elliptical cycle equivalent to the first order Fourier series of the step cycle with  $T_m = 1.5$  and  $\Delta T = \pi/2$ . The orange dotted line corresponds to the step cycle for the same maximal and minimal temperatures of the previous cycle,  $T_H = 3/2 + \pi/4$  and  $T_C = 3/2 - \pi/4$ . 54
- Figure 3.7 Distribution of the work per cycle  $p(W) \times W$  in log-lin scale for the step cycle with  $T_H = 2$  and  $T_C = 1$  on the top (a) and for the elliptical cycle with  $T_m = 3/2$  and  $\Delta T = \pi/2$  on the bottom (b). The parameters used  $m = k_2 = k_L = \gamma = 1$ ,  $L_m = 3/2$ ,  $\Delta L = 1$  and  $\Omega = \pi/100$ . 55
- Figure 3.8 Distribution of the work per cycle  $p(-W)/P(W) \times W$  in log-lin scale for the step cycle with  $T_H = 2$  and  $T_C = 1$  on the top and for the elliptical cycle with  $T_m = 3/2$  and  $\Delta T = \pi/2$ . The parameters used  $m = k_2 = k_L = \gamma = 1$ ,  $\Delta L = 1$  and  $\Omega = \pi/100$ . 56
- Figure 3.9 On the top (a) the distribution of the instantaneous power  $p(w) \times w$  in log-lin and lin-lin in the inset for the elliptical cycle with  $T_m = 3/2$ ,  $\Delta T = \pi/2$  and  $m = k_2 = k_L = \gamma = 1$ ,  $k_4 = 1.5$ ,  $L_m = 3/2$ ,  $\Delta L = 1$  and  $\Omega = \pi/100$ . On the bottom (b) the step cycle with the same parameters (reminding that  $T_m$  is the average temperature and  $\Delta T$  the temperature gap.) 57
- 3.9(a) 57
- 3.9(b) 57
- Figure 3.10 The fluctuation relation  $p(-w)/p(w) \times w$  in log-lin scale for the step cycle with parameters  $T_H = 2$ ,  $T_C = 1$ ,  $m = k_2 = k_L = \gamma = 1$ ,  $k_4 = 1.5$ ,  $L_m = 3/2$ ,  $\Delta L = 1$  and  $\Omega = \pi/100$ . 58
- Figure 4.1 On the top (a) the potential, on the bottom (b) the probability density for the position  $x$  for different values of the exponent  $\alpha$ . In the linear regime,  $\alpha = 2$ , the density is symmetric, for over linear values of  $\alpha$  we recover the effect displayed in figure 2.8. For sub linear values of  $\alpha$  the bias switches direction and the expected position shifts to the right of the minimal potential. 61
- 4.1(a) 61
- 4.1(b) 61
- Figure 4.2 On the top (a) we plot the difference between the expected position  $\langle x \rangle$  and the minimal potential position  $x_m$  for different values of  $\alpha$ . Note that for  $\alpha < 2$  the difference is positive, hence  $\langle x \rangle > x_m$  and negative for values of  $\alpha > 2$ . On the bottom (b) we plot the effects of temperature on the value of the expected coordinate for different values of  $\alpha$ . 63
- 4.2(a) 63

- 4.2(b) 63
- Figure 4.3 The ensemble average of the position for different numbers of cycles  $N_C$ , the cycle used was the step cycle. For  $N_C = 10000$  the ensemble average is already quite close to the equilibrium expectation. The values are  $k_\alpha = k_L = m = \gamma = \Delta L 1$ ,  $L_m = 1.5$ ,  $T_H = 2$ ,  $T_C = 1$  66
- Figure 4.4 The ensemble average of the expected position on the top left, internal energy on the top right, instantaneous power bellow left and a comparisson between of the instantaneous power during the hot phase in red and cold phase in dotted blue. The values used are  $k_\alpha = k_L = m = \gamma = \Delta L = 1$ ,  $L_m = 1.5$ ,  $T_H = 2$ ,  $T_C = 1$  for the exponent  $\alpha = 1.2$ . 67
- Figure 4.5 The ensemble average of the expected position on the top left, internal energy on the top right, instantaneous power bellow left and a comparisson between of the instantaneous power during the hot phase in red and cold phase in dotted blue. The values used are  $k_\alpha = k_L = m = \gamma = \Delta L = 1$ ,  $L_m = 1.5$ ,  $T_H = 2$ ,  $T_C = 1$  for the exponent  $\alpha = 2.0$ . 68
- Figure 4.6 The ensemble average of the expected position on the top left, internal energy on the top right, instantaneous power bellow left and a comparisson between of the instantaneous power during the hot phase in red and cold phase in dotted blue. The values used are  $k_\alpha = k_L = m = \gamma = \Delta L = 1$ ,  $L_m = 1.5$ ,  $T_H = 2$ ,  $T_C = 1$  for the exponent  $\alpha = 2.2$ . 69
- Figure 4.7 The ensemble average of the expected position on the top left, internal energy on the top right, instantaneous power bellow left and a comparisson between the instantaneous power during the hot phase in red and cold phase in dotted blue, the area between curves is the work output. The values used are  $k_\alpha = k_L = m = \gamma = \Delta L 1$ ,  $L_m = 1.5$ ,  $T_H = 2$ ,  $T_C = 1$  for the exponent  $\alpha = 6.0$ . 70
- Figure 4.8 Distribution of the work per cycle  $p(W) \times W$  for different values of  $\alpha$  using the step cycle operating between  $T_H = 2$  and  $T_C = 1$ . The cycle period is  $\tau = 200$  or  $\Omega = \pi/100$  and  $m = k_\alpha = k_L = \gamma = \sigma = 1$ . The solid lines are defined by equation 4-25 using the respective  $\mathcal{W}$  and  $\sigma_W$  for each  $\alpha$ . We highlight how the average work shifts from positive for  $\alpha < 2$  to negative  $\alpha > 2$  and exactly in  $\alpha = 2$  the average work is zero. 71
- Figure 4.9 The fluctuation relations  $p(-W)/p(W) \times W$  presented in the log-linear scale for the different values of  $\alpha$  presented in figure 4.8. The solid blue lines were obtained using equation 4-25 with the respective values of  $\mathcal{W}$  and  $\sigma_W$ . 72
- 4.9(a) 72
- 4.9(b) 72
- 4.9(c) 72
- Figure 4.10 Average work performed by the machine on a  $\mathcal{W} \times \alpha$  plot with  $m = 1 = \gamma = k_L = k_\alpha$ . The cycle used was the step cycle with  $L_m = 3/2$ ,  $\Delta L = 1$ ,  $T_C = 1$  and  $T_H = 2$ . 73

- Figure 4.11 Average work performed by the machine on a  $\mathcal{W} \times \alpha$  plot with  $m = \gamma = k_L = k_\alpha = \sigma = 1$ . The cycle used was the elliptical cycle with  $L_m = 3/2$ ,  $\Delta L = 1$ ,  $T_C = 1$  and  $T_H = 2$ . The internal potential of the particle represented in the blue line also contains a quadratic pinning  $V_i(x) = k_\alpha |x/\sigma|^\alpha / \alpha + k_2(x-L)^2/2$ , where  $k_2 = 1$ . The pinning does not affect the qualitative behaviour, only decreases the overall work output. By increasing the cycle period to  $\tau = 1000$ , we observe that the points more disconnected to the curve get closer. 73
- Figure 4.12 A large set of isentropic processes with sublinear potentials ( $\alpha = 0.75$ ) on the top (a). There is a very brief range of values of displacements where the potential will be asymmetric. Starting with  $L = 0$  the potential is clearly symmetric, early displacements cause great asymmetry but as the displacements increase, the external potential  $V_e$  becomes dominant over the sublinear internal potential effectively decoupling  $L$  and  $S$ . Bottom figure (b) represents the this decoupling effect. The parameters used were  $m = k_L = 1$  and  $k_\alpha = 1.5$ . 76
- 4.12(a) 76
- 4.12(b) 76
- Figure 4.13 The isentropic trajectories of overlinear potentials ( $\alpha = 8$ ) on the top (a). Early increases in  $L$  will intensify the potential asymmetry and increase its temperature. On the bottom (b), a specific isentropic trajectory demonstrates that, even for very large displacements,  $L$  and  $S$  never decouple. Note that in order to obtain temperature shifts it is necessary employ displacements ten time larger. The parameters used were  $m = k_L = 1$  and  $k_\alpha = 1.5$ . 77
- 4.13(a) 77
- 4.13(b) 77
- Figure 4.14 Representation of a Carnot cycle for a nonlinear Brownian machine. The dashed lines are the isentropic processes while the solid lines represent the internal temperature of the particle, defined as  $\langle v^2 \rangle / m$ , where the adiabaticity was achieved by removing the contact with the heat sources. The present cycle verifies exactly the isentropic relations proposed on equation 4-33. The parameters used were  $m = \gamma = k_L = \sigma = 1$  and  $k_\alpha = 5$ . 78
- Figure 4.15 Representation of a Carnot cycle for a nonlinear Brownian machine. The solid lines represent the internal temperature of the particle, defined as  $\langle v^2 \rangle / m$ , where the adiabaticity was achieved by removing the contact with the heat sources. Note that in order to obtain a  $\Delta T = 1$ , we had to displace the potential by  $\Delta L \approx 700$ , which severely limits the applicability of the isentropics in experimental situations. The parameters used were  $m = \gamma = k_L = \sigma = 1$  and  $k_\alpha = 2.5$ . 79
- Figure B.1 This is a visual representation of the broken averages. The dark blue represents the early time average and the light blue represents the late time average. 88

# 1 Introduction

When Nicolas Sadi Carnot embarked upon the quest to understand the intrinsic nature of thermal machines, the world had already been irreversibly changed by the industrial revolution. The economical value of steam engines in industry was quite clear, and that caused the development of machines to greatly outpace any physical theory to describe it.

Looking at history from our privileged position, it's easy to understate the achievement made by Carnot. His book "Réflexions sur la puissance motrice du feu et sur les machines propres à développer cette puissance" (Reflections on the Motive Power of Fire) was published in 1824; Josiah Willard Gibbs would only be born in 1839, Ludwig Boltzmann in 1834, Hermann von Helmholtz would only publish his treatise on the conservation of energy 1847, and Rudolf Clausius would state the first law of thermodynamics in 1850.

Whilst Newton claimed that he could see further by standing in the shoulders of giants, the french military engineer had very few shoulders to stand on when it came to investigating the thermodynamic properties of machines. His work contained a very simple mathematical framework, nevertheless he managed, in a remarkable feature of careful investigation and intuition, to obtain cornerstone properties of a machine, as well as the notion of a maximum efficiency

$$\xi_C = 1 - \frac{T_C}{T_H}, \quad (1-1)$$

which still today, after so much development in the field of statistical physics, stands as an insurmountable boundary in efficiency.

Almost two hundred years later, with a vast array of techniques to manipulate ever smaller systems, the possibility of creating a one particle microscopic engine was elevated from a simple thought experiment to an attainable experimental reality.

The principles of equilibrium statistical mechanics were developed analysing systems so large that their internal fluctuations are negligible and macroscopic physics ruled them. One particle systems, however, are strongly affected by fluctuations, the proverbial scenario where a glass unshatters it-

self would be still a rare, but present effect. In this regime, highly driven by fluctuations, kinesin molecular motors are known to convert chemical energy from molecules of adenosinetriphosphate (ATP) into work, at near 60% efficiency [1, 2].

Several interesting mechanisms for working machines have been proposed and studied through the years, like ratchet potentials in both classical [3, 4] and quantum [5] mechanics. Such systems are influenced by unbiased fluctuations that, when combined with the asymmetric dynamic induced by the ratchet potential lead to the transport of particles.

Another alternative mechanism is to consider a Brownian particle subjected to a harmonic potential of controllable stiffness  $k(t)$  in contact with a heat bath of controlled temperature. Such systems have been extensively studied both analytically and numerically [6–10]. We will label such machines as *modulated frequency models*.

Throughout there have been many experimental realizations of one particle heat engines, from molecular engines that convert the internal chemical energy into work [11], photonic engines [12], colloidal Brownian particles trapped in elliptical well potentials [13] and to optical laser traps [14], ions confined in a linear Pauli trap [15] and a single optically trapped Brownian particle [16].

Brownian motors have also been studied extensively within the framework of quantum mechanics [8, 17–32]. Fascinating results have been obtained such as thermal machines driven by vacuum forces [33] and reversible engines for electrons [34].

For artificial systems operating at maximum power, the reported values for the efficiency are coherent with the values of the Carnot cycle under the maximum power constraint, discovered by Novikov [35] and rediscovered by Curzon and Ahlborn [36]. We call this the Novikov-Curzon-Ahlborn limit (NCA).

It is also possible to create Brownian information machines that operate using feedback from information obtained through constant measurements of the system [12, 37–40]. Information machines are capable of breaking the classical Carnot limit [41], which does not violate the second law of thermodynamics when we take into account the entropy generated by the measurement process.

Small systems operating under realistic conditions may not reach the Carnot limit due to several causes, such as irreversible heat flows [42, 43] or the presence of friction. Furthermore, the generated power, a very important characteristic of a thermal machine, does not easily reach maxima near quasi-

static conditions, despite some arguments that point to a possible surpassing of the NCA limit for systems with broken time-reversal symmetry [44]. There is also some evidence that high efficiency is possible at finite power [45]. However, in general, the efficiency at maximum power does depend on the protocol parameter space [46, 47].

$$\xi_{NCA} = 1 - \sqrt{\frac{T_C}{T_H}}. \quad (1-2)$$

The properties of nonlinearities in stochastic models is also studied in the similar context of energy harvesters. Such devices are capable of converting natural occurring vibrations into useful energy. The linear energy harvester is very limited, since it can only effectively convert fluctuations at frequencies close to its harmonic mode. With the addition of nonlinearities, the spectrum of useful frequencies widens, increasing the practical applicability of such devices [48, 48–52].

In this thesis we propose a model where the Brownian particle is subjected to a nonlinear potential being deformed by an external harmonic potential and, following the same asymmetry principle that makes machines with ratchet potentials possible, is capable of directing the fluctuations of an unbiased heat source. Manipulating the point of application of the external potential  $L$  and the bath temperature  $T$ , we can use the directed fluctuations to convert heat into work.

The first half of chapter 2 will be dedicated to the definition of the model we shall employ on the rest of this work. We will attempt to explain the role of each element in the dynamical equation 2-2 as well as the cycles we will be using. We will also provide an intuitive explanation on the nature of nonlinear machines and how a nonlinear potential can be used as a means to convert heat into work.

In the second half of chapter 3 we will consider that the internal potential is strongly quadratic with a small quartic correction. If the nonlinearity  $k_4$  is small enough, we will be able to use perturbation theory to expand the solutions of 2-2 in series of  $k_4$ . The work and heat output are then obtained for our cycle choices up to the first order of  $k_4$  and we comment on the advantages and limitations of this approach.

By relaxing the restriction of small  $k_4$  and imposing that the cycle time is large enough for the system to be considered, at least to some extent, in equilibrium with the heat bath, we are capable of employing classical statistical mechanics. In chapter 4 we use this new framework to recover the analytical results obtained in the previous chapter for small  $k_4$  and uncover the behaviour

of work and heat output for large  $k_4$ . Turning to numerical calculation of the equilibrium probability distributions we are capable of obtaining results for larger values for  $k_4$ . However, even the maximum work output obtained is still on a scale ten times lower than the heat intake.

One of the main concepts of our work is that the nonlinearities are merely a tool for obtaining asymmetric potentials, so we extend the range of nonlinearities in chapter 5 to a more general internal potential. We investigate the internal potential  $V_i(x) \propto |x|^\alpha$ , which we label as  $\alpha$ -type potential and proceed to investigate the effect the exponent alpha has on work and heat outputs. Analytical results are presented for very specific cases, most of the results however can only be obtained numerically.

The efficiency of the elliptical cycles is very poor when compared to the expected Carnot efficiency. We create the same effect of an adiabatic process by imposing that the system entropy remains unchanged in the branches that connect the isotherms. We obtain that the isentropic trajectories are intrinsically connected with the nonlinearities and, more importantly, the exponent of the potential. In order to obtain a meaningful temperature difference between the hot and cold phases, we end up having to deform the potential with values of  $\Delta L$  orders of magnitude larger than  $\Delta T$ , imposing several restrictions on the actual applicability of such trajectories in an experimental scenario.

Lastly, we present a brief summary of all the results obtained in this work. We also present clearly the core concepts we have learned with this study and a brief glimpse of the possible directions we may take from here. The first two chapters consist of a detailed version of the results published by Defaveri et. al. [53], while Chapter 4 contains results of an yet unpublished work. The nonlinear models presented in Chapter 2 and 4 are our original contribution to the study of Brownian machines and more specifically, how nonlinearities in the potential can be used to convert heat into work.

## 2

### Perturbative Approach

We will start this chapter providing a simple explanation of the model to be used throughout the thesis. We explain how linear machines cannot produce net work output, how non-linearities are essential to creating asymmetric potentials, and how that asymmetry is responsible for the efficiency of the machine.

The potential considered will consist of quadratic and quartic terms, and by imposing that the energy contained in the quartic mode be much smaller than in the quadratic one it is possible to employ perturbation theory and obtain analytical results.

#### 2.1

##### The Model

We consider a system composed by a single Brownian particle (which will abbreviate BP) with mass  $m$  subjected to a potential  $V(x)$ , with  $x$  being the position coordinate (for the momentum we will be using small capital  $p$ ). Throughout this chapter we will consider  $V(x) = \frac{k_2}{2}x^2 + \frac{k_4}{4}x^4$ . The system is then driven by an external linear force  $F_e = -k_L(x - L(t))$ , where we (the experimentalist in a practical situation) have full control of  $L$ . Using a simple mechanical analogy, this force can be seen as a spring connected to a piston located at position  $L$  (see figure 2.1). The potential associated with this force is  $V_e(x) = \frac{k_L}{2}(x - L)^2$ , therefore we cannot alter the concavity of the potential (or the stiffness of the spring) like in the case of the modulated frequency model, only the position where it is applied.

The system is also in contact with a heat bath, which we shall model using the stochastic force  $\eta(t)$ . In an experimental situation, a heat bath could consist of a viscous liquid [14, 16] composed by a very large number of particles when compared to the system. From the perspective of the BP, since the bath is composed of such a large number of particles, following the central limit theorem, the distribution of the stochastic force is Gaussian with cumulants:

$$\langle \eta(t) \rangle_C = 0 \quad ; \quad \langle \eta(t)\eta(t') \rangle_C = 2m\gamma T(t)\delta(t - t'), \quad (2-1)$$

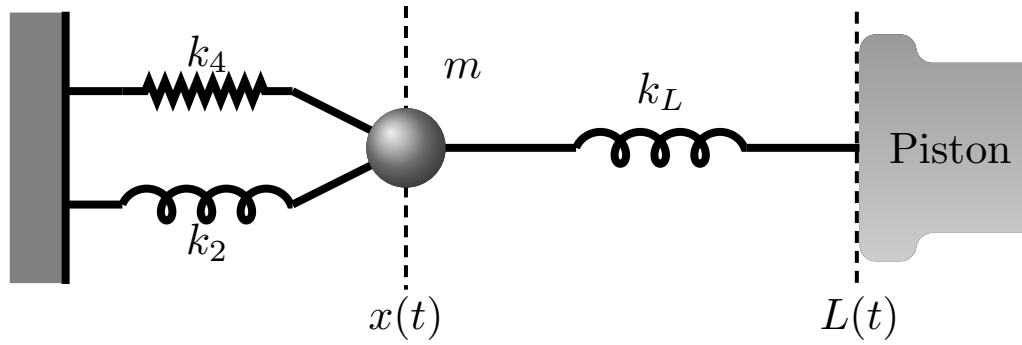


Figure 2.1: An analogous mechanical representation of our Brownian machine.

where  $\langle \rangle_C$  represents the cumulants. The Dirac delta term imposes that there is no correlation between two different instants in time. We are capable of exerting full control over the bath temperature  $T(t)$ . There is also a dissipative interaction between the heat bath and the system (fluctuation dissipation theorem).

We will impose periodic protocols over  $L(t)$  and  $T(t)$  to account for the machine's operation cycles. The particle is free to visit all points in the axis. Since the potential will become too steep for large values of  $x$ , we may interpret  $L(t)$  as a *soft* volume, since it can extend the range where the particle is more likely to be found. In a more standard machine the phase space is composed of the volume and temperature  $(V, T)$ , we will use  $(L, T)$ .

The final equation of motion is the Langevin-type equation [54–56]

$$m\ddot{x} + m\gamma\dot{x} + V'_i(x) = -k_L(x - L) + \eta(t), \quad (2-2)$$

where  $\gamma$  represents the exchange rate between the bath and the system and the main potential we shall study is  $V_i(x) = \frac{k_2}{2}x^2 + \frac{k_4}{4}x^4$ . By adding and subtracting  $k_L(x - L)\dot{L}$  on both sides of equation 2-2 and performing some algebra we can write

$$\begin{aligned} \left[ m\ddot{x} + V'(x) \right] \dot{x} &= \left[ \eta(t) - m\gamma\dot{x} - k_L(x - L) \right] \dot{x} \\ \left[ m\ddot{x} + V'(x) \right] \dot{x} - k_L x \dot{L} + k_L L \dot{L} &= k_L L \dot{L} - k_L x \dot{L} + \left[ \eta(t) - m\gamma\dot{x} - k_L(x - L) \right] \dot{x} \\ \underbrace{\frac{d}{dt} \left[ \frac{m}{2} \dot{x}^2 + V(x) + \frac{k_L}{2} (x - L)^2 \right]}_{dU/dt} &= \underbrace{-k_L(x - L)\dot{L}}_{dW/dt} + \underbrace{\left( \eta(t)\dot{x} - m\gamma\dot{x}^2 \right)}_{dQ/dt}, \end{aligned} \quad (2-3)$$

where we recover the familiar result of the First Law of Thermodynamics  $dU = dW + dQ$ . Note that the internal energy is an exact differential term, indicating that it does not depend on the trajectory in the phase space while the

work and heat are inexact differentials individually but when added together become exact.

### 2.1.1 Step and elliptical cycles

In order to perform an adiabatic transformation upon a macroscopic system, one would simply remove any contact between the heat bath and the system's particles. When dealing with a microscopic system however, it becomes experimentally harder to remove the contact between system particles and external bath.

An alternative [14–16] to disconnecting the heat bath from the system is to evaluate *isentropic* trajectories. We will discuss this topic carefully in chapter 5 and appendix D. Note however that only isentropy and adiabaticity are only equivalent when dealing with classical statistical mechanics, on a realistic single particle system the adiabatical restriction is

$$\frac{dQ}{dt} = 0, \quad (2-4)$$

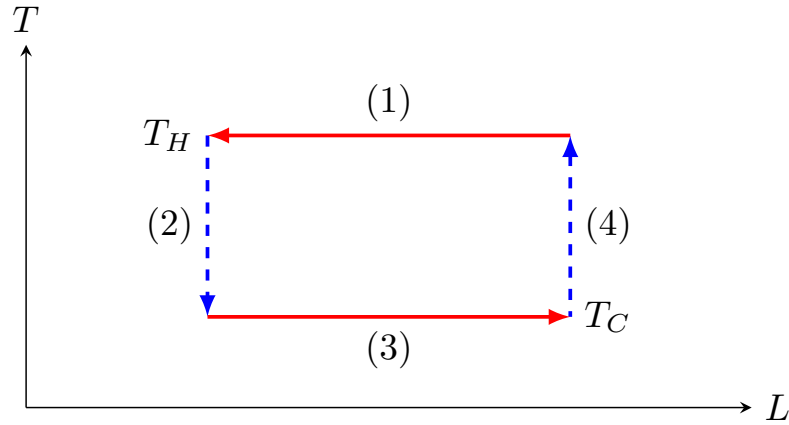
so there is no heat flow between bath and BP.

By imposing that the cycle period  $\tau$  is much larger than  $1/\gamma$ , or equivalently that  $\Omega \ll \gamma$ , we ensure that as the system navigates the phase space of  $(L, T)$ , there will be enough time for the system to equilibrate at least partially with the bath.

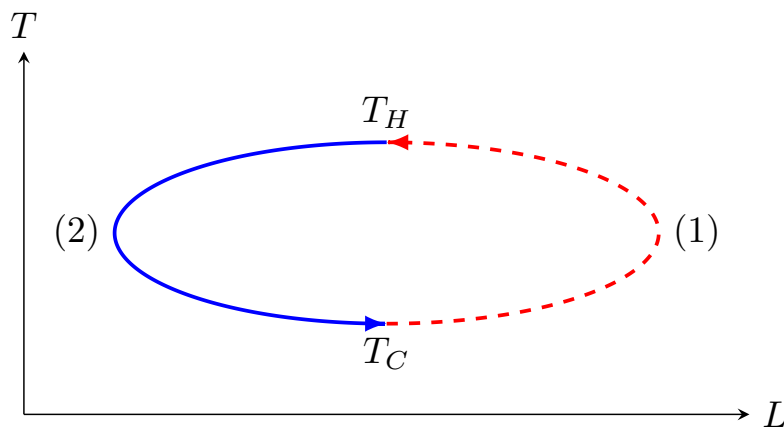
For the piston position we will use the protocol [53]

$$L(t) = L_m + \frac{\Delta L}{2} \cos(\Omega t), \quad (2-5)$$

and for the bath temperature we shall use two distinct protocols: the step cycle, where the Brownian particle first undergoes a compression phase ( $L_m + \Delta L/2 \rightarrow L_m - \Delta L/2$ ) while in contact with a heat source of temperature  $T_H$ , after we instantaneously switch the heat source for a colder one of temperature  $T_C$ , following by an expansion back to the starting value of  $L$  ( $L_m - \Delta L/2 \rightarrow L_m + \Delta L/2$ ). At the end, we switch the heat source back to the original ( $T_H$ ) and the cycle restarts. The alternative is the elliptical cycle, where  $L$  and  $T$  are constantly changing but very slowly. The temperature



(a)



(b)

Figure 2.2: Figure on top represents a step cycle (a) and the elliptical cycle is represented on the bottom (b). For the step cycle, compression phase ( $L_m + \Delta L/2 \rightarrow L_m - \Delta L/2$ ) is performed (labelled 1) in contact with the hot source ( $T_H$ ), at the end there we instantaneously switch (labelled 2) with the cold source ( $T_C$ ) following by an expansion ( $L_m - \Delta L/2 \rightarrow L_m + \Delta L/2$ , labelled 3). At the end we instantaneously switch back to the hot source (labelled 4). For the elliptical cycle, both  $T$  and  $L$  change continuously with the BP absorbing heat while  $T$  increases (labelled 1) and rejecting heat when  $T$  decreases (labelled 2).

protocols are

$$T^{\text{step}}(t) = \begin{cases} T_H & \text{if } n\tau < t < (n+1/2)\tau \\ T_C & \text{if } (n+1/2)\tau < t < (n+1)\tau \end{cases} \quad (2-6)$$

$$T^{\text{ell}}(t) = T_m + \frac{\Delta T}{2} \sin(\Omega t), \quad (2-7)$$

where we can write that  $T_H = T_m + \Delta T/2$  and  $T_C = T_m - \Delta T/2$ , in other words,  $T_H$  and  $T_C$  represent the maximum and minimum temperature respectively while  $\Delta T$  is the gap between the two and  $T_m$  the average temperature. The cycles are represented in figure 2.2.

Since the step cycle is very similar to the Stirling cycle we would like to draw attention to the fact that, unlike in an actual Stirling machine, during the isocoric trajectories (constant  $L$ ) the system *does* exchange heat with the reservoirs which decreases the overall efficiency, we shall obtain how much in the end of this chapter.

### 2.1.2

#### Work Calculations

The work rate into the system is written as

$$\frac{dW}{dt} = -k_L(x - L)\dot{L} = P_W(t). \quad (2-8)$$

The work output per cycle of the  $n$ -th cycle is defined as

$$W_n = \int_{(n-1)\tau}^{n\tau} dt P_W(t) = \int_{(n-1)\tau}^{n\tau} dt \left\{ -k_L(x - L)\dot{L} \right\}, \quad (2-9)$$

which is a stochastic discrete variable (since  $x$  is also stochastic), and  $\tau$  is the period of a cycle. We are going to define the expected work output  $\mathcal{W}$  as both the average over ensembles and a time average over a very large number of cycles:

$$\mathcal{W} = \lim_{N \rightarrow \infty} \frac{1}{N} \sum_{n=0}^N \langle W_n \rangle, \quad (2-10)$$

here we introduce the notation that  $W$  (or any function  $F$ ) represents the value of an individual cycle while  $\mathcal{W}$  ( $\mathcal{F}$ ) represents the cycle expectation. Both the work output per cycle and the instantaneous power have a stochastic nature, however because the work is defined already as a time average over the instantaneous power, it will fluctuate far less.

Also we would like to draw attention to the sign when defining the work

as in 2-3: we are taking the perspective of the particle, therefore if  $\mathcal{W} > 0$  the particle is gaining work while if  $\mathcal{W} < 0$  then the particle is providing work to the piston, and by extension us. Thus we define the useful work as  $-\mathcal{W}$ .

### 2.1.3

#### Heat calculations

The instantaneous heat flow is represented by two terms with distinct roles

$$\frac{dQ}{dt} = \left[ \eta(t)v(t) - m\gamma v^2(t) \right] = P_Q(t), \quad (2-11)$$

where the first term  $\eta(t)\dot{x}$ , that we will henceforth refer as *fluctuation term* is the only term capable of injecting energy into the system. The second term, the *dissipation term*, is always removing energy from the system. In the experimental scenario it represents the interaction between the system and a medium composed of several smaller particles, and the large Brownian particle collides with the smaller bath particles constantly.

If the system is at a higher temperature than the bath, the dissipation term will be dominant over the fluctuation until the particle reaches thermal equilibrium at the same temperature as the heat bath; if the particle is at a lower temperature, the fluctuation term will dominate the energy exchange heating up the system.

We would like to also draw attention to the fact that the fluctuation is quite noisy; in fact, it becomes clear when evaluating its second moment:

$$\left\langle \left( \eta(t)\dot{x}(t) \right)^2 \right\rangle = \langle \eta(t)\eta(t) \rangle \langle v(t)v(t) \rangle + \dots, \quad (2-12)$$

that its variance is divergent since  $\langle \eta(t)\eta(t) \rangle \propto \delta(0)$ . This is a characteristic of the Langevin model, which has a too broad spectrum. In comparison, the dissipation fluctuates far less.

The heat intake  $\mathcal{Q}_H$  of the system is defined in the time interval where the heat flow is positive,  $\langle P_Q(t) \rangle > 0$ , while the expelled heat  $\mathcal{Q}_C$  is defined when  $\langle dQ/dt \rangle < 0$ . Of course if  $\langle P_Q(t) \rangle = 0$  there is no heat exchange between the heat bath and the system. The average heat flow is

$$\left\langle \frac{dQ}{dt} \right\rangle = \langle \eta(t)\dot{x}(t) \rangle - m\gamma \langle \dot{x}^2(t) \rangle = \gamma(T(t) - T_i(t)), \quad (2-13)$$

where the first result is explained in the appendix A and we have defined  $T_i$  as the system's internal temperature. This picture is quite straightforward, the average heat flow is proportional to the difference between the bath

temperature and the system temperature and the role of  $\gamma$  is the rate with which this exchange happens and if the system is at the bath temperature, there will be no heat exchange.

We can bring a lot of clarity to the heat flow between reservoir and system by analysing the linear problem:

$$m\ddot{x} + m\gamma\dot{x} + m\omega^2x = \eta(t), \quad (2-14)$$

where  $\eta$  has the same properties as the ones outlined in equation 2-1. Knowing that the Green function of the damped harmonic oscillator (assuming that  $\gamma < \omega$ ) is

$$G(t) = e^{-\gamma t/2} \frac{\sin\left(t\sqrt{\omega^2 - \gamma^2/4}\right)}{m\sqrt{\omega^2 - \gamma^2/4}}, \quad (2-15)$$

we can write the solution of 2-14 as

$$x(t) = \int_{-\infty}^t G(t-s)\eta(s)ds, \quad (2-16)$$

and

$$v(t) = \int_{-\infty}^t \dot{G}(t-s)\eta(s)ds + \underbrace{G(0)}_{=0}\eta(t) = \int_{-\infty}^t \dot{G}(t-s)\eta(s)ds. \quad (2-17)$$

Using the result from appendix A we can write that  $\langle\eta(t)v(t)\rangle = \gamma T(t)$  and using the previous equation we can write that

$$\begin{aligned} \langle v^2(t) \rangle &= \int_{-\infty}^t \langle \eta(s_1)\eta(s_2) \rangle \dot{G}(t-s_1)\dot{G}(t-s_2) ds_1 ds_2 \\ &= 2m\gamma \int_{-\infty}^t T(t)\dot{G}^2(t-s) ds. \end{aligned} \quad (2-18)$$

In order to understand how our system will behave with the abrupt changes in temperature, let us solve previous equation considering the particle was in contact with a heat bath of temperature  $T_1$  for  $t < 0$  and for  $t > 0$  we instantaneously change the bath temperature to  $T_2 > T_1$ . The solution is:

$$\begin{aligned} m\gamma\langle v^2(t) \rangle &= 2m^2\gamma^2 \int_{-\infty}^t T(t)\dot{G}^2(t-s) ds. \\ &= \gamma T_2 - \gamma(T_2 - T_1)e^{-\gamma t} \left\{ \frac{\omega^2 - \frac{\gamma^2}{4} \cos\left(t\sqrt{4\omega^2 - \gamma^2} + \phi_0\right)}{\omega^2 - \gamma^2/4} \right\} \end{aligned} \quad (2-19)$$

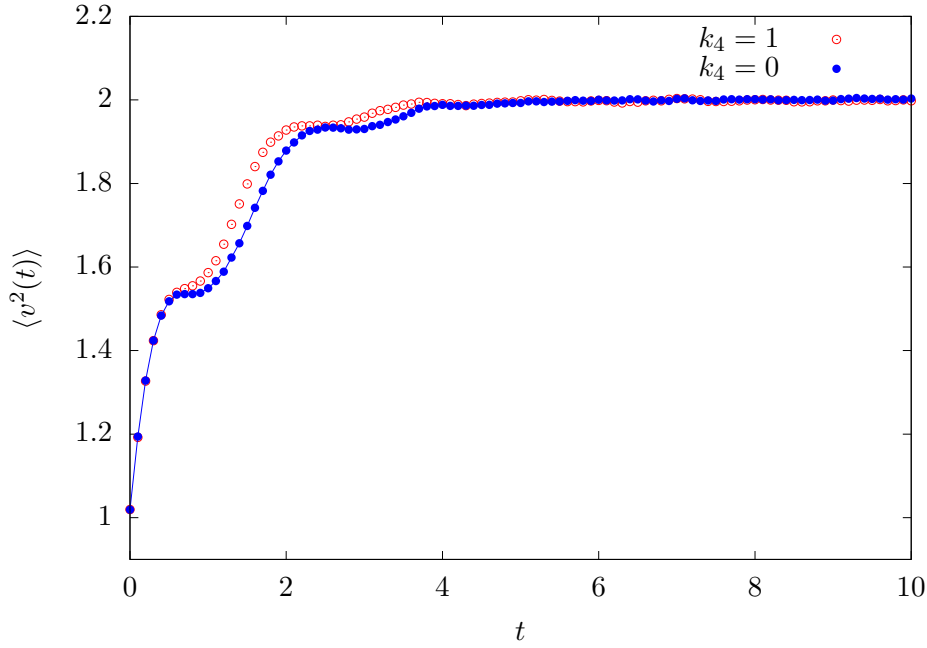


Figure 2.3: We present here the ensemble averages obtained through numerical simulations of equation 2-14. The parameters used were  $\gamma = \omega = m = 1$ .

where the phase is

$$\phi_0 = \arctan \left( \frac{\gamma}{\sqrt{4\omega^2 - \gamma^2}} \right). \quad (2-20)$$

We can demonstrate now two very intuitive results

$$m\gamma\langle v^2(0) \rangle = \gamma T_1 \quad ; \quad m\gamma\langle v^2(t \gg 1/\gamma) \rangle = \gamma T_2, \quad (2-21)$$

as we have stated before,  $\gamma$  is the time scale of the heat exchange between the reservoir and the system. By imposing that  $\tau\gamma \ll 1$ , the system will require but a small fraction of the overall cycle time to equilibrate with the bath. We have performed numerical simulations of  $\langle v^2 \rangle$  for non-linear potentials to demonstrate that the time scale of the temperature is still quite close to the linear system, the results are shown in figure 2.3.

Considering now that the system is in contact with a reservoir with the same temperature as the one in the elliptical cycle

$$m\gamma\langle v^2(t) \rangle = \gamma T_m + A(\Omega)\gamma\Delta T \sin(\Omega t) - B(\Omega)\gamma\Delta T \cos(\Omega t), \quad (2-22)$$

where we have defined:

$$A(\Omega) = \frac{2\gamma(4\omega^4 + \gamma^2\Omega^2 - 3\omega^2\Omega^2 + \Omega^4)}{(\gamma^2 + \Omega^2)(4\gamma^2\Omega^2 + (\Omega^2 - 4\omega^2)^2)}$$

$$B(\Omega) = \frac{\Omega(8\omega^4 + \gamma^2\Omega^2 - 6\omega^2\Omega^2 + \Omega^4)}{(\gamma^2 + \Omega^2)(4\gamma^2\Omega^2 + (\Omega^2 - 4\omega^2)^2)}.$$

Considering that  $\Omega \ll \omega$  and  $\Omega \ll \gamma$  we can write equation 2-22 as

$$m\gamma\langle v^2(t) \rangle \approx \gamma T_m + \frac{\gamma\Delta T}{2} \sin(\Omega t) - \frac{\Omega\Delta T}{2} \cos(\Omega t), \quad (2-23)$$

in order to obtain the heat flow between system and reservoir:

$$P_Q(t) = \langle \eta(t)v(t) \rangle - m\gamma\langle v^2(t) \rangle \approx \frac{\Omega\Delta T}{2} \cos(\Omega t). \quad (2-24)$$

This term is very small, however we must include it in our calculations, note that when integrating in the time interval where  $P_Q$  is positive we obtain the absorbed heat ( $Q_H$ ), we will obtain

$$Q_H = \int_{\tau/2}^{3\tau/2} dt P_Q(t) = \Delta T, \quad (2-25)$$

which is clearly non-negligible. We performed numerical simulations to demonstrate the validity of equation 2-22 even for nonlinear systems, the results are shown in figure 2.4.

## 2.2

### The Role of Non-Linearities

Now we shall go into detail on the role that the nonlinearities in the potential  $V(x)$  have in the conversion of heat into work. Let us take first a purely mathematical perspective, if the internal potential were to be linear, the Langevin equation describing the system becomes

$$m\ddot{x} + m\gamma\dot{x} + k_2x = -k_L(x - L) + \eta(t), \quad (2-26)$$

which can be easily solved using the Laplace Transform  $\mathcal{L}(x) = \tilde{x}(s)$ :

$$\underbrace{(ms^2 + m\gamma s + k_2 + k_L)}_{R(s)} \tilde{x}(s) = -k_L\tilde{L}(s) + \tilde{\eta}(s)$$

$$\tilde{x}(s) = \frac{\tilde{\eta}(s)}{R(s)} - \frac{k_L\tilde{L}(s)}{R(s)}, \quad (2-27)$$

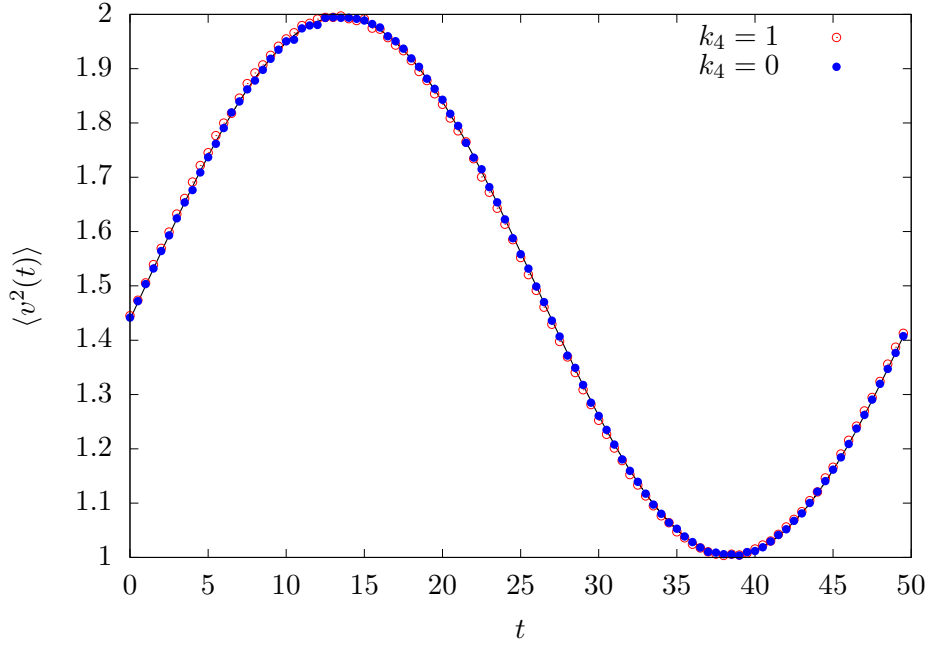


Figure 2.4: We present here the ensemble averages obtained through numerical simulations of equation 2-14 with the elliptical temperature. The parameters used where  $\gamma = \omega = m = 1$ . The solid line represents the result for the linear case 2-22.

so we conclude that the average power (or the expected power) is proportional to the expected position

$$\left\langle \frac{dW}{dt} \right\rangle = -k_L (\langle x \rangle - L) \dot{L}, \quad (2-28)$$

but the expected position depends only on  $\tilde{L}(s)$ :

$$\langle \tilde{x}(s) \rangle = -\frac{k_L \tilde{L}(s)}{R(s)}, \quad (2-29)$$

and is completely independent of the temperature. In other words, if we were to disconnect the system from the heat bath, the expected power would not depend on  $T$ ! Thus, the linear machine is incapable of converting heat into work.

From a mathematical perspective it is very easy to explain this result. Equation 2-8 shows us that the work rate is linearly dependent on the position  $x$ , and from equation 2-2 the position is linearly dependent on  $L$  and  $\eta(T)$ . If the governing Langevin equation were non-linear, like for instance

$$m\ddot{x} + m\gamma\dot{x} + k_2x + k_4x^3 = -k_L(x - L) + \eta(t), \quad (2-30)$$

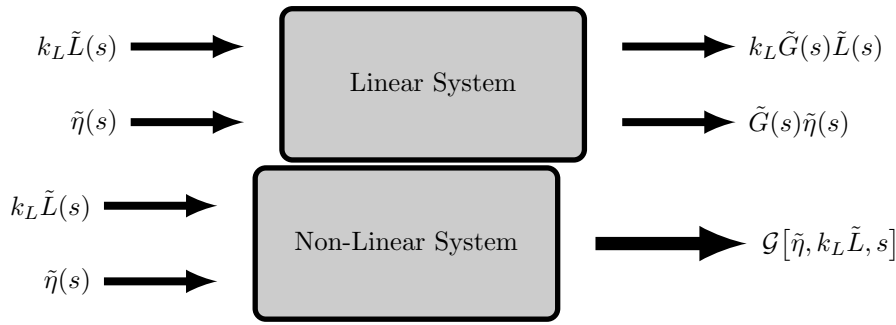


Figure 2.5: Visual representation of a dynamical equation. In the linear case, on top, the answer consists on the sum of the two individual entries contributions while for the nonlinear system, bottom, the answer consists in a non-trivial combination of the two.

now  $x$  is no longer a linear sum of the independent responses from  $L$  and  $\eta$ , and in this case there will be mixing of the dynamic from the bath and from the external piston (see figure 2.5).

However we are still left with questions. For instance, not all non-linear systems are capable of converting heat into work (we demonstrate this in chapter 3), the non-linearity is necessary but no sufficient. So let us take a more physical approach to the problem of: what makes a machine?

Consider a system of  $N$  ideal gas particles at temperature  $T$ . Following the law of ideal gasses, the pressure necessary to constrain these particles inside a box of volume  $V$  obeys

$$pV = NT, \quad (2-31)$$

where we are taking the temperature in energy units ( $k_B = 1$ ). The particles of the gas are in constant collision with the walls of the box, and from 2-31 we can conclude that the higher the temperature, the higher the pressure on the walls.

Consider that one of the walls of this volume  $V$  is a piston, when the gas particles are at a high temperature  $T_2$ , the particles will collide with the piston and drive its displacement which in turn becomes a source of work. The gas particles are now performing this work in the external environment, this process converts the heat contained within the gas particles into work (see a representation in figure 2.6).

We cannot just stop here. As stated in the previous chapter, the correct way to operate machines is through cycles, so we must return our piston to its original position. If this compression is performed while the system remains at temperature  $T_2$ , then the pressure that the gas particles apply to the piston will be the same and we would be required to spend the same amount of work we

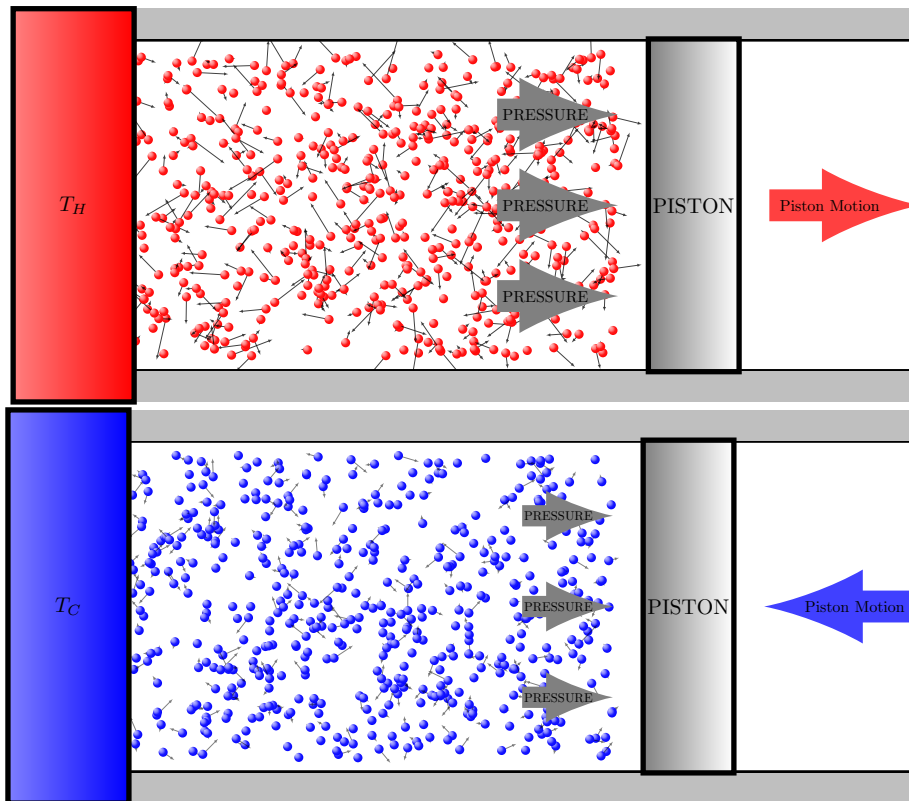


Figure 2.6: A simple representation of two stages of a machine. With the high temperature  $T_H$ , we move the piston in the direction of the pressure from the particles. With the lower temperature  $T_C$ , because the pressure on the piston is now lower, we require less work to push it back to its original position, thus having a net gain of work at the end of the cycle.

just managed to obtain in the expansion phase. However, if the temperature has been lowered to  $T_1 < T_2$ , now the pressure on the piston walls is lower following 2-31. Once the original volume is restored we return the system particles to their original temperature.

We described above a very simple machine (roughly a Stirling cycle) in order to highlight the most important aspect of a machine: the fluctuations must have some sort of bias. In this case, the fluctuations drive the system to occupy an even larger volume, which is why we require the pressure  $p$  to keep the particles contained inside a given volume. When the system is at a high temperature, use this tendency to occupy more volume, let the particles spend their energy pushing the piston even further and then, with the system at a lower temperature, we shall face less resistance from the particles and we can push the piston back to its original gaining net work.

When we move to a setting composed of a single particle it becomes less intuitive. The BP is subjected to the effective potential  $V(x) = \frac{k_2}{2}x^2 + \frac{k_L}{2}(x - L)^2$ , the Langevin equation governing the evolution of such system is equation 2-26. Using purely mathematical principles we have concluded that

such potential cannot convert heat into work. We can reach the same conclusion from a much clearer physical perspective simply by looking at the potential.

In figure 2.7 we can see the probability distribution obtained using equilibrium statistical mechanics (more on that in chapter 3), notice how the position expectation is the same as the minimal potential  $x_m$  regardless of the temperature. That is because the external potential we introduced,  $V_e$  did not break the symmetry of the effective potential, the particle finds the same resistance when fluctuating to the left or to the right of the minimum, and since the work output is linearly proportional to the expectation of  $x$  as shown in 2-8, the net work is going to be null.

When we introduce a non-harmonic potential into the problem,  $V(x) = \frac{k_2}{2}x^2 + \frac{k_4}{4}x^4 + \frac{k_L}{2}(x - L)^2$ , we have that for different values of  $L$  the potential is no longer symmetric, it becomes deformed and, as a result, to the left of the minimal position ( $x < x_m$ ) it becomes softer meanwhile to the right of the minimal ( $x > x_m$ ) it becomes steeper. The fluctuations of  $\eta(t)$  are unbiased, but the particle has less opposition to fluctuating to the left of the minimum than to the right of it. The asymmetry in the potential created a preferred direction to the BP and, as a result, stronger fluctuations shift the expected position even further from the minimal potential as we can see in figure 2.8.

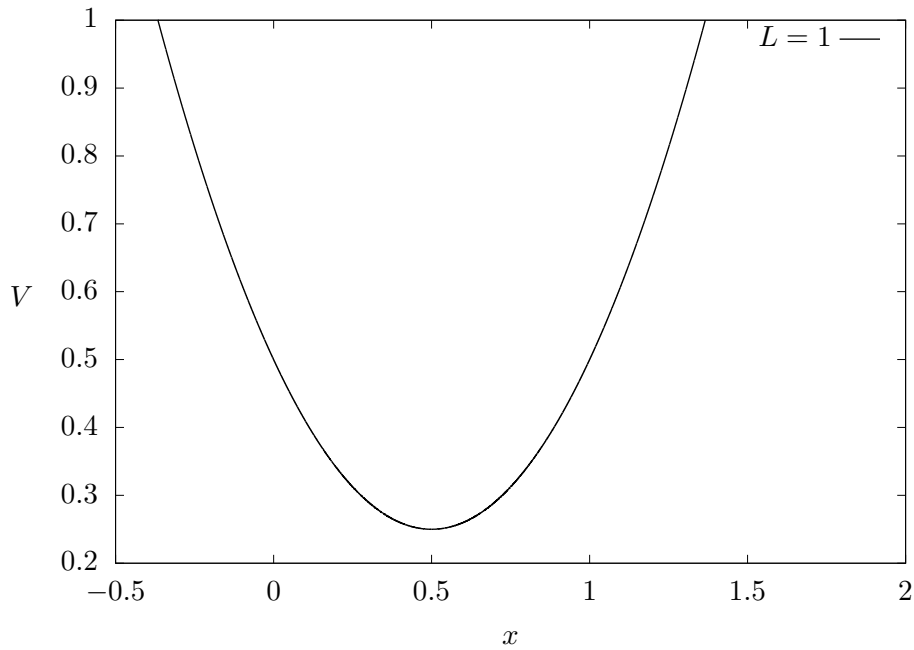
Now the parallel is clear, when the system is at a higher temperature we will follow the preferred direction of the particle and perform a contraction, and at a lower temperature, with weaker opposition by the fluctuations,  $L$  will revert to its original position performing an expansion. The work output in both branches will be different and the net work production of the cycle will be non-zero. We illustrate this point in figure 2.9.

## 2.3

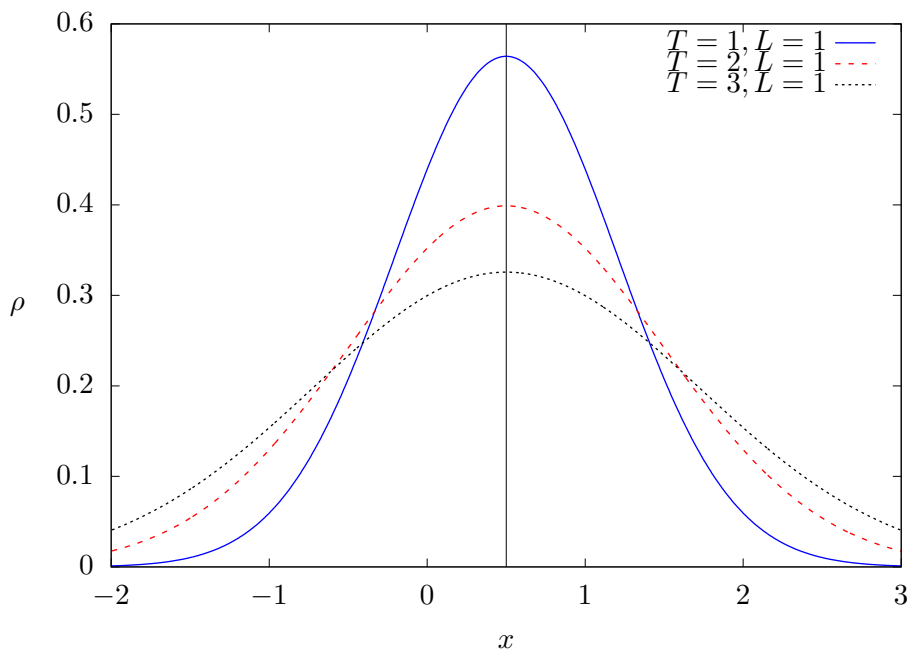
### Perturbative Approach

The task of solving a non-linear differential equation is quite challenging, the vast majority array of methods, like both the Fourier and Laplace transform, or the Green Function method work better when the equations are linear. In order to extract analytical results from equation 2-30 we will employ perturbation theory to expand the solutions as series of the non-linear term  $k_4$ .

The use of harmonic potentials is not only due to the simplicity that it provides when it comes to obtaining analytical solutions, it also represents a first approximation to a naturally occurring confining potential. It is a natural

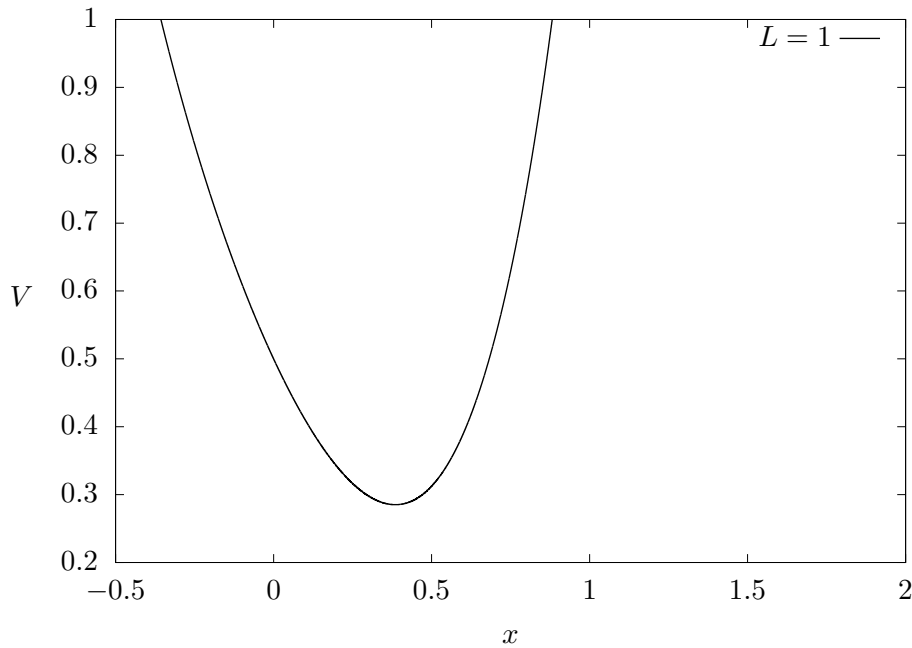


2.7(a):

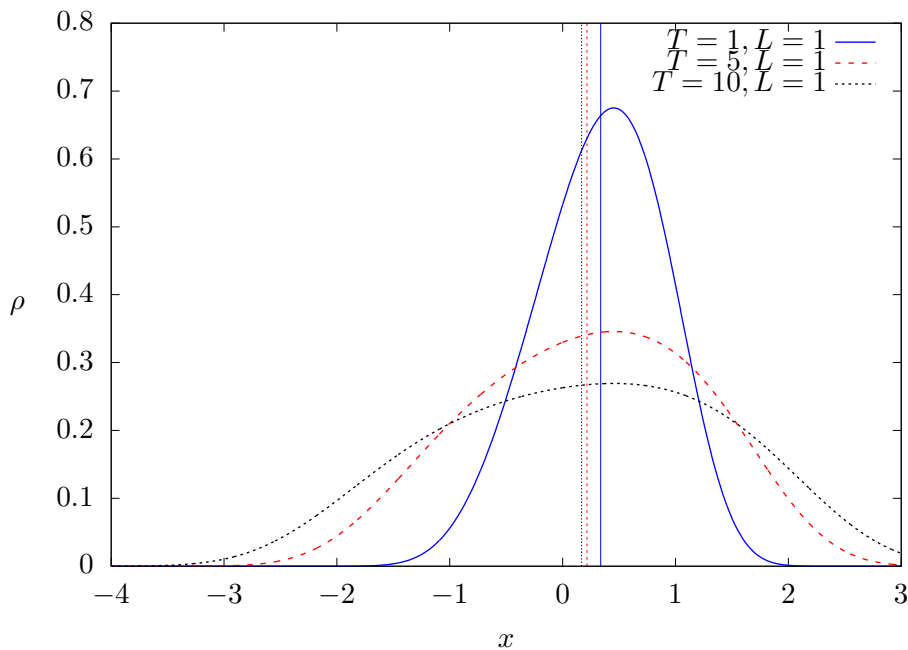


2.7(b):

Figure 2.7: The figure on the top represents (a) the effective potential  $V(x) = \frac{k_2}{2}x^2 + \frac{k_L}{2}(x-L)^2$  and on the bottom (b) represents the probability distribution of the particle at different temperatures. The solid black line represents  $\langle x \rangle$ , which does not change with the temperature. We have considered  $k_2 = 1$  and  $k_L = 1$ .



2.8(a):



2.8(b):

Figure 2.8: The figure on the top (a) represents the effective potential  $V(x) = \frac{k_2}{2}x^2 + \frac{k_4}{4}x^4 + \frac{k_L}{2}(x - L)^2$  and on the bottom (b) represents the probability distribution of the particle at different temperatures. The solid black line represents  $\langle x \rangle$ , which increases with the temperature. We have considered  $k_2 = 1$ ,  $k_L = 1$  and  $k_4 = 1$ .

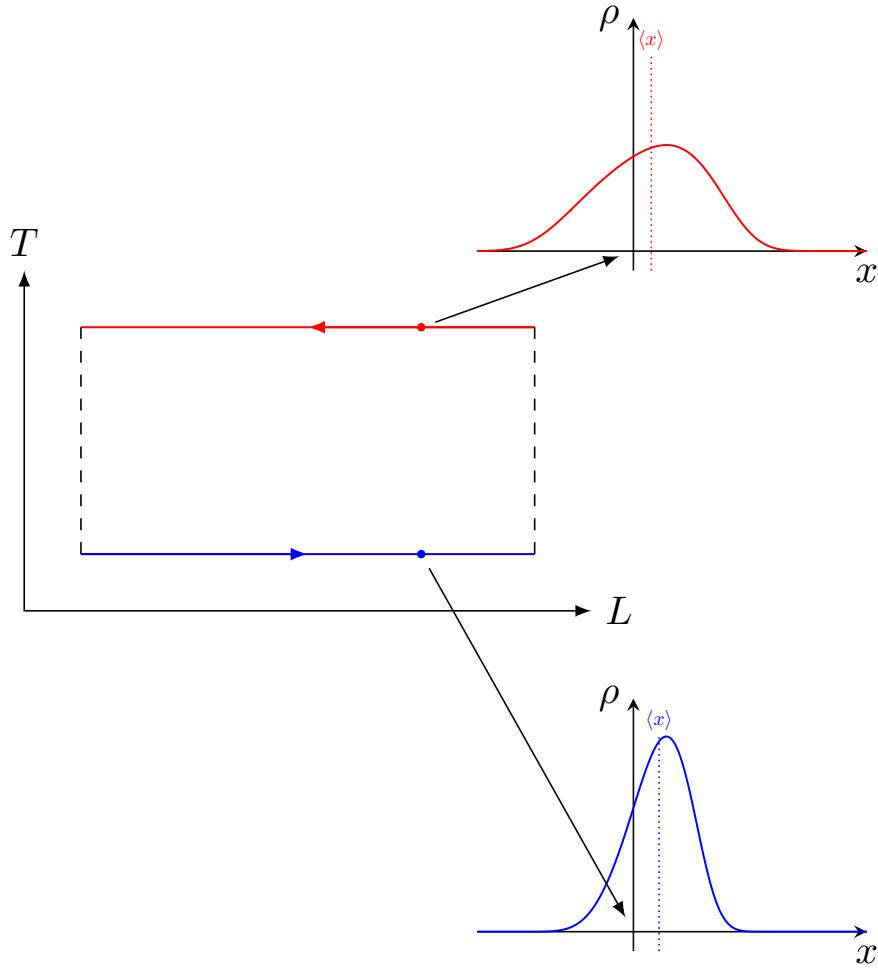


Figure 2.9: The step cycle is represented where we have highlighted the same displacement  $L$  but for different temperatures in order to compare compression with expansion phases. The power output for the fixed value of  $L$  is  $P_W = -k_L(\langle x \rangle_{T_H} - \langle x \rangle_{T_C})\dot{L}$ , which is negative since  $\langle x \rangle_{T_H} > \langle x \rangle_{T_C}$ .

first step to introduce the second term of such an expansion,

$$V_i(x) = V_0 + \frac{V_i''(0)}{2}x^2 + \frac{V_i^{(4)}(0)}{24}x^4 + \mathcal{O}(x^6) \approx \frac{k_2}{2}x^2 + \frac{k_4}{4}x^4, \quad (2-32)$$

which also justifies the use of perturbation theory. The coordinates can be perturbatively expanded as [53, 57–59].

$$x = x_0 + k_4x_1 + \mathcal{O}(k_4^2) \quad ; \quad v = v_0 + k_4v_1 + \mathcal{O}(k_4^2), \quad (2-33)$$

and after replacing these terms in equation 2-30 and separating according to  $k_4$  we obtain the following recursive relationship

$$\begin{aligned} \mathcal{O}(k_4^0) & : \quad m\dot{v}_0 + m\gamma v_0 + k_2x_0 = -k_L(x_0 - L) + \eta(t) \\ \mathcal{O}(k_4^1) & : \quad m\dot{v}_1 + m\gamma v_1 + k_2x_1 = -x_0^3. \end{aligned} \quad (2-34)$$

The first equation is the linear approximation ( $k_4 = 0$ ) and can be solved using Laplace transform or Green's function, with the solution of  $x_0(t)$  we can now solve the differential equation for  $x_1(t)$  using  $x_0$  as a driving force.

Following the assumption that the energy in the harmonic mode  $\phi_2$  is much larger than in the quartic mode  $\phi_4$  ( $\phi_2 \gg \phi_4$ ), the average energy  $\mathcal{U}$  calculated as

$$\mathcal{U} = \langle U \rangle = \left\langle \frac{m}{2}v^2 + \frac{k_2}{2}x^2 + \frac{k_4}{4}x^4 + \frac{k_L}{2}(x-L)^2 \right\rangle \quad (2-35)$$

can also be expanded in a series of  $k_4$  to the first order

$$\begin{aligned} \mathcal{U} &\approx \frac{m}{2}\langle v_0^2 \rangle + \frac{k_2 + k_L}{2}\langle x_0^2 \rangle + \frac{k_4}{4}\langle x_0^4 \rangle = \\ &= \frac{m}{2}(\langle v_0^2 \rangle_c + \langle v_0 \rangle_c^2) + \frac{k_2 + k_L}{2}(\langle x_0^2 \rangle_c + \langle x_0 \rangle_c^2) + \frac{k_4}{4}(3\langle x_0^2 \rangle_c^2 + \langle x_0 \rangle_c^4) \end{aligned}$$

since the energy, up to the first order expansion in  $k_4$  is only a function of the zero order terms  $x_0$  and  $v_0$ , we can evaluate previous equation directly, leading to the result

$$\underbrace{T + \frac{m}{2}\langle v_0 \rangle^2 + \frac{k_2 + k_L}{2}\langle x_0 \rangle^2}_{\phi_2} + \underbrace{\frac{3k_4 T^2}{(k_2 + k_L)^2} + \frac{k_4}{4}\langle x_0 \rangle^4}_{\phi_4}, \quad (2-36)$$

and by separating the thermal components from the deterministic ones we can write the two restrictions

$$1 \gg \frac{k_4 T}{(k_2 + k_L)^2} \quad ; \quad 1 \gg \frac{k_4 L_m^2}{k_2 + k_L}, \quad (2-37)$$

where  $L_m$  is the average value of  $L(t)$  in time. Both restrictions must be respected simultaneously for the expansion to be a valid approximation.

By taking the Laplace transform of 2-34 we have that

$$\begin{aligned} \tilde{x}_0(s) &= \frac{k_L \tilde{L}(s)}{mR(s)} + \frac{\tilde{\eta}(s)}{mR(s)} \\ \tilde{x}_1(s) &= -\lim_{\epsilon \rightarrow 0} \int \frac{dq_1 dq_2 dq_3}{(2\pi)^3 mR(s)} \frac{\tilde{x}_0(iq_1 + \epsilon) \tilde{x}_0(iq_2 + \epsilon) \tilde{x}_0(iq_3 + \epsilon)}{s - iq_1 - iq_2 - iq_3 - 3\epsilon}, \end{aligned} \quad (2-38)$$

where we have made use of the result in appendix B:

$$\mathcal{L}\{x_0^3(t)\} = \lim_{\epsilon \rightarrow 0} \int \frac{dq_1 dq_2 dq_3}{(2\pi)^3} \frac{\tilde{x}_0(iq_1 + \epsilon) \tilde{x}_0(iq_2 + \epsilon) \tilde{x}_0(iq_3 + \epsilon)}{s - iq_1 - iq_2 - iq_3 - 3\epsilon}, \quad (2-39)$$

we have also defined that  $R(s) = s^2 + \gamma s + \omega^2$  (and  $k_2 + k_L = m\omega^2$ ).

## 2.4

### Work Output

Let us remind ourselves of the work expression

$$\begin{aligned}\mathcal{W} &= \lim_{N \rightarrow \infty} \frac{1}{N} \int_0^{N\tau} -k_L \{ \langle x \rangle - L(t) \} \dot{L}(t) dt \\ &= \lim_{N \rightarrow \infty} -\frac{k_L}{N} \int_0^{\tau N} \langle x \rangle \dot{L} dt.\end{aligned}\quad (2-40)$$

We can also expand  $\mathcal{W}$  as a series of  $k_4$

$$\begin{aligned}\mathcal{W} &= \mathcal{W}_0 + k_4 \mathcal{W}_1 + \mathcal{O}(k_4^2) = \lim_{N \rightarrow \infty} -\frac{k_L}{N} \int_0^{\tau N} \left\{ \langle x_0 \rangle + k_4 \langle x_1 \rangle + \mathcal{O}(k_4^2) \right\} \dot{L} dt \\ &= -\lim_{N \rightarrow \infty} \frac{k_L}{N} \int_0^{\tau N} \langle x_0 \rangle \dot{L} dt - \lim_{N \rightarrow \infty} \frac{k_L k_4}{N} \int_0^{\tau N} \langle x_1 \rangle \dot{L} dt + \mathcal{O}(k_4^2).\end{aligned}\quad (2-41)$$

In order to perform the calculations we will make use of the techniques outlined in appendix B, where the time average is expressed in terms of the Laplace transform of our functions

$$\begin{aligned}\mathcal{W}_0 &= -\lim_{N \rightarrow \infty} \lim_{\epsilon \rightarrow 0} \int_{-\infty}^{\infty} \frac{dq_1 dq_2}{(2\pi)^2} k_L \tau (iq_1 + iq_2 + 2\epsilon) \langle \tilde{x}_0(iq_1 + \epsilon) \rangle \tilde{L}(iq_2 + \epsilon) \\ \mathcal{W}_1 &= -\lim_{N \rightarrow \infty} \lim_{\epsilon \rightarrow 0} \int_{-\infty}^{\infty} \frac{dq_1 dq_2}{(2\pi)^2} k_L \tau (iq_1 + iq_2 + 2\epsilon) \langle \tilde{x}_1(iq_1 + \epsilon) \rangle \tilde{L}(iq_2 + \epsilon).\end{aligned}$$

### 2.4.1

#### Zerth order

Since the average of the zeroth term in the position

$$\begin{aligned}\langle \tilde{x}_0(s) \rangle &= \left\langle \frac{k_L \tilde{L}(s)}{mR(s)} + \frac{\tilde{\eta}(s)}{mR(s)} \right\rangle \\ &= \frac{k_L \tilde{L}(s)}{mR(s)},\end{aligned}\quad (2-42)$$

and there is no dependence on the temperature, the zeroth order work is identical for both step and elliptical cycles

$$\begin{aligned}\mathcal{W}_0 &= -\lim_{N \rightarrow \infty} \lim_{\epsilon \rightarrow 0} \int_{-\infty}^{\infty} \frac{dq_1 dq_2}{(2\pi)^2} k_L \tau (iq_1 + iq_2 + 2\epsilon) \langle \tilde{x}_0(iq_1 + \epsilon) \rangle \tilde{L}(iq_2 + \epsilon) \\ &= -\lim_{N \rightarrow \infty} \lim_{\epsilon \rightarrow 0} \int_{-\infty}^{\infty} \frac{dq_1 dq_2}{(2\pi)^2} k_L^2 \tau (iq_1 + iq_2 + 2\epsilon) \frac{\tilde{L}(iq_1 + \epsilon) \tilde{L}(iq_2 + \epsilon)}{mR(iq_1 + \epsilon)} \\ &= \frac{\pi m \gamma k_L^2 \Delta L^2}{4(k_2 + k_L)^2} \Omega + \mathcal{O}(\Omega^4),\end{aligned}\quad (2-43)$$

since the sign of the output is positive, the machine is absorbing the work. This represents an irreversible loss for  $\Omega > 0$ , caused by the mechanical friction between the BP and the surrounding bath particles, as attested by the factor  $\gamma$  in the numerator.

## 2.4.2

### First Order

The average of the first order term of the position starts to become quite cumbersome

$$\begin{aligned}
\langle \tilde{x}_1(s) \rangle &= - \lim_{\epsilon \rightarrow 0} \frac{1}{mR(s)} \int \frac{dq_1 dq_2 dq_3}{(2\pi)^3} \frac{\langle \tilde{x}_0(iq_1 + \epsilon) \tilde{x}_0(iq_2 + \epsilon) \tilde{x}_0(iq_3 + \epsilon) \rangle}{s - iq_1 - iq_2 - iq_3 - 3\epsilon}, \\
&= - \lim_{\epsilon \rightarrow 0} \frac{1}{mR(s)} \int \frac{dq_1 dq_2 dq_3}{(2\pi)^3} \frac{\langle \tilde{x}_0(iq_1 + \epsilon) \rangle \langle \tilde{x}_0(iq_2 + \epsilon) \rangle \langle \tilde{x}_0(iq_3 + \epsilon) \rangle}{s - iq_1 - iq_2 - iq_3 - 3\epsilon} - \\
&\quad - \lim_{\epsilon \rightarrow 0} \frac{3}{mR(s)} \int \frac{dq_1 dq_2 dq_3}{(2\pi)^3} \frac{\langle \tilde{x}_0(iq_1 + \epsilon) \rangle \langle \tilde{x}_0(iq_2 + \epsilon) \tilde{x}_0(iq_3 + \epsilon) \rangle}{s - iq_1 - iq_2 - iq_3 - 3\epsilon} \\
&= \lim_{\epsilon \rightarrow 0} \frac{1}{mR(s)} \int \frac{dq_1 dq_2 dq_3}{(2\pi)^3} \frac{\frac{k_L^3 \tilde{L}(iq_1 + \epsilon) \tilde{L}(iq_2 + \epsilon) \tilde{L}(iq_3 + \epsilon)}{m^3 R(iq_1 + \epsilon) R(iq_2 + \epsilon) R(iq_3 + \epsilon)}}{s - iq_1 - iq_2 - iq_3 - 3\epsilon} + \\
&\quad + \lim_{\epsilon \rightarrow 0} \frac{3}{mR(s)} \int \frac{dq_1 dq_2 dq_3}{(2\pi)^3} \frac{\frac{k_L \tilde{L}(iq_1 + \epsilon) \langle \tilde{\eta}(iq_2 + \epsilon) \tilde{\eta}(iq_3 + \epsilon) \rangle}{m^3 R(iq_1 + \epsilon) R(iq_2 + \epsilon) R(iq_3 + \epsilon)}}{s - iq_1 - iq_2 - iq_3 - 3\epsilon}, \tag{2-44}
\end{aligned}$$

and the first order of the work output is enormously more cumbersome, we will limit ourselves here to calculate the reduced

$$\mathcal{W}_1 = - \lim_{N \rightarrow \infty} \lim_{\epsilon \rightarrow 0} \int_{-\infty}^{\infty} \frac{dq_1 dq_2}{(2\pi)^2} k_L k_4 \tau (iq_1 + iq_2 + 2\epsilon) \langle \tilde{x}_0(iq_1 + \epsilon) \rangle \tilde{L}(iq_2 + \epsilon).$$

For the first order correction we obtain terms that do not depend on the cycle time ( $\Omega$ )

$$\begin{aligned}
\mathcal{W}_1^{\text{ell}} &= - \frac{3\pi k_L k_4 L_m \Delta L \Delta T^{\text{ell}}}{4(k_2 + k_L)^3} - \frac{3\pi m \gamma k_4 k_L^2 \Delta L^2}{2(k_2 + k_L)^4} \left\{ T_m + \frac{k_L^2 (\Delta L^2 + 16L_m)}{16(k_2 + k_L)} \right\} \Omega \\
\mathcal{W}_1^{\text{step}} &= - \frac{3k_L k_4 L_m \Delta L \Delta T^{\text{step}}}{(k_2 + k_L)^3} - \frac{3\pi m \gamma k_4 k_L^2 \Delta L^2}{2(k_2 + k_L)^4} \left\{ T_m + \frac{k_L^2 (\Delta L^2 + 16L_m)}{16(k_2 + k_L)} \right\} \Omega.
\end{aligned}$$

Note that all the main ingredients we intuitively expect a working machine to possess are present: we have  $L_m$ , which ensures that the potential deformation remains biased (if we had  $L_m = 0$  the deformation on the positive side would be compensated by the equivalent on the negative side), and of course  $\Delta T$ .

The terms dependent on cycle period do not violate the second law thanks to the presence of the much larger zeroth term  $\mathcal{W}_0$  which is a consequence of the restriction imposed in 2-37. In other words, they are not too large.

Also, we decided to label the temperature difference specifying the cycle

( $\Delta T^{\text{step}}$  and  $\Delta T^{\text{ell}}$ ) because if we consider  $\Delta T^{\text{ell}} = 4\Delta T^{\text{step}}/\pi$ , all terms in the first order become identical. It is simple to understand this relation when one looks at the Fourier series of the step cycle temperature:

$$T(t) = T_m + \frac{2}{\pi}\Delta T^{\text{step}}\sin(\Omega t) + \frac{2}{3\pi}\Delta T^{\text{step}}\sin(3\Omega t) + \dots \quad (2-45)$$

by choosing that  $\Delta T^{\text{ell}} = 4\Delta T^{\text{step}}/\pi$  the elliptical cycle becomes the first order expansion of the step cycle.

## 2.5 Heat Exchanges

Following the definition of heat rate outlined in section 2.1.3, the amount of heat exchanged in the time interval between 0 and  $t$  is

$$\mathcal{Q}(t) = \int_0^t ds \langle \eta(s)v(s) - m\gamma v^2(s) \rangle. \quad (2-46)$$

Using the result of appendix A, we have that

$$\mathcal{Q}(t) = \gamma \int_0^t ds \{ T(s) - m \langle v^2(s) \rangle \}. \quad (2-47)$$

In order to evaluate the heat exchanged we need to evaluate  $\langle v^2(t) \rangle$ . In section 2.1.3 we have also outlined the phases in which the system is either absorbing or rejecting heat to/from reservoir. For the elliptical cycle the heat is absorbed when the bath temperature rises, in the step cycle its absorbed when the system is in contact with the higher temperature. To evaluate the heat only in the desired regions we will make use of the early and late time averages defined in appendix B.

$$\mathcal{Q}_H = \overline{\langle \eta(t)v(t) - m\gamma v^2(t) \rangle}^{\text{early}} = T_m + \frac{\Delta T}{2} - m\gamma \overline{\langle v^2(t) \rangle}^{\text{early}} \quad (2-48)$$

$$\mathcal{Q}_C = \overline{\langle \eta(t)v(t) - m\gamma v^2(t) \rangle}^{\text{late}} = T_m - \frac{\Delta T}{2} - m\gamma \overline{\langle v^2(t) \rangle}^{\text{early}} \quad (2-49)$$

For reasons that will become clear by the end of the section, we will only calculate the zeroth order of  $\langle v^2(t) \rangle$ . The early and late time averages are written as

$$\begin{aligned}
\overline{v_0^2(t)}^{\text{early}} &= \lim_{N \rightarrow \infty} \lim_{\epsilon \rightarrow 0} \int_{-\infty}^{\infty} \frac{dq_1 dq_2}{(2\pi)^2} \tau_E(iq_1 + iq_2 + 2\epsilon) \langle \tilde{v}_0(iq + \epsilon) \tilde{v}_0(iq_2 + \epsilon) \rangle \\
&= \lim_{N \rightarrow \infty} \lim_{\epsilon \rightarrow 0} \int_{-\infty}^{\infty} \frac{dq_1 dq_2}{(2\pi)^2} \tau_E(iq_1 + iq_2 + 2\epsilon) (iq_1 + \epsilon)(iq_2 + \epsilon) \times \\
&\times \langle \tilde{x}_0(iq + \epsilon) \tilde{x}_0(iq_2 + \epsilon) \rangle \\
&= \lim_{N \rightarrow \infty} \lim_{\epsilon \rightarrow 0} \int_{-\infty}^{\infty} \frac{dq_1 dq_2}{(2\pi)^2} \tau_E(iq_1 + iq_2 + 2\epsilon) (iq_1 + \epsilon)(iq_2 + \epsilon) \times \\
&\times \left\{ \frac{k_L^2 \tilde{L}(iq_1 + \epsilon) \tilde{L}(iq_2 + \epsilon)}{m^2 R(iq_1 + \epsilon) R(iq_2 + \epsilon)} + \frac{\langle \tilde{\eta}(iq_1 + \epsilon) \tilde{\eta}(iq_2 + \epsilon) \rangle}{m^2 R(iq_1 + \epsilon) R(iq_2 + \epsilon)} \right\} \quad (2-50)
\end{aligned}$$

$$\begin{aligned}
\overline{v_0^2(t)}^{\text{late}} &= \lim_{N \rightarrow \infty} \lim_{\epsilon \rightarrow 0} \int_{-\infty}^{\infty} \frac{dq_1 dq_2}{(2\pi)^2} \tau_L(iq_1 + iq_2 + 2\epsilon) \langle \tilde{v}_0(iq + \epsilon) \tilde{v}_0(iq_2 + \epsilon) \rangle \\
&= \lim_{N \rightarrow \infty} \lim_{\epsilon \rightarrow 0} \int_{-\infty}^{\infty} \frac{dq_1 dq_2}{(2\pi)^2} \tau_L(iq_1 + iq_2 + 2\epsilon) (iq_1 + \epsilon)(iq_2 + \epsilon) \times \\
&\times \langle \tilde{x}_0(iq + \epsilon) \tilde{x}_0(iq_2 + \epsilon) \rangle \\
&= \lim_{N \rightarrow \infty} \lim_{\epsilon \rightarrow 0} \int_{-\infty}^{\infty} \frac{dq_1 dq_2}{(2\pi)^2} \tau_L(iq_1 + iq_2 + 2\epsilon) (iq_1 + \epsilon)(iq_2 + \epsilon) \times \\
&\times \left\{ \frac{k_L^2 \tilde{L}(iq_1 + \epsilon) \tilde{L}(iq_2 + \epsilon)}{m^2 R(iq_1 + \epsilon) R(iq_2 + \epsilon)} + \frac{\langle \tilde{\eta}(iq_1 + \epsilon) \tilde{\eta}(iq_2 + \epsilon) \rangle}{m^2 R(iq_1 + \epsilon) R(iq_2 + \epsilon)} \right\} \quad (2-51)
\end{aligned}$$

with results

$$\overline{v_0^2(t)}^{\text{early}} = \frac{\pi k_L^2 \Delta L^2}{8(k_2 + k_L)^2} \Omega + \frac{2T_m - \Delta T}{2m} \quad (2-52)$$

$$\overline{v_0^2(t)}^{\text{late}} = \frac{\pi k_L^2 \Delta L^2}{8(k_2 + k_L)^2} \Omega + \frac{2T_m + \Delta T}{2m}. \quad (2-53)$$

Replacing our findings in

$$\mathcal{Q}_H = T_m + \frac{\Delta T}{2} - \frac{\pi m \gamma k_L^2 \Delta L^2}{8(k_2 + k_L)^2} \Omega - \frac{2T_m - \Delta T}{2m} = \Delta T - \frac{\pi m \gamma k_L^2 \Delta L^2}{8(k_2 + k_L)^2} \quad (2-54)$$

$$\mathcal{Q}_C = T_m - \frac{\Delta T}{2} - \frac{\pi m \gamma k_L^2 \Delta L^2}{8(k_2 + k_L)^2} \Omega - \frac{2T_m + \Delta T}{2m} = -\Delta T - \frac{\pi m \gamma k_L^2 \Delta L^2}{8(k_2 + k_L)^2} \quad (2-55)$$

note that if we add both terms we would get the heat exchange of the entire cycle

$$\mathcal{Q} = \mathcal{Q}_1 + \mathcal{Q}_2 = -\frac{\pi m \gamma k_L^2 \Delta L^2}{4(k_2 + k_L)^2} \Omega, \quad (2-56)$$

which, in accordance with the first law of thermodynamics  $\mathcal{Q} + \mathcal{W} = 0$ , at the end of a cycle.

Unlike the result obtained for the work output, the heat does contain

terms that do not depend on the cycle duration, this is why we will not be calculating beyond the zeroth order, these terms will be dominant when compared to the first order. For the work output, we could always choose  $\Omega$  to be so small that only the stationary terms remain relevant, but even then the efficiency of our machine would be

$$\text{efficiency} = \frac{3\pi k_L k_4 L_m \Delta L}{4(k_2 + k_L)^3} \frac{\Delta T}{\Delta T} = \frac{3\pi k_L k_4 L_m \Delta L}{4(k_2 + k_L)^3} \ll 1 \quad (2-57)$$

which is much smaller than the Carnot efficiency. In experimental situations, the efficiency can also be quite low [15].

## 2.6

### Final Remarks

In this chapter we presented the quartic model and its relevant properties. We focussed on providing a simple and intuitive perspective while describing the role of each component in our equations of motion.

Employing perturbation theory we are able to solve equation 2-2 analytically up to any order of  $k_4$ ; a task which is easier said than done when one considers how the components become quite cumbersome. Nevertheless, the biggest downfall of this approach is that, for the cycles we employed, the heat absorption is gigantic when compared to the work produced, rendering the efficiency quite insignificant.

In the next chapter we will attempt to improve the machine by investigating larger nonlinearities. However, in order to achieve this higher range of  $k_4$  we will be making an equilibrium hypothesis, which is only consistent with Gaussian heat baths. If we were dealing with more exotic types of reservoirs (of Poissonian nature for instance), then perturbation theory would be our only tool to investigate these problems.

### 3 The Quasi-Static Regime

In the previous chapter we analysed the nonlinear machine using perturbation theory to obtain analytical results. This decision greatly narrows the range of values of  $k_4$  we may investigate.

We will now soften the restrictions on  $k_4$  by imposing more severe ones to the cycle time. Previously we have considered that the cycle duration was the largest time scale of the problem (or  $\Omega \ll \omega_2, \gamma$ ), such a restriction was taken not only to obtain the approximation but also due to the fact that in an experimental situation, we would expect the piston position (a parameter which varies as a known protocol) will operate much slower than the internal vibrations of the system. Now we will consider that the cycle time is long enough ( $\Omega \rightarrow 0$ ) so that at all points we may consider the system and bath to be in equilibrium with each other. This new restriction we shall henceforth refer as *quasi-static* regime.

Within this regime, we are allowed to invoke the heavy machinery that is classical statistical mechanics (Boltzmann and Gibbs), which will in turn allow for analytical predictions to be made.

#### 3.1 Equilibrium Distribution

Consider that our system is in equilibrium with a heat bath of temperature  $T$  with its ensemble distribution written as

$$\rho(x, p) = \frac{1}{Z} e^{-\mathcal{H}(x, p)/T}, \quad (3-1)$$

where  $Z$  is the partition function defined as

$$Z = \int dx dp e^{-\mathcal{H}(x, p)/T}. \quad (3-2)$$

The system Hamiltonian can be written as,

$$\mathcal{H}(x, p, L) = \frac{p^2}{2m} + \frac{k_2}{2} x^2 + \frac{k_4}{4} x^4 + \frac{k_L}{2} (x - L)^2, \quad (3-3)$$

the work gained (or lost) to change the parameter  $L$  by  $dL$  is

$$d\mathcal{W} = \left\langle \frac{\partial \mathcal{H}}{\partial L} \right\rangle dL = F_L dL. \quad (3-4)$$

where  $F_L = -k_L \langle x - L \rangle$  is the conjugate of  $L$ . The work rate can also be written in terms of the free energy  $F$  as

$$d\mathcal{W} = -k_L (\langle x \rangle - L) dL = \frac{\partial}{\partial L} \left\{ \underbrace{-T \ln \mathcal{Z}(L, T)}_{F(L, T)} \right\} \Big|_T dL. \quad (3-5)$$

In a full cycle, the amount of work that can be produced is evaluated as

$$\mathcal{W} = \oint \frac{\partial}{\partial L} F(L, T) \Big|_T dL, \quad (3-6)$$

where we draw attention to the fact that the derivative with respect to  $L$  is taken at constant  $T$  while the integration is made on a trajectory in the phase-space of  $L \times T$  which implies a dependency between  $T$  and  $L$ . Since the step cycle is composed of two branches where the temperature is constant, separating the integration in two

$$\begin{aligned} \mathcal{W}^{\text{step}} &= \int_{L_2}^{L_1} \frac{\partial}{\partial L} F(L, T_H) dL + \int_{L_1}^{L_2} \frac{\partial}{\partial L} F(L, T_C) dL = \\ &= F(L_1, T_H) - F(L_2, T_H) + F(L_2, T_C) - F(L_1, T_C), \end{aligned} \quad (3-7)$$

and since the sudden changes in temperature happen with a constant  $L$ , there will be no work change. It is also possible to express the previous result using the partition functions

$$\mathcal{W}^{\text{step}} = T_H \ln \frac{Z(L_2, T_H)}{Z(L_1, T_H)} - T_C \ln \frac{Z(L_2, T_C)}{Z(L_1, T_C)}. \quad (3-8)$$

So far we have expressed our cycles using mainly figure 2.2 as representation since we can control only  $L$  and  $T$  directly. However, that representation is not as clear as a pressure by volume ( $p \times V$ ) representation for the ideal gas. With the tools of classical statistics we are able to, at least numerically, present them in a clearer way, using the First law we obtain

$$\oint_{\text{cycle}} d\mathcal{U} = \oint_{\text{cycle}} T dS + \oint_{\text{cycle}} F_L dL = 0, \quad (3-9)$$

we can now express the work output using two sets of conjugated variables

$$\oint_{\text{cycle}} F_L dL = - \oint_{\text{cycle}} T dS = \mathcal{W}, \quad (3-10)$$

which we have represented for a particular case in figure 3.1. We can now demonstrate the statement made in subsection 2.2, consider a hypothetical system with Hamiltonian

$$\mathcal{H}_{\text{sym}}(x, p) = \frac{p^2}{2m} + \frac{k_2}{2}(x - L)^2 + \frac{k_4}{4}(x - L)^4, \quad (3-11)$$

the potential is clearly nonlinear, so the mathematical restriction is obeyed, however it remains symmetrical for any value of  $L$  as shown in figure 3.2. Because of that, the particles will have no preferred direction, oscillating equally in both directions as

$$\langle x \rangle_{\text{sym}} = L, \quad (3-12)$$

making

$$\oint_{\text{cycle}} F_L dL = 0. \quad (3-13)$$

### 3.2

#### Small Nonlinearity Approximation ( $k_4 \rightarrow 0$ )

For small non-linearities we find ourselves in the same regime of the previous chapter 2 so we must recover the results which do not depend on cycle time. The partition function can be approximated as

$$Z \approx \int_{-\infty}^{\infty} dx dp \left\{ 1 - \frac{k_4}{4T} x^4 \right\} e^{-\beta \left\{ \frac{p^2}{2m} + \frac{k_2}{2} x^2 + \frac{k_4}{4} (x-L)^2 \right\}} = Z_0 + k_4 Z_1, \quad (3-14)$$

where  $\beta = 1/T$ . We also defined the linear partition function as

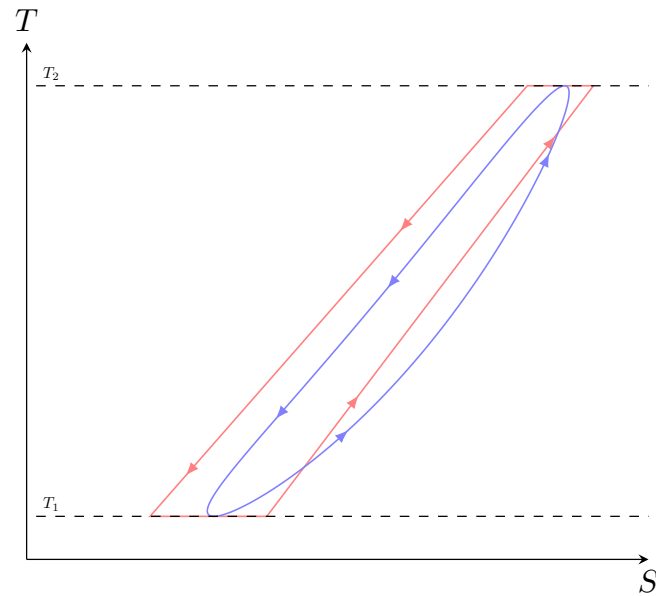
$$Z_0 = 2\pi T \sqrt{\frac{m}{k_2 + k_L}} e^{-\frac{k_2 k_L L^2}{2T(k_2 + k_L)}} \quad (3-15)$$

and first nonlinear the correction

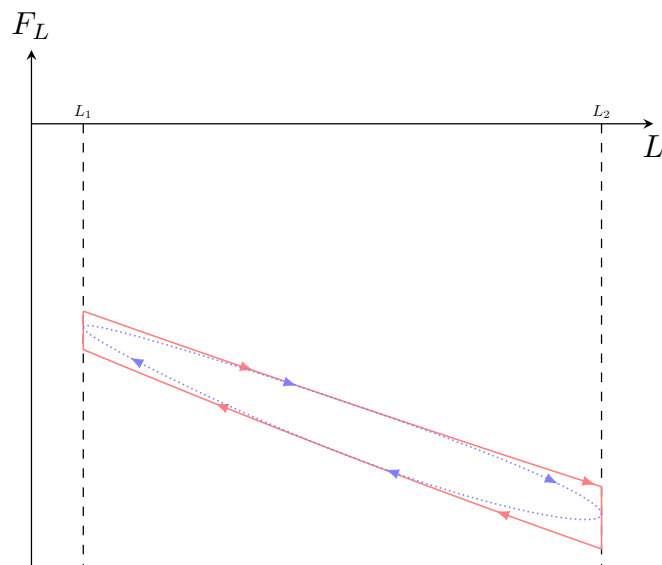
$$Z_1 = \frac{\pi}{(k_2 + k_L)^2} \sqrt{\frac{m}{k_2 + k_L}} \left\{ \frac{k_L^4 L^4}{2(k_2 + k_L)^2} + \frac{6k_L^2 L^2 T}{k_2 + k_L} + 3T^2 \right\}. \quad (3-16)$$

and using the definition of the work output in Eq. (3-5) we obtain

$$\begin{aligned} d\mathcal{W} &\approx -k_L \int_{-\infty}^{\infty} dx dp x \frac{\left\{ 1 - \frac{k_4}{4T} x^4 \right\}}{Z_0 + k_4 Z_1} e^{-\beta \left\{ \frac{p^2}{2m} + \frac{k_2}{2} x^2 + \frac{k_4}{4} (x-L)^2 \right\}} dL + k_L L dL \\ &\approx \frac{k_L k_2}{k_2 + k_L} L dL + k_4 \frac{k_L^4 L^3 + 3k_2 k_L L T + 3k_L^3 L T}{(k_2 + k_L)^3} dL. \end{aligned} \quad (3-17)$$



3.1(a):



3.1(b):

Figure 3.1: Here we represent a cycle from the perspective of the conjugated variables, the top figure (a) represents the plot of temperature versus entropy ( $T \times S$ ) while the bottom figure (b) represents the plot of  $F_L \times L_m$  which is equivalent to the  $p \times V$  plot of an ideal gas. Following 3-10, the work output is the area between the two lines. The red line represents the step cycle while the blue dotted line represents the elliptical cycle. Both cases have  $L_m$ ,  $\Delta L$ ,  $T_m$  and  $\Delta T$ .

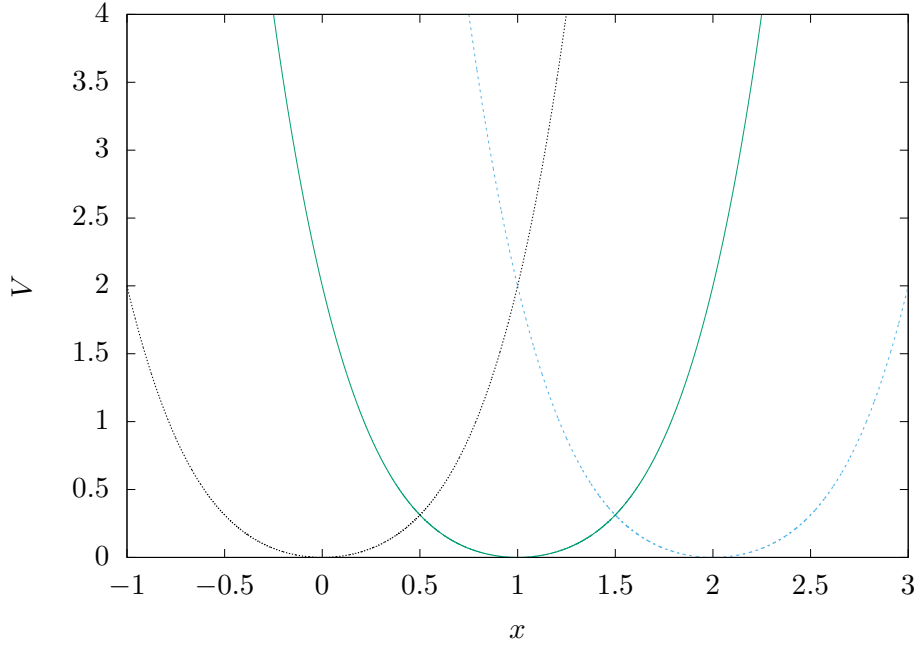


Figure 3.2: Nonlinear potentials that remain symmetric.

Using previous equation to calculate the work output we obtain

$$\begin{aligned}\mathcal{W}^{\text{ell}} &= -\frac{3\pi k_L k_4 L_m \Delta L \Delta T^{\text{ell}}}{4(k_2 + k_L)^3} \\ \mathcal{W}^{\text{step}} &= -\frac{3k_L k_4 L_m \Delta L \Delta T^{\text{step}}}{(k_2 + k_L)^3},\end{aligned}$$

thus recovering the results presented in chapter 2 when one takes the limit  $\Omega \rightarrow 0$ . Using the same approximation we write the internal energy up to the first order of  $k_4$

$$\mathcal{U} \approx T + \frac{k_2 k_L}{2(k_2 + k_L)} L^2 + k_4 \left\{ \frac{k_L^4 L^4}{4(k_2 + k_L)^4} - \frac{3T^2}{4(k_2 + k_L)^2} \right\}, \quad (3-18)$$

and using the conservation of energy

$$dQ = d\mathcal{U} - d\mathcal{W},$$

we obtain the heat exchanged for the step

$$Q_H^{\text{step}} = +\Delta T + \frac{3k_4 \Delta T}{2(k_2 + k_L)^2} \left\{ \frac{k_L^2 L_m \Delta L}{(k_2 + k_L)} - T_m \right\} + \frac{3k_4 k_L^2 T_m L_m \Delta L}{2(k_2 + k_L)^3} + \mathcal{O}(k_4^2) \quad (3-19)$$

$$Q_C^{\text{step}} = -\Delta T + \frac{3k_4 \Delta T}{2(k_2 + k_L)^2} \left\{ \frac{k_L^2 L_m \Delta L}{(k_2 + k_L)} + T_m \right\} - \frac{3k_4 k_L^2 T_m L_m \Delta L}{2(k_2 + k_L)^3} + \mathcal{O}(k_4^2) \quad (3-20)$$

and elliptical cycles

$$\mathcal{Q}_H^{\text{ell}} = +\Delta T + \frac{3\pi k_4 \Delta T}{4(k_2 + k_L)^2} \left\{ \frac{k_L^2 L_m \Delta L}{(k_2 + k_L)} - T_m \right\} + \frac{3k_4 k_L^2 T_m L_m \Delta L}{2(k_2 + k_L)^3} + \mathcal{O}(k_4^2) \quad (3-21)$$

$$\mathcal{Q}_C^{\text{ell}} = -\Delta T + \frac{3\pi k_4 \Delta T}{4(k_2 + k_L)^2} \left\{ \frac{k_L^2 L_m \Delta L}{(k_2 + k_L)} + T_m \right\} - \frac{3k_4 k_L^2 T_m L_m \Delta L}{2(k_2 + k_L)^3} + \mathcal{O}(k_4^2) \quad (3-22)$$

leading to the same efficiency as equation 2-57.

Now consider that, like in the Stirling engine, during the isochoric process (represented by path (1) in figure 2.2) the heat exchange is internal. The resulting heat exchange becomes

$$\mathcal{Q}_H^{\text{hyp}} = \frac{3k_L k_4 L_m \Delta L T_H}{(k_2 + k_L)^3} \quad (3-23)$$

$$\mathcal{Q}_C^{\text{hyp}} = \frac{3k_L k_4 L_m \Delta L T_C}{(k_2 + k_L)^3}, \quad (3-24)$$

leading to the Carnot efficiency

$$\xi = -\frac{\mathcal{W}}{\mathcal{Q}_H} = \frac{\Delta T}{T_H} = \xi_C. \quad (3-25)$$

With such results we can now state with certainty that the low efficiency is a direct consequence of the isochoric branch.

### 3.2.1

#### Large Nonlinearity Approximation ( $k_4 \rightarrow \infty$ )

In the quasi-static regime it is also possible to study the limit where the nonlinearity is very large, in this case the majority of the energy is contained in the quartic mode rather than the harmonic one. After performing a change of variables in the definition of the partition function:  $k_4 \rightarrow 4T/\epsilon^4$  and  $x \rightarrow \epsilon y$  we obtain

$$Z = \sqrt{\pi m T} e^{-\frac{k_L}{2T} L^2} \int_{-\infty}^{\infty} \epsilon dy e^{-\frac{k_2 + k_L}{2T} \epsilon^2 y^2 + \frac{k_L L}{T} L \epsilon y} e^{-y^4}. \quad (3-26)$$

The limit  $\epsilon \rightarrow 0$  ( $k_4 \rightarrow \infty$ ) yields the approximate value

$$Z \approx \frac{\sqrt{\pi m T}}{2} e^{-\frac{k_L}{2T} L^2} \epsilon \left\{ \Gamma\left(\frac{1}{4}\right) - \epsilon^2 \left[ \frac{k_2 + k_L}{2T} - \frac{k_L^2}{2T^2} \right] \Gamma\left(\frac{3}{4}\right) \right\} + \mathcal{O}(\epsilon^3), \quad (3-27)$$

leading to the work rate

$$\begin{aligned} d\mathcal{W} &= k_L L dL \left\{ 1 - \epsilon^2 k_L \frac{\Gamma(3/4)}{\Gamma(1/4)} \right\} + \mathcal{O}(\epsilon^4) \\ &= k_L L dL \left\{ 1 - \frac{1}{\sqrt{k_4}} \frac{2k_L \Gamma(3/4)}{\sqrt{T} \Gamma(1/4)} \right\} + \mathcal{O}(1/k_4), \end{aligned} \quad (3-28)$$

where  $\Gamma(x)$  is the Gamma function. The work produced in a complete cycle is

$$\mathcal{W} = -\frac{1}{\sqrt{k_4}} \oint dL \frac{2k_L^2 L \Gamma(3/4)}{\sqrt{T(L)} \Gamma(1/4)} + \mathcal{O}(1/k_4). \quad (3-29)$$

The work output of the step cycle is quite straightforward

$$\mathcal{W}^{\text{step}} = -\frac{2k_L^2 L_m \Delta L (\sqrt{T_H} - \sqrt{T_C}) \Gamma(3/4)}{\sqrt{k_4 T_H T_C} \Gamma(1/4)}, \quad (3-30)$$

while the elliptical cycle requires a bit more effort, first we parametrize the trajectory using a new variable  $\theta$  as

$$L(\theta) = L_m + \frac{\Delta L}{2} \cos(\theta); \quad dL = -\frac{\Delta L}{2} \sin(\theta) d\theta; \quad T(\theta) = T_m + \frac{\Delta T}{2} \sin(\theta) \quad (3-31)$$

making the work output

$$\mathcal{W}^{\text{ell}} = -\frac{2k_L^2 L_m \Delta L \Gamma(3/4)}{\sqrt{k_4 T_m} \Gamma(1/4)} \int_{2\pi}^0 d\theta \frac{1 + \frac{\Delta L}{2L_m} \cos \theta}{\sqrt{1 + \frac{\Delta T}{2T_m} \sin \theta}} \sin \theta, \quad (3-32)$$

we point out that the integration is always positive. Notice that both elliptical and step cycles present the same asymptotic behaviour of  $1/\sqrt{k_4}$ .

The internal energy is

$$\begin{aligned} \mathcal{U} &= \frac{1}{2} k_L L^2 + \frac{3T}{4} + \epsilon^2 \left\{ \frac{(k_2 + k_L)T - 3k_L^2 L^2}{2\sqrt{2T} \Gamma(1/4)^2} \right\} \\ &= \frac{1}{2} k_L L^2 + \frac{3T}{4} + \frac{1}{\sqrt{k_4}} \left\{ \frac{(k_2 + k_L)T - 3k_L^2 L^2}{\sqrt{2T} \Gamma(1/4)^2} \right\} \end{aligned} \quad (3-33)$$

where the zeroth term of the expansion corresponds to the internal energy of a massive particle subjected to a quartic potential. Using these results with the First law of thermodynamics we obtain the heat outputs

$$\mathcal{Q}_H^{\text{step}} = \mathcal{Q}_H^{\text{ell}} = \frac{3}{4} \Delta T + \mathcal{O}(1/\sqrt{k_4}) \quad (3-34)$$

$$\mathcal{Q}_C^{\text{step}} = \mathcal{Q}_C^{\text{ell}} = -\frac{3}{4} \Delta T + \mathcal{O}(1/\sqrt{k_4}), \quad (3-35)$$

leading to efficiencies that are also of the order of the approximation  $\mathcal{O}(1/\sqrt{k_4})$ .

### 3.3

#### Convergence Issue

Employing the procedure described in the previous two sections numerically we can directly evaluate for defined sets of parameters the value of the coefficients of our expansion using any cycle. Take the work output expanded up to the  $N$ -th order, in the limit of small nonlinearity

$$\mathcal{W} = \sum_{n=1}^N w_n k_4^n, \quad (3-36)$$

and in the large  $k_4$  limit

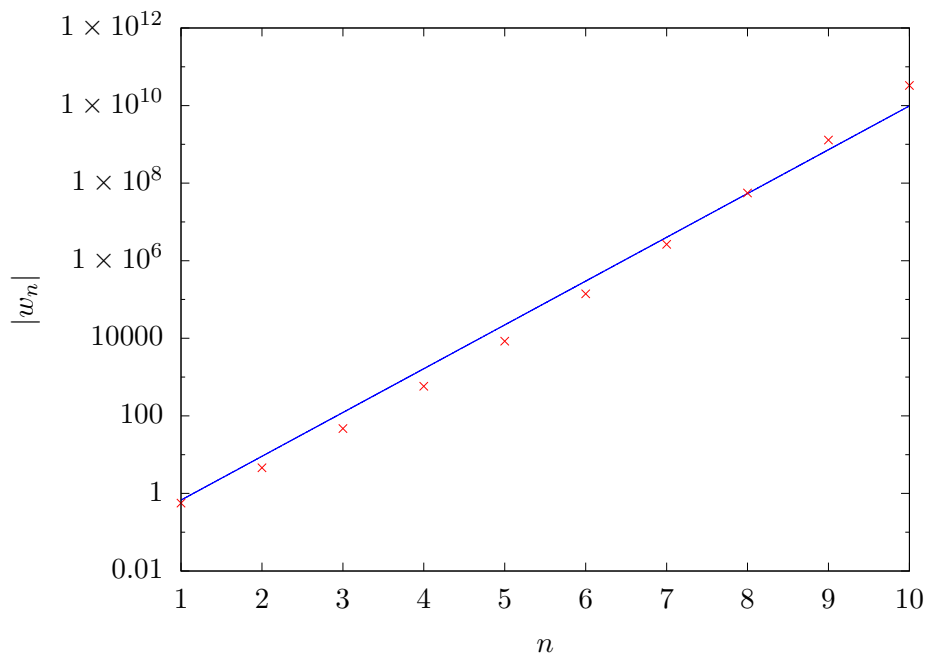
$$\mathcal{W} = \sum_{n=1}^N w'_n k_4^{-n/2}, \quad (3-37)$$

one could assume that by increasing the value of  $N$  we would systematically increase the range of validity of our approximation but that is not the case. The series alternates but the absolute value of each  $w_n$  increases exponentially as shown in figure 3.3 [53].

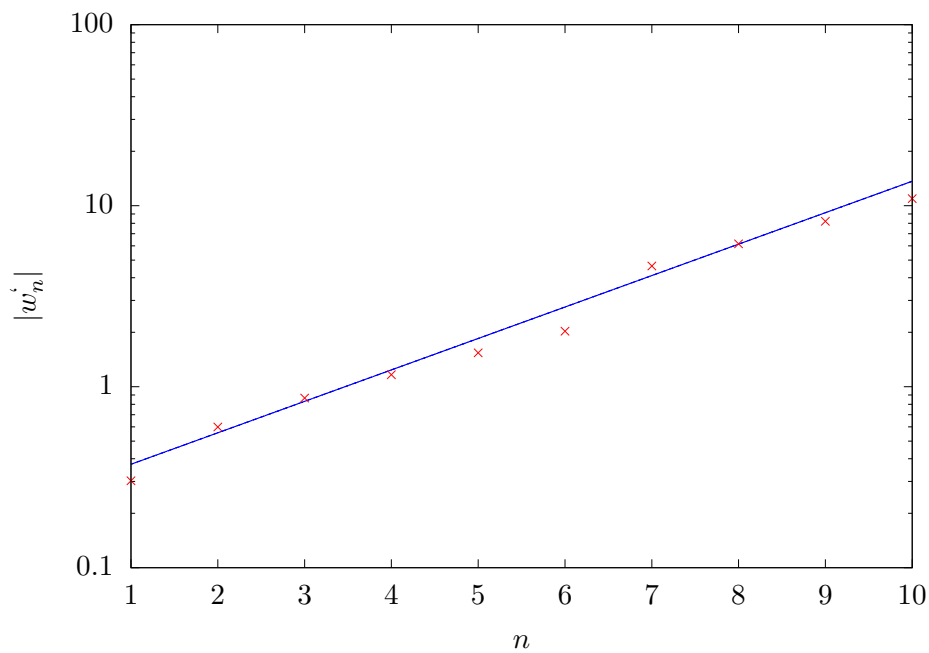
Comparing previous results with numerical calculations shown in Fig. 3.4 [53] we observe that increasing the order of our expansions does improve accuracy of the result, but cannot overcome a range of validity for small  $k_4$  (or large  $k_4$ ) that does not provide any insight on the point of maximal work output. This is an unfortunate consequence of the fact that we have chosen to expand highly convergent Gaussians by means of polynomial series, which will always diverge for a sufficiently high value of the variable (in our case the position  $x$ ). Thus, if for instance  $k_4$  is large (but not so large as to justify the large value expansion) the integration in  $Z$  will cover a large domain where the polynomial begins to diverge from the Gaussian.

To circumvent this problem we decided to employ a less intuitive approximation, but one that presents absolute convergence and can be used for any range of  $k_4$ . Starting by redefining the partition function as

$$\begin{aligned} Z &= \sqrt{\pi m T} \int_{-\infty}^{\infty} e^{-\frac{k_2}{2T} x^2 - \frac{k_L}{2T} (x-L)^2 - \frac{k_4}{4T} x^4} dx \\ &= \frac{\sqrt{\pi m T}}{2} \int_{-\infty}^{\infty} \left\{ e^{-\frac{k_L}{2T} (x-L)^2} + e^{-\frac{k_L}{2T} (x+L)^2} \right\} e^{-\frac{k_2}{2T} x^2 - \frac{k_4}{4T} x^4} \\ &= \sqrt{\pi m T} e^{-\frac{k_L L^2}{2T}} \int_{-\infty}^{\infty} \sinh\left(\frac{k_L L}{T} x\right) e^{-\frac{k_2}{2T} x^2 - \frac{k_L}{2T} x^2 - \frac{k_4}{4T} x^4}, \quad (3-38) \end{aligned}$$



3.3(a):



3.3(b):

Figure 3.3: The red points represent the absolute values of the expansion constants, on the top (a) we represent the approximation for small nonlinearities, the figure on the bottom (b) for large nonlinearities. For small nonlinearities the values grow so rapidly that by the tenth term we already have values up to  $10^{12}$ , for large nonlinearities the growth is much more tamed, but still very clear. The auxiliary blue line highlights how the growth is exponential in both cases. The values used are  $\Delta T = \Delta L = m = k_2 = k_L = 1$  and  $L_m = T_m = 1.5$ .

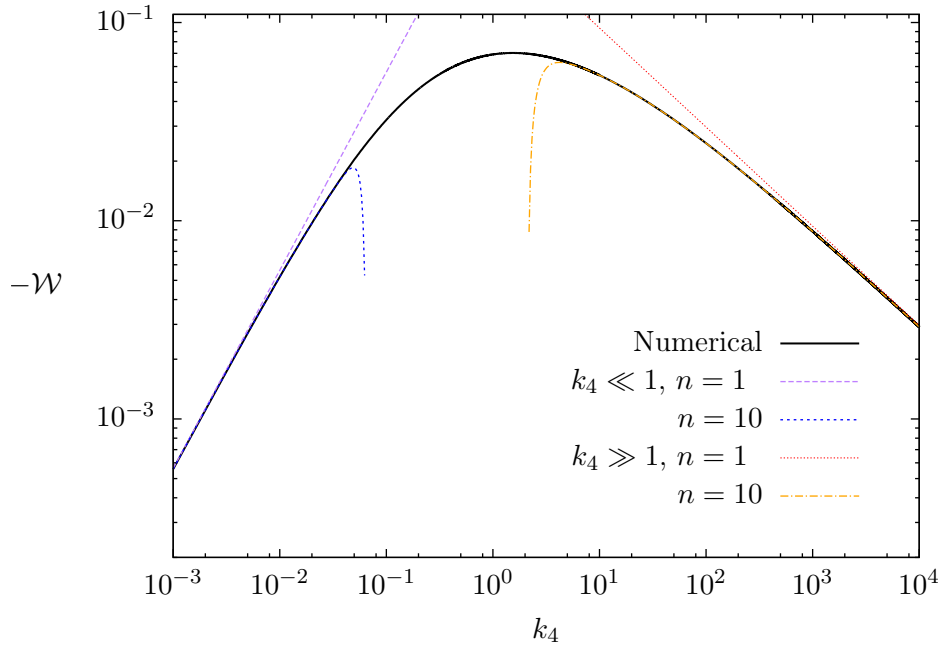


Figure 3.4: The solid (black) line represents the numerical integration of equation 3-6, using our analytical expansions for the step cycle. The dotted lines, blue and violet depict expansions of equation 3-6 for small values of  $k_4$  while the dot-dashed lines, orange and red, depict expansions for large values of  $k_4$ . For both cases we display the first and tenth orders to illustrate how there is no conversion radius. The values used are  $\Delta T = \Delta L = m = k_2 = k_L = 1$  and  $L_m = T_m = 3/2$ .

we can now expand the hyperbolic sine as a polynomial series. Because  $\sinh(x)$  does not converge, the polynomial representation remains good approximation to the original function even when we drastically increase the value of  $x$ . The series for the hyperbolic sine are

$$\sinh(x) = \sum_{n=0}^{\infty} \frac{x^{2n+1}}{(2n)!}, \quad (3-39)$$

that we may use to evaluate the partition function

$$Z = \sqrt{\pi m T} e^{-\frac{k_L L^2}{2T}} \int_{-\infty}^{\infty} \sum_{n=0}^{\infty} \frac{1}{(2n)!} \left( \frac{k_L L}{T} x \right)^{2n+1} e^{-\frac{k_2}{2T} x^2 - \frac{k_L}{2T} x^2 - \frac{k_4}{4T} x^4}, \quad (3-40)$$

which can be calculated exactly using the confluent hypergeometric function

$$M(a, b, z) = \frac{1}{\Gamma(a)} \int_0^{\infty} e^{-zt} t^{a-1} (1+t)^{b-a-1} dt, \quad (3-41)$$

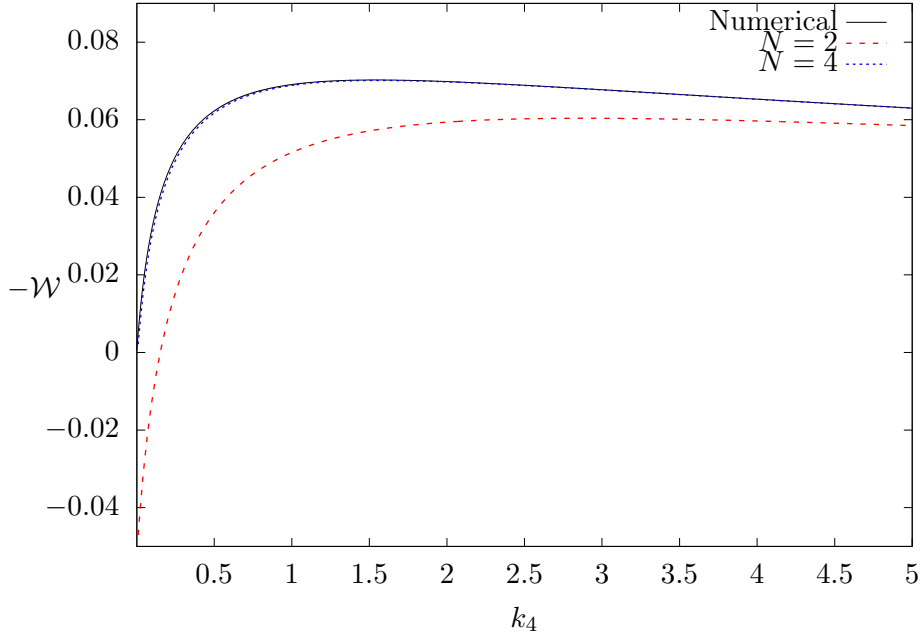


Figure 3.5: The solid black line represents the numerical integration of equation 3-6 while the dashed red line represents the absolutely convergent expansion for  $N = 2$  and the dotted blue line for  $N = 4$ . The values used are  $\Delta T = \Delta L = m = k_2 = k_L = 1$  and  $L_m = T_m = 3/2$ .

as

$$Z = \sqrt{\pi m T} e^{-\frac{k_L + k_2}{2T} L^2} \sum_{n=0}^{\infty} \left( \frac{\sqrt{2} k_L L}{(k_4 T^3)^{1/4}} \right)^{2n} \frac{\Gamma\left(n + \frac{1}{2}\right)}{(2n)! 2^{n+\frac{1}{2}}} \times \\ \times M\left(\frac{1}{4} + \frac{n}{2}, \frac{1}{2}, \frac{(k_2 + k_L)^2}{4k_4 T}\right). \quad (3-42)$$

Albeit being quite cumbersome, this approximation converges far better than the first two as we show in figure 3.5. However, because of the non trivial algebraic role of our parameters ( $L$ ,  $T$ , etc), it unfortunately does not provide much insight on the interplay of such parameters in the final answer.

### 3.4

#### Numerical Approach

Having analysed the system using the equilibrium approach, we now turn to numerical integration to validate our findings. We start by writing equation 2-2 as [54, 55]

$$\begin{aligned} \dot{p} &= -\gamma p - k_L(x - L) - k_2 x - k_4 x^3 + \eta(t), \\ \dot{x} &= \frac{p}{m} \end{aligned} \quad (3-43)$$

now we use equation A-7 from Appendix A

$$dp_t = \left\{ -\gamma p_t - k_2 x_t - k_4 x_t^4 - k_L(x_t - L_t) \right\} dt + dG_t \quad (3-44)$$

$$dx_t = \frac{p_t}{m} dt. \quad (3-45)$$

where  $dG_t$  is the Wiener process defined according to equation A-3

$$dG_t = \int_t^{t+dt} \eta(t') dt'. \quad (3-46)$$

We shall employ the forward Euler method to solve equation 2-2, the time will be discretized in steps of duration  $\delta t = 0.0001$ , the current instant of time will be  $t_n = n\delta t$ . Every cycle will consist of  $N_S$  steps defined as  $N_S = \tau/\delta t$  ( $\tau$  is the protocol period) and we will perform a total of  $N_C = 100000$  of cycles.

The discrete version of equation 3-43 is

$$\begin{aligned} p_{n+1} &= p_n + \delta t \left( -\gamma p_n - k_2 x_n - k_4 x_n^3 - k_L[x_n - L(t_n)] \right) + dG_n \\ x_{n+1} &= x_n + \delta t \left( \frac{p_n}{m} \right), \end{aligned} \quad (3-47)$$

with the Wiener process defined by

$$dG_n = \int_{n\delta t}^{(n+1)\delta t} \eta(t') dt'. \quad (3-48)$$

From the correlation of  $dG_n$

$$\begin{aligned} \langle dG_n dG_m \rangle &= \int_{n\delta t}^{(n+1)\delta t} dt' \int_{m\delta t}^{(m+1)\delta t} dt'' \langle \eta(t') \eta(t'') \rangle \\ &= 2\gamma m T(t_n) \delta t \delta_{n,m}, \end{aligned} \quad (3-49)$$

we can conclude that  $|dG_n| \propto \sqrt{\delta t}$ . Using a stochastic discrete variable with Gaussian distribution that obeys

$$\langle \phi_n \rangle_C = 0 \quad ; \quad \langle \phi_n \phi_m \rangle_C = \delta_{n,m}, \quad (3-50)$$

we define

$$\psi_n = \sqrt{2\gamma m T(t_n)} \phi_n, \quad (3-51)$$

where we have

$$dG_n = \phi_n \sqrt{\delta t}. \quad (3-52)$$

The discrete equations of motion become

$$\begin{aligned} p_{n+1} &= p_n + \delta t \left( -\gamma p_n - k_2 x_n - k_4 x_n^3 - k_L [x_n - L(t_n)] \right) + \sqrt{\delta t} \phi_n \\ x_{n+1} &= x_n + \delta t \left( \frac{p_n}{m} \right), \end{aligned} \quad (3-53)$$

which, as a consequence of  $|dG_n| \propto \sqrt{\delta t}$ , will have precision of  $\sqrt{\delta t}$  [60, 61]. The work output of the  $m$ -cycle is defined as

$$W_m = -k_L \sum_{n=0}^{N_S} (x_n - L_n) \dot{L}(t_n) \delta t \quad (3-54)$$

with the expected work

$$\mathcal{W} = \frac{1}{N_C} \sum_{m=1}^{N_C} W_m. \quad (3-55)$$

The heat output is written as

$$Q_m = \sum_{n=0}^N \left\{ \left( \frac{p_{n+1} + p_n}{2} \right) \psi_n - \gamma p_n^2 \right\} \delta t, \quad (3-56)$$

where we are making explicit use of the Stratonovich definition, which is necessary for  $Q$  to have its physical representation, as demonstrated in Appendix A. Likewise, the expected heat during each phase is

$$Q_H = \frac{1}{N_C} \sum_{m=1}^{N_C/2} Q_m \quad (3-57)$$

$$Q_C = \frac{1}{N_C} \sum_{m=N_C/2}^{N_C} Q_m. \quad (3-58)$$

All cycles are evaluated back to back, meaning that  $(x_{N_S}, p_{N_S})$  of the last cycle will be the initial conditions  $(x_0, p_0)$  of the next cycle. At the start of every program we run a couple of cycles to ensure the information of the initial conditions have been erased.

### 3.5 Numerical Results

In this section we present the results. The validity of the analytical quasi-static approach is confirmed in figure 3.6 where the the work output defined by 3-55 is evaluated by different values of the nonlinearity  $k_4$ . Not only the dot-dashed green line is within statistical error, but it is also in accordance with the results in Chapter 1 that indicate the equilibrium result as a maximal point

only achievable for extremely slow cycles.

Regardless of whether elliptical or step cycles are considered, the work produced per cycle has shown the emergence of a Gaussian distribution defined as

$$p(W) = \frac{1}{\sqrt{2\pi\sigma_W^2}} e^{-\frac{(w-W)^2}{2\sigma_W^2}}, \quad (3-59)$$

where the variance is evaluated as

$$\sigma_W = \sqrt{\frac{1}{N_C} \sum_{m=1}^{N_C} W_m^2 - \mathcal{W}^2}. \quad (3-60)$$

To explain this result, we return to the definition of the work output as 3-55 [53]. The equilibrium approach considers that on a given instant the probability distribution of the position  $x_n$  will obey equation 3-1, the work output is written as

$$W_m \propto \frac{1}{N_S} \sum_{n=1}^{N_S} x_n \dot{L}_n \delta t, \quad (3-61)$$

which, following the central limit theorem, since  $\rho(x) \propto e^{-(k_L/2T)x^2 - (k_4/4T)x^4}$ , will converge to a Gaussian distribution. The results are presented in figure 3.7 [53]. From equation 3-59 we derive the standard fluctuation relation

$$\frac{p(-W)}{p(W)} = \exp \left\{ 2 \frac{\mathcal{W}}{\sigma_W^2} W \right\}, \quad (3-62)$$

shown to be true in figure 3.8 [53]. We also investigated the instantaneous power

$$w \equiv P_W(t_n), \quad (3-63)$$

and we have verified that its probability does not resemble the work Gaussians, which is expected since the instantaneous power is driven more directly by the bath fluctuations. The distributions present a peculiar shape, with a central point of much higher probability as shown in figures 3.9 [53] and 3.10. As it was indicated by both the small and large  $k_4$  approximations, the absorbed heat  $\mathcal{Q}_H$  was found to be roughly similar for both step and elliptical cycles. The values obtained were also much larger than the maximum power, making the efficiency for both cycles inferior to 10%, five times less than the associated Carnot efficiency.

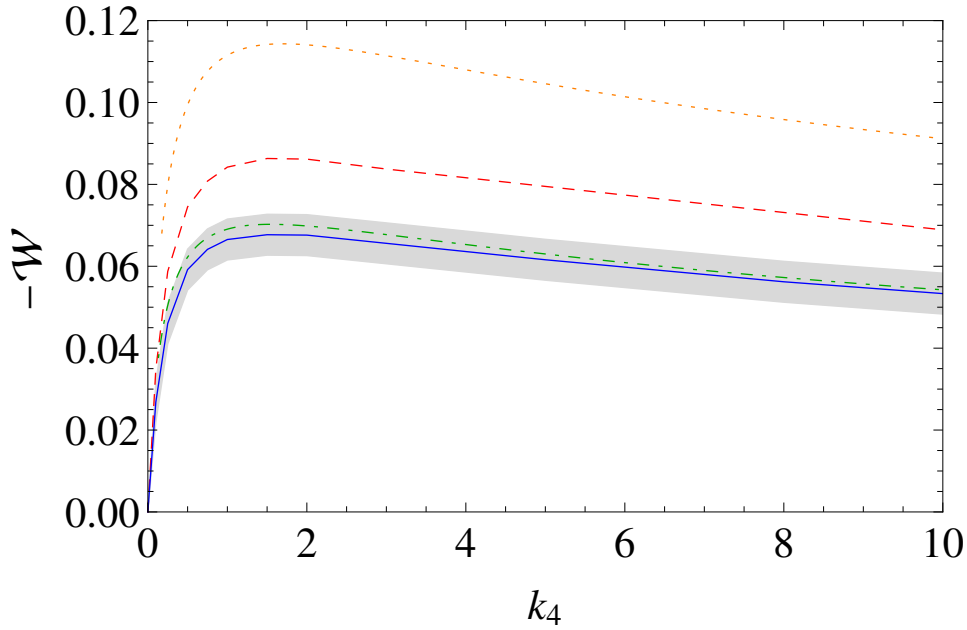


Figure 3.6: Average work performed by the machine  $-\mathcal{W} \times k_4$  with  $m = k_2 = k_L = \gamma = 1$ ,  $L_m = 3/2$ ,  $\Delta L = 1$  and  $\Omega = \pi/100$ . The solid blue line corresponds to the step cycle with  $T_H = 2$  and  $T_C = 1$ , whereas the green dotdashed line depicts the analytical results assuming the local equilibrium approach which yields maximum at  $k_4 = 1.47$ . The red dashed line corresponds to the elliptical cycle equivalent to the first order Fourier series of the step cycle with  $T_m = 1.5$  and  $\Delta T = \pi/2$ . The orange dotted line corresponds to the step cycle for the same maximal and minimal temperatures of the previous cycle,  $T_H = 3/2 + \pi/4$  and  $T_C = 3/2 - \pi/4$ .

### 3.6

#### Final Remarks

Within the quasi-static limit we were able to recover, with significant less algebraic effort, the same stationary results as in Chapter 2 for the case of small nonlinearities. We were also able to investigate the opposite limit where the nonlinearities play the dominant role. However, as figure 3.4 illustrates, the  $k_4$  value that maximizes the work output is out of the range of both approximations.

Making use of numerical analysis we extended the validity of these results outside the quasi-static limit, as figure 3.6 clearly shows, it is possible to make accurate predictions of the dependence of the work output with the nonlinear term  $k_4$  even despite finite time effects.

The efficiency is still quite low, however if we compared with the expected efficiency from Chapter 1, where  $\eta$  was on the order of the perturbative restriction, the 10% represents a monumental step forward, even though we are still five times short of the maximum Carnot efficiency.

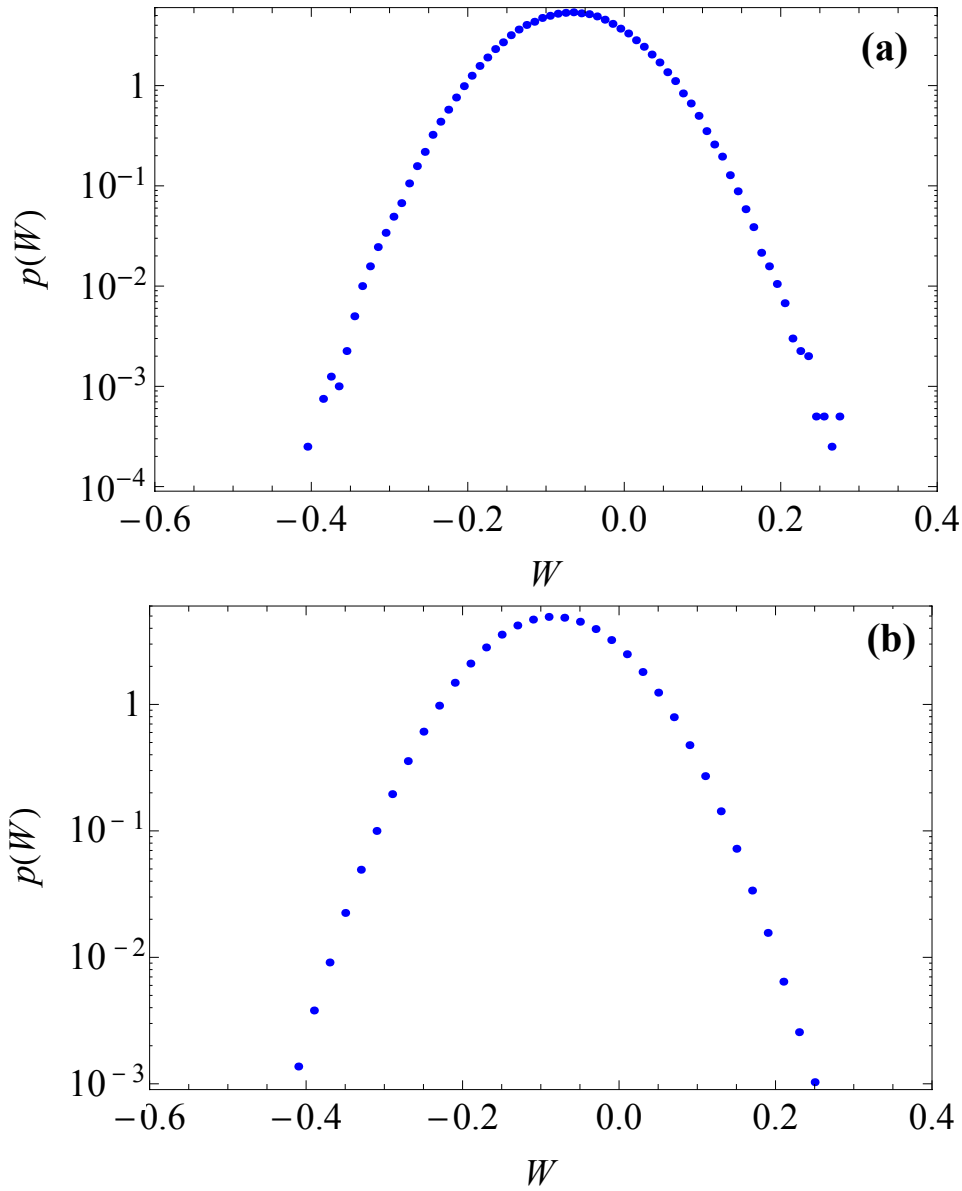


Figure 3.7: Distribution of the work per cycle  $p(W) \times W$  in log-lin scale for the step cycle with  $T_H = 2$  and  $T_C = 1$  on the top (a) and for the elliptical cycle with  $T_m = 3/2$  and  $\Delta T = \pi/2$  on the bottom (b). The parameters used  $m = k_2 = k_L = \gamma = 1$ ,  $L_m = 3/2$ ,  $\Delta L = 1$  and  $\Omega = \pi/100$ .

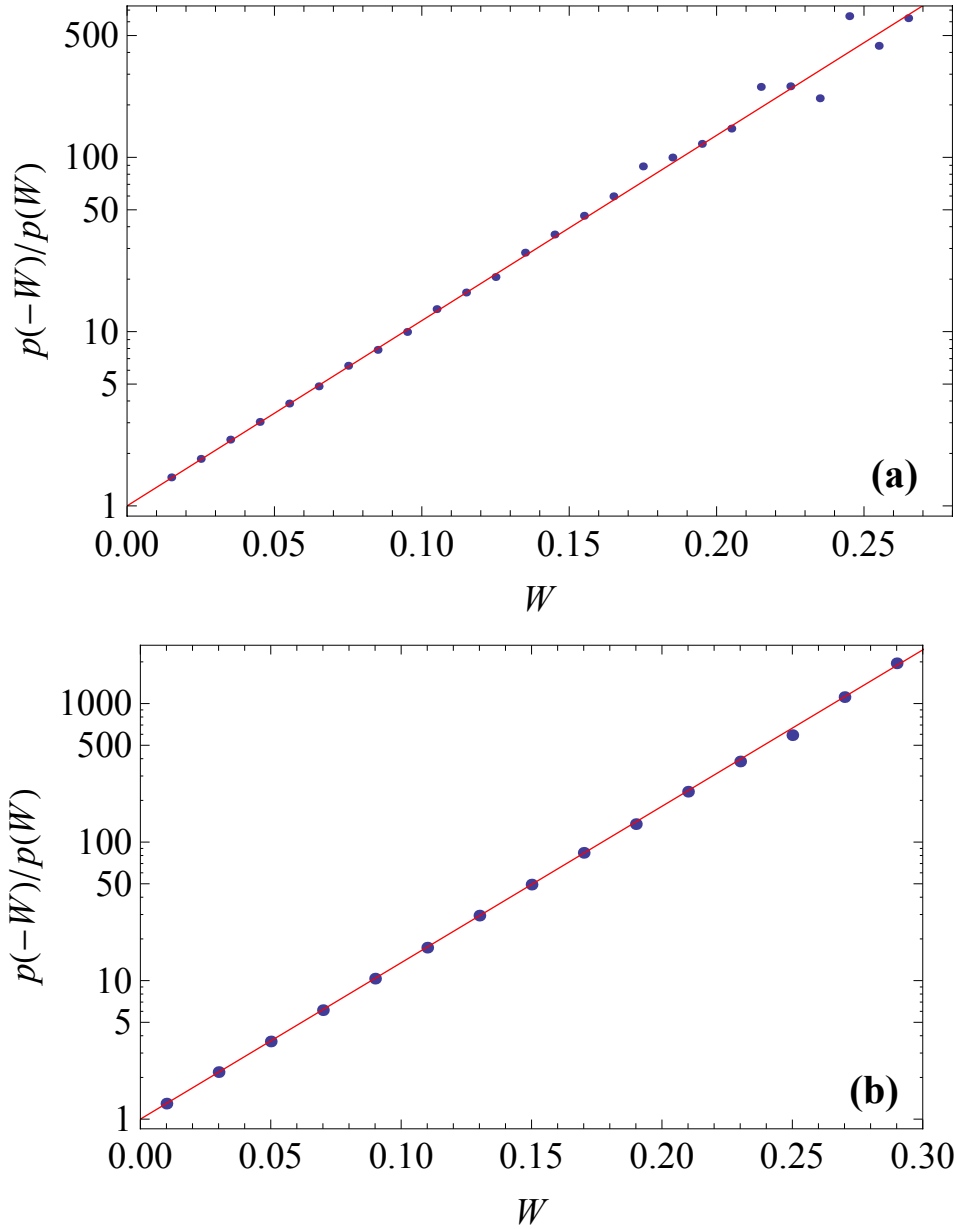
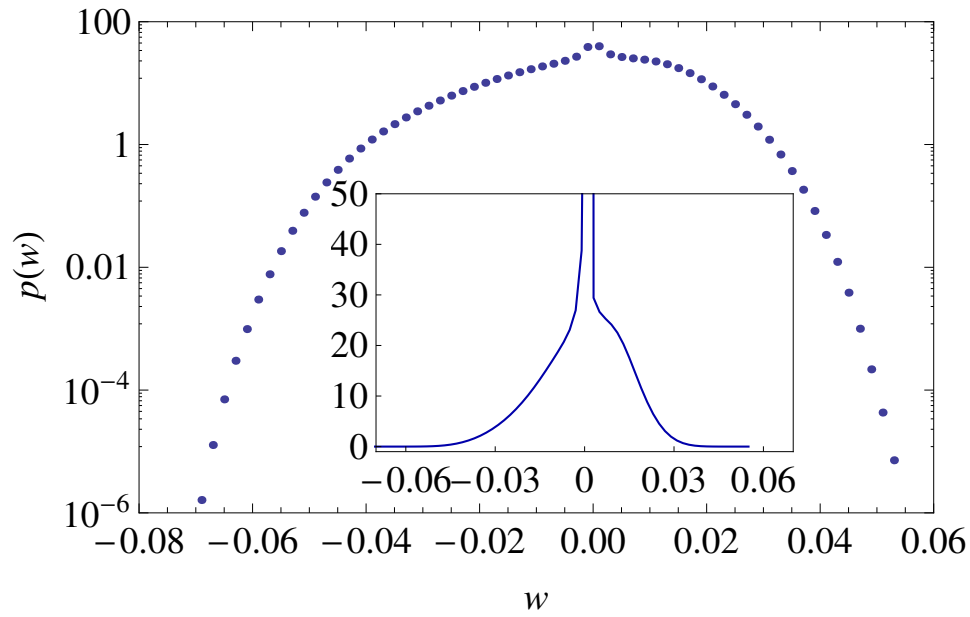
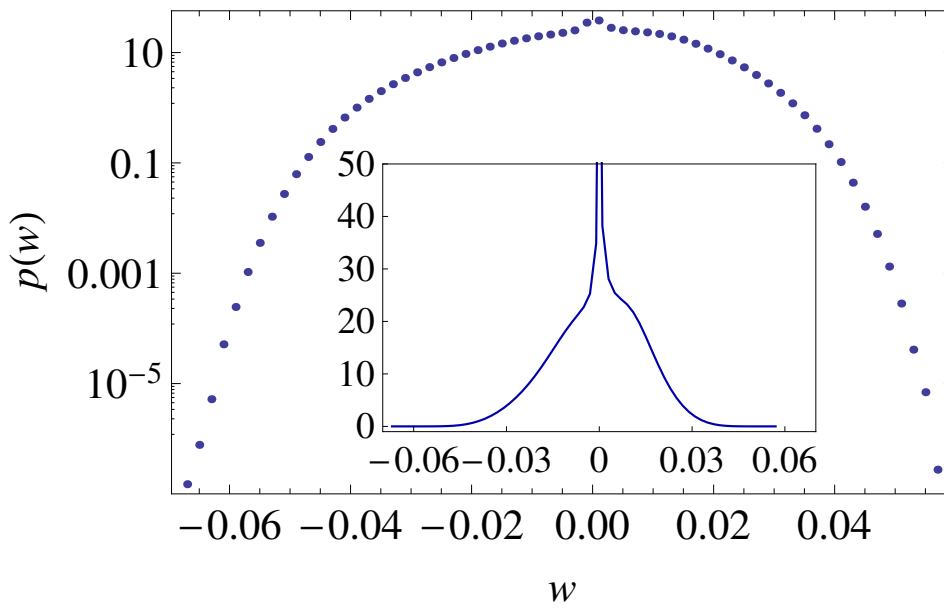


Figure 3.8: Distribution of the work per cycle  $p(-W)/P(W) \times W$  in log-linear scale for the step cycle with  $T_H = 2$  and  $T_C = 1$  on the top and for the elliptical cycle with  $T_m = 3/2$  and  $\Delta T = \pi/2$ . The parameters used  $m = k_2 = k_L = \gamma = 1$ ,  $\Delta L = 1$  and  $\Omega = \pi/100$ .



3.9(a):



3.9(b):

Figure 3.9: On the top (a) the distribution of the instantaneous power  $p(w) \times w$  in log-lin and lin-lin in the inset for the elliptical cycle with  $T_m = 3/2$ ,  $\Delta T = \pi/2$  and  $m = k_2 = k_L = \gamma = 1$ ,  $k_4 = 1.5$ ,  $L_m = 3/2$ ,  $\Delta L = 1$  and  $\Omega = \pi/100$ . On the bottom (b) the step cycle with the same parameters (reminding that  $T_m$  is the average temperature and  $\Delta T$  the temperature gap.)

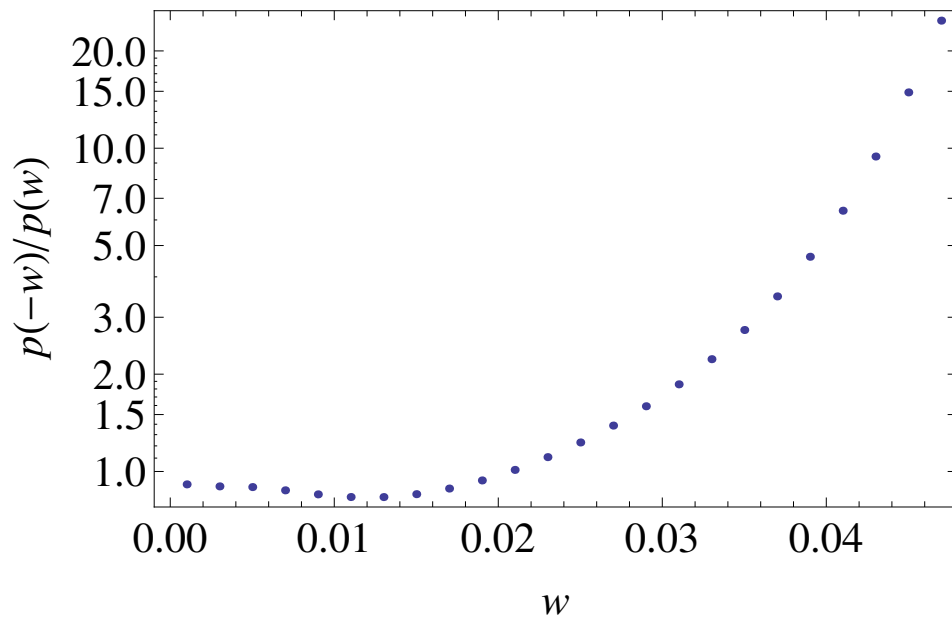


Figure 3.10: The fluctuation relation  $p(-w)/p(w) \times w$  in log-lin scale for the step cycle with parameters  $T_H = 2$ ,  $T_C = 1$ ,  $m = k_2 = k_L = \gamma = 1$ ,  $k_4 = 1.5$ ,  $L_m = 3/2$ ,  $\Delta L = 1$  and  $\Omega = \pi/100$ .

## 4

### Generalized Nonlinear Machines

In the previous chapters we have studied extensively the properties of a machine composed of a single particle under the influence of a nonlinear quartic potential as  $k_4x^4/4$ , which in nature could represent a FPUT- $\alpha$  potential [62]. In a more realistic situation we may be faced with more exotic types of potentials [52, 63]. Motivated by this, we dedicate Chapter 4 to study a more general class of nonlinear potential.

#### 4.1

##### The $\alpha$ -type Potential

As we have stated previously in chapter 2, the nonlinearity is responsible for making the potential asymmetric under deformations. Previously we dedicated our analysis to the role that the nonlinearity played in the work output, however by focusing our attention merely on  $k_4$ , which controls the intensity of the nonlinear potential, we now will focus on the exponent.

We define the  $\alpha$ -type potential as

$$V_\alpha(x) = \frac{k_\alpha}{\alpha} \left| \frac{x}{\sigma} \right|^\alpha \quad (4-1)$$

which is very similar to the potential defined by Rossello et al [52] in the context of energy harvesters, for integer exponents. The  $\alpha$ -type is more general since we shall consider  $\alpha$  to be a real positive number. The force related can be written as

$$F_\alpha(x) = \begin{cases} -\frac{k_\alpha}{\sigma} \left| \frac{x}{\sigma} \right|^{\alpha-1} & \text{for } x > 0 \\ 0 & \text{for } |x| = 0 \\ \frac{k_\alpha}{\sigma} \left| \frac{x}{\sigma} \right|^{\alpha-1} & \text{for } x < 0 \end{cases} , \quad (4-2)$$

and the equivalent Langevin equation of motion

$$m\ddot{x} + m\gamma\dot{x} = -k_L(x - L) + F_\alpha(x) + \eta(t). \quad (4-3)$$

Immediately it becomes clear that the perturbative approach used in Chapter 2 is not very useful when attempting to provide analytical solutions to this

non analytical force. Therefore we shall focus our analysis to numerical results, providing analytical solutions to a few distinct limits of  $\alpha$ : for very large values of  $\alpha$  the potential will behave like a perfect wall, confining the particle in the length  $|x| < x_0$  where

$$x_0 = \lim_{\alpha \rightarrow \infty} \sigma \left( \frac{\alpha T}{k_\alpha} \right)^{\frac{1}{\alpha}} \rightarrow \sigma, \quad (4.4)$$

therefore the confinement does not depend on parameters like  $k_\alpha$  or  $T$ .

## 4.2

### The Role of $\alpha$ in the asymmetry

In section 2.2 of Chapter 2 we demonstrated how the quartic nonlinearity becomes asymmetric when deformed by an external quadratic potential. The asymmetry creates a bias in the motion of the BP causing the expected position  $\langle x \rangle$  to shift from the of minimal potential position  $x_m$ .

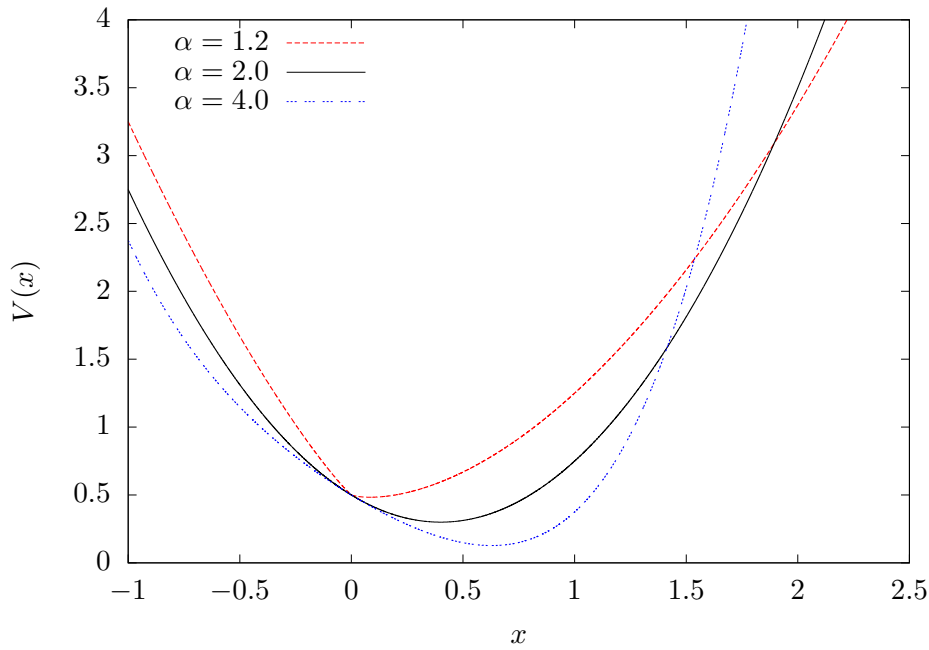
We highlight in figure 4.1, for different values of the exponent below the quadratic (sublinear) the asymmetry become steeper on the left side of  $x_m$  and softer on the right, while values above the threshold (superlinear) have the same behaviour as outlined in section 2.2 of Chapter 2.

The  $\alpha$ -type potential is the internal potential of the BP, centred at the origin pinning the particle to it. The external potential  $V_e(x) = k_L(x - L)^2/2$  is centred at position  $L$ , and it represents our interaction with the BP. We act to effectively pull the particle from the origin using our external potential. In the linear case,  $\alpha = 2$ , the superposition of parabolic potentials is also a parabola.

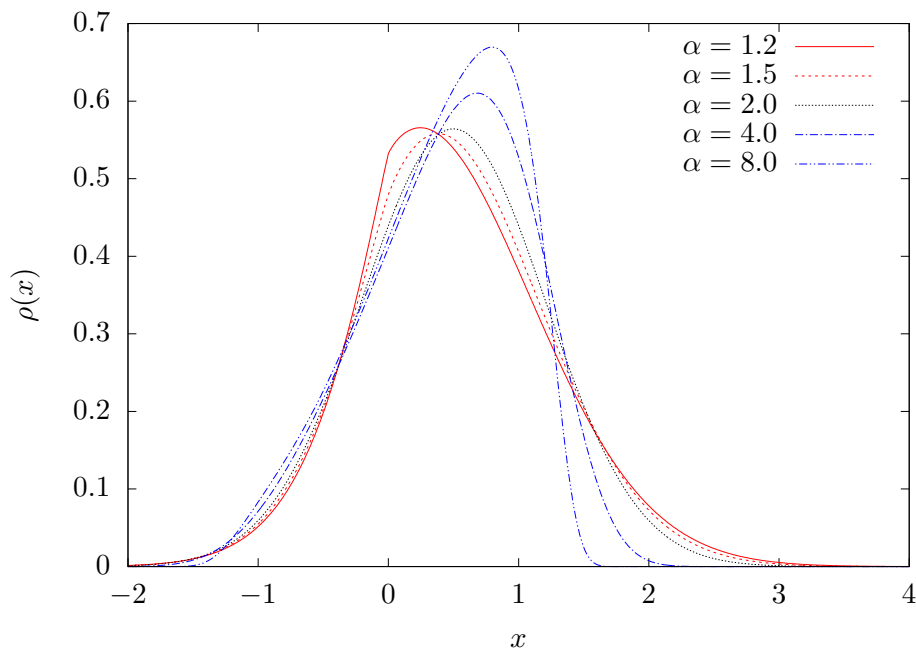
When we consider the superlinear,  $\alpha > 2$  limit, the internal potential now grows more rapidly with distance than our applied external potential, meaning that the more we pull, the more it resists - hence the asymmetry. Introducing fluctuations with the heat bath this asymmetric potential makes it easier for the particle to fluctuate back to the origin rather than further from it.

The sublinear,  $\alpha < 2$ , limit acts exactly the opposite. Now the external potential grows faster with the distance, so when connected to a heat bath the particle will fluctuate more easily in the direction to the left of the minimal potential. Because of that, using the same cycles as Chapters 2 and 3, we expect the machine to behave as a refrigerator, due to its bias inversion.

This effect is demonstrated on the top of figure 4.2, where we plot the difference between the expectation and the minimal potential keeping the temperature and the displacement fixed, and change the value of the exponent from the sublinear to the superlinear limits. For  $\alpha < 2$  we have that  $\langle x \rangle > x_m$ ,



4.1(a):



4.1(b):

Figure 4.1: On the top (a) the potential, on the bottom (b) the probability density for the position  $x$  for different values of the exponent  $\alpha$ . In the linear regime,  $\alpha = 2$ , the density is symmetric, for over linear values of  $\alpha$  we recover the effect displayed in figure 2.8. For sub linear values of  $\alpha$  the bias switches direction and the expected position shifts to the right of the minimal potential.

the particle moves in the direction of the displacement, and for  $\alpha > 2$  we have  $\langle x \rangle < x_m$ , the particle moves away from the displacement, back to the origin.

On the right of figure 4.2 we show how the effect of increasing temperature is different from the sub- and superlinear cases. We plot the expectation of the coordinate  $x$  divided by the minimal potential one  $x_m$ , for  $T = 0$ , where there is no fluctuation, we have clearly that

$$\langle x \rangle_{T \rightarrow 0} = x_m. \quad (4-5)$$

As the temperature increases and the fluctuations become stronger, the bias induced by the potential becomes clear. For superlinear, the new expectation follows the flatter side of the potential, becoming less than  $x_m$ , while for the sublinear case the deformation is stronger and pulls the particle towards  $L$ , causing the expectation to become larger than  $x_m$ .

### 4.3

#### Numerical Approach

Even within the equilibrium approach, the complexity in the definition of the  $\alpha$ -type potential makes it quite difficult to analytically solve the problem, so we will be analysing the system mainly numerically. We start with the equations of motion

$$\dot{p} = -\gamma p + F_\alpha(x) - k_L(x - L) + \eta(t) \quad (4-6)$$

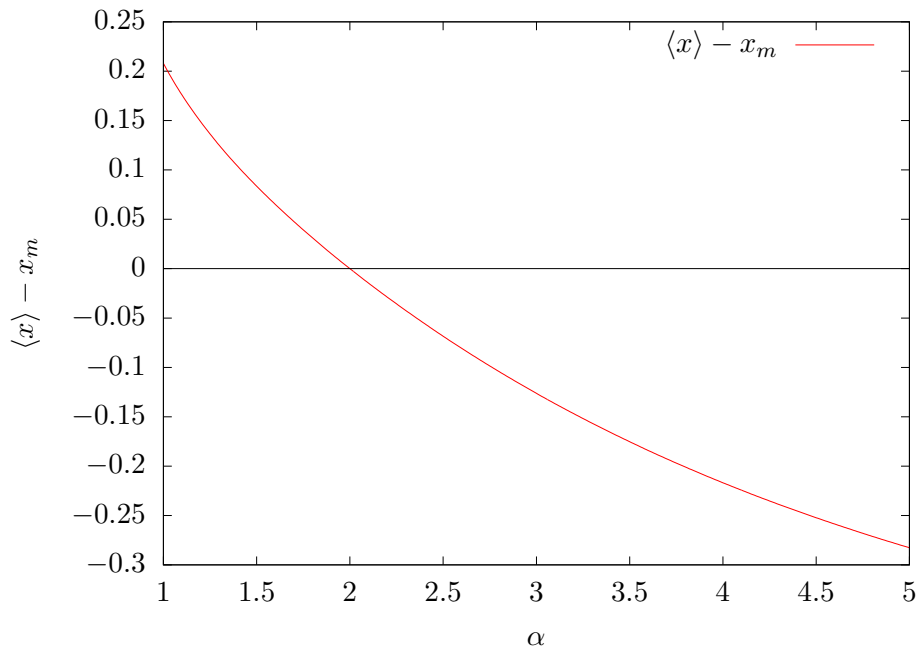
$$\dot{x} = \frac{p}{m}, \quad (4-7)$$

using equation A-7 from Appendix A we write

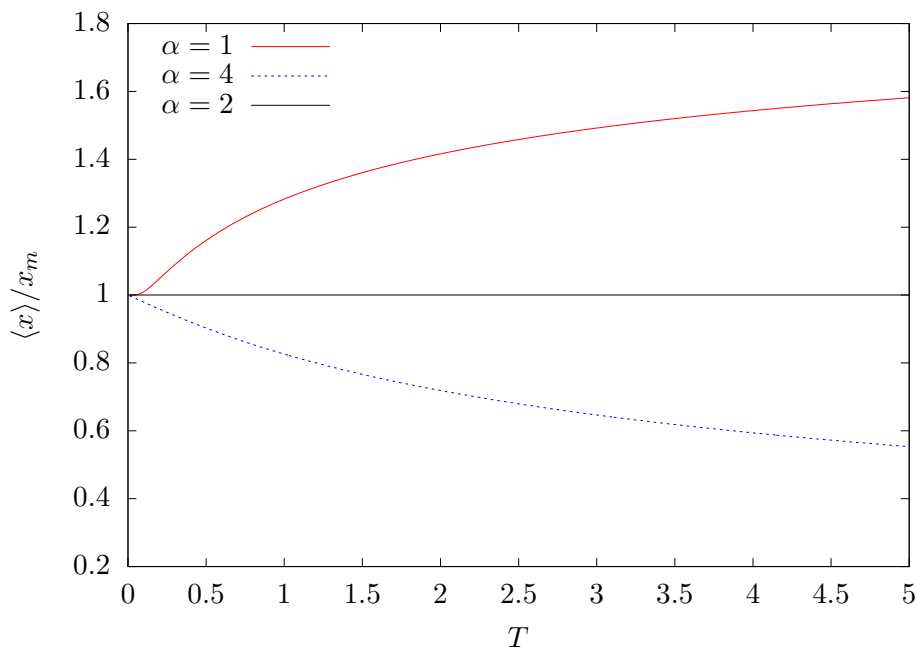
$$\begin{aligned} dp_t &= \{-\gamma p_t + F_\alpha(x_t) - k_L(x_t - L_t)\} dt + dG_t \\ dx_t &= \frac{p_t}{m} dt. \end{aligned} \quad (4-8)$$

Unlike in previous chapter where we employed the forward Euler method, we will now use the Henon method which is a second order Runge-Kutta method for stochastic differential equations. The time will be discretized in steps of duration  $\delta t = 0.0001$ , current instant of time will be  $t_n = n\delta t$ . Every cycle consists of  $N_S$  steps defined as  $N_S = \tau/\delta t$  ( $\tau$  is the protocol period) and we will perform a total of  $N_C = 100000$  cycles.

While the forward Euler method uses only the slope at the current instant



4.2(a):



4.2(b):

Figure 4.2: On the top (a) we plot the difference between the expected position  $\langle x \rangle$  and the minimal potential position  $x_m$  for different values of  $\alpha$ . Note that for  $\alpha < 2$  the difference is positive, hence  $\langle x \rangle > x_m$  and negative for values of  $\alpha > 2$ . On the bottom (b) we plot the effects of temperature on the value of the expected coordinate for different values of  $\alpha$ .

to calculate the step as

$$\kappa_{x1} = \frac{p_n}{m} \quad (4-9)$$

$$\kappa_{p1} = -\gamma p_n - F_\alpha(x_n) - k_L(x_n - L_n) = h(x_n, p_n, L_n), \quad (4-10)$$

the Henon method takes a "super" slope as an average of the current slopes  $(\kappa_{x1}, \kappa_{p1})$  with a step forward slope

$$\kappa_{x2} = \frac{p_n}{m} + \delta t \kappa_{p1} \quad (4-11)$$

$$\kappa_{p2} = h(x_n + \delta t \kappa_{x1}, p_n + \delta t \kappa_{p1} + \delta t \psi_n, L_{n+1}) \quad (4-12)$$

to increase the accuracy of the answer from  $\sqrt{\delta t}$  to  $\delta t$

$$x_{n+1} = x_n + \delta t \left( \frac{\kappa_{x1} + \kappa_{x2}}{2} \right) \quad (4-13)$$

$$p_{n+1} = p_n + \delta t \left( \frac{\kappa_{p1} + \kappa_{p2}}{2} \right) + \delta t \psi_n. \quad (4-14)$$

Here we use the same definition of  $\psi_n$  as in equation 3-51.

In the previous chapter we analysed the instantaneous distribution of the work rate defined in equation 3-63, the results, however, consisted of an awkward shape [53]. Instead of evaluating the instantaneous work rate at any time, now we will calculate several ensemble averages defined as

$$\langle x(t) \rangle = \int dx dp \rho(x, p) x, \quad (4-15)$$

$$\langle P_W(t) \rangle = \int dx dp \rho(x, p) \{-k_L(x - L)\}, \quad (4-16)$$

$$\langle \mathcal{H}(t) \rangle = \int dx dp \rho(x, p) \mathcal{H}(x, p). \quad (4-17)$$

where  $\rho(x, p)$  is the equilibrium probability distribution for the  $\alpha$ -type model. In our discretized version we will interpret the ensemble average as an instantaneous average over several cycles

$$\langle x(t) \rangle = \frac{1}{N_C} \sum_{m=1}^{N_C} x(t + m\tau), \quad (4-18)$$

$$\langle P_W(t) \rangle = \frac{1}{N_C} \sum_{m=1}^{N_C} P_W(t + m\tau), \quad (4-19)$$

$$\langle \mathcal{H}(t) \rangle = \frac{1}{N_C} \sum_{m=1}^{N_C} \mathcal{H}(t + m\tau). \quad (4-20)$$

We will also evaluate the work produced during the  $m$ -th cycle

$$W_m = -k_L \sum_{n=0}^{N_S} (x_n - L_n) \dot{L}(t_n) \delta t \quad (4-21)$$

and the expected work

$$\mathcal{W} = \frac{1}{N_C} \sum_{m=1}^{N_C} W_m. \quad (4-22)$$

In the following we will use the step cycle, with the displacement defined as

$$L(t) = L_m + \frac{\Delta L}{2} \cos(\Omega t), \quad (4-23)$$

and the temperature

$$T^{\text{step}}(t) = \begin{cases} T_H & \text{if } n\tau < t < (n+1/2)\tau \\ T_C & \text{if } (n+1/2)\tau < t < (n+1)\tau \end{cases} \quad (4-24)$$

and will evaluate for different values of the exponent  $\alpha$ .

#### 4.4 Numerical Results

Using the ensemble averages, we further validate the predictions of the equilibrium approach. In figure 4.3, it becomes quite clear how the equilibrium averages correctly predict the position behaviour and by increasing the number of cycles we can increase its precision.

The results for the ensemble averages of the expected position, expected internal energy, and instantaneous power are presented in figures 4.4 to 4.7. Our predictions obtained using equilibrium theory agree quite well with numerical results, the only problem is, of course, on the instants immediately after the sudden temperature jumps of the step cycle.

Within the quasi-static regime, the system is considered to be at thermal equilibrium with the heat bath at all times, however in a realistic scenario, the BP will require some time to thermalize, in section 2.1.3 of Chapter 2 we evaluated that the necessary time is on the magnitude of  $1/\gamma$ . Since the time required to thermalize is so small when compared to the overall time cycle that the approach is still accurate ( $1/\gamma \approx 1 \ll \tau = 100$ ). We also illustrate the work production by plotting side by side a comparison between the instantaneous power of the hot phase (in dotted red) and the cold phase (in solid blue) on the lower right side in figures 4.4 to 4.7. As the value of  $\alpha$  approaches 2, the values become closer and closer, meaning all the work gained

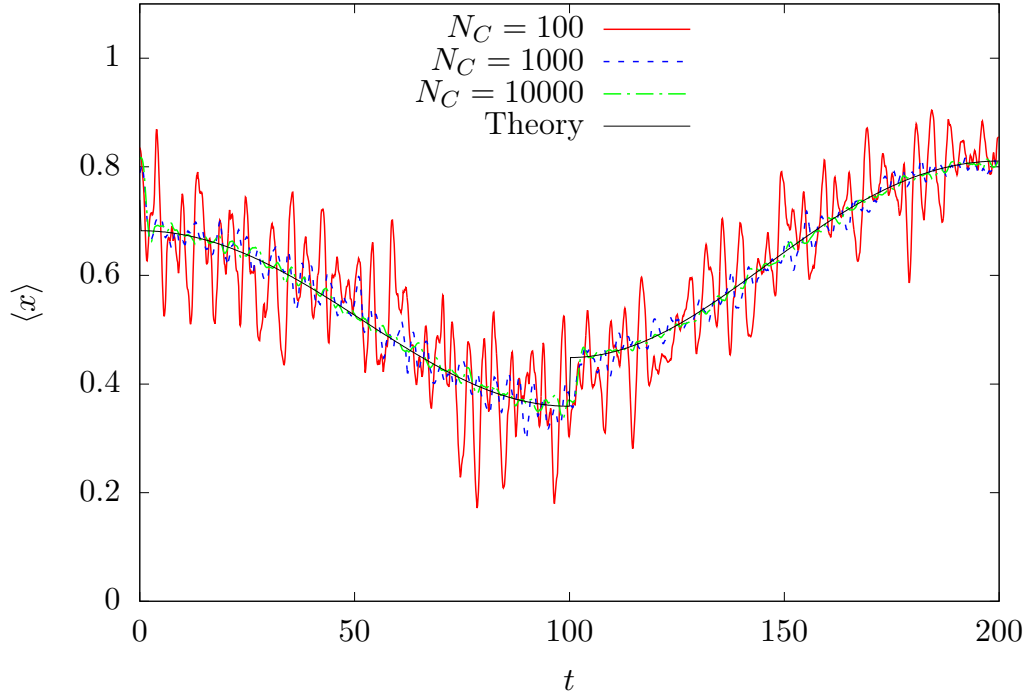


Figure 4.3: The ensemble average of the position for different numbers of cycles  $N_C$ , the cycle used was the step cycle. For  $N_C = 10000$  the ensemble average is already quite close to the equilibrium expectation. The values are  $k_\alpha = k_L = m = \gamma = \Delta L1$ ,  $L_m = 1.5$ ,  $T_H = 2$ ,  $T_C = 1$

is also lost, until it crosses the linear threshold and changes sign, confirming that indeed, for  $\alpha < 2$  the machine behaves like a refrigerator.

Our results regarding the work produced per cycle show the emergence of a Gaussian distribution for  $W$ , demonstrating that the result in Chapter 3 does not depend on the  $\alpha$ . The work distribution can be written as

$$p(W) = \frac{1}{\sqrt{2\pi\sigma_W^2}} e^{-\frac{(w-\mathcal{W})^2}{2\sigma_W^2}}, \quad (4-25)$$

which we present in figure 4.8. We also conclude that the distributions must obey the standard fluctuation relation

$$\frac{p(-W)}{p(W)} = \exp\left\{2\frac{\mathcal{W}}{\sigma_W^2}W\right\}. \quad (4-26)$$

This result is displayed in figure 4.9, where we point out that the values of  $\mathcal{W}$  and  $\sigma_W$  were obtained from the simulations. The work output follows the equilibrium distribution quite closely as shown in figure 4.10 for the step cycle. We also present the results for the elliptical cycle, which displayed better

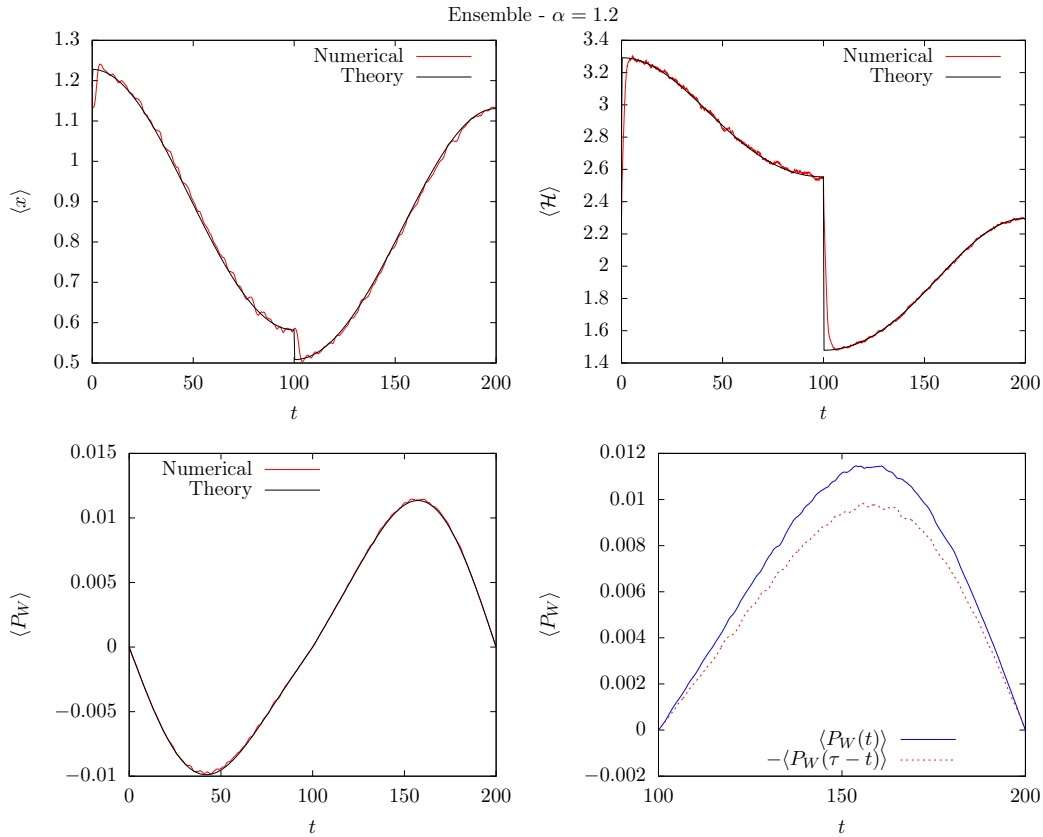


Figure 4.4: The ensemble average of the expected position on the top left, internal energy on the top right, instantaneous power below left and a comparison between of the instantaneous power during the hot phase in red and cold phase in dotted blue. The values used are  $k_\alpha = k_L = m = \gamma = \Delta L = 1$ ,  $L_m = 1.5$ ,  $T_H = 2$ ,  $T_C = 1$  for the exponent  $\alpha = 1.2$ .

conversion to the expectation than the step cycle. The heat absorbed remain close to the temperature gap  $\Delta T = 1$ , making the best efficiency close to 15%.

#### 4.5 Adiabaticity versus isentropy

During an adiabatic process, the system and the heat bath do not exchange heat. In a macroscopic system it is possible to perform such process simply by removing contact between the heat source and the system using some sort of thermal isolation. The microscopic equivalent of that scenario would be to take the Langevin equation

$$m\ddot{x} + V'(x) = -k_L(x - L) + \eta(t) - m\gamma v \quad \longrightarrow \quad m\ddot{x} + V'(x) = -k_L(x - L) + \eta(t) - m\gamma v \quad (4.27)$$

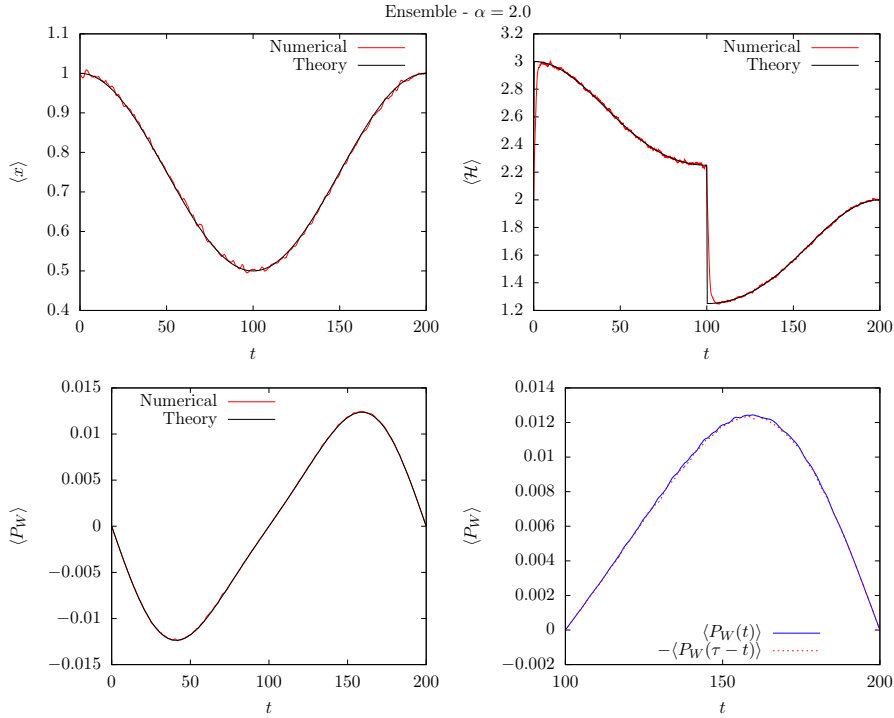


Figure 4.5: The ensemble average of the expected position on the top left, internal energy on the top right, instantaneous power bellow left and a comparisson between of the instantaneous power during the hot phase in red and cold phase in dotted blue. The values used are  $k_\alpha = k_L = m = \gamma = \Delta L = 1$ ,  $L_m = 1.5$ ,  $T_H = 2$ ,  $T_C = 1$  for the exponent  $\alpha = 2.0$ .

When considering a microscopic system, however in an experimental situation the system is often immersed on a viscous fluid which represents the heat bath and cannot be easily separated [14, 16, 64]. Alternatively, from the definition of an adiabatic process, one could also impose that

$$\left\langle \frac{dQ}{dt} \right\rangle = \langle \eta(t)v(t) - m\gamma v^2(t) \rangle = 0, \quad (4-28)$$

but even on a linear case this approach requires the solution of a nontrivial integral differential equation.

The most common and by far the simplest alternative is to impose an *isentropic* condition: take the definition of entropy for the equivalent probability distribution [6, 64, 65]

$$S = - \int dx dp \rho(x, p) \ln \rho(x, p), \quad (4-29)$$

and impose that the entropy remains constant throughout the process

$$dS = \frac{\partial S}{\partial L} dL + \frac{\partial S}{\partial T} dT = 0. \quad (4-30)$$

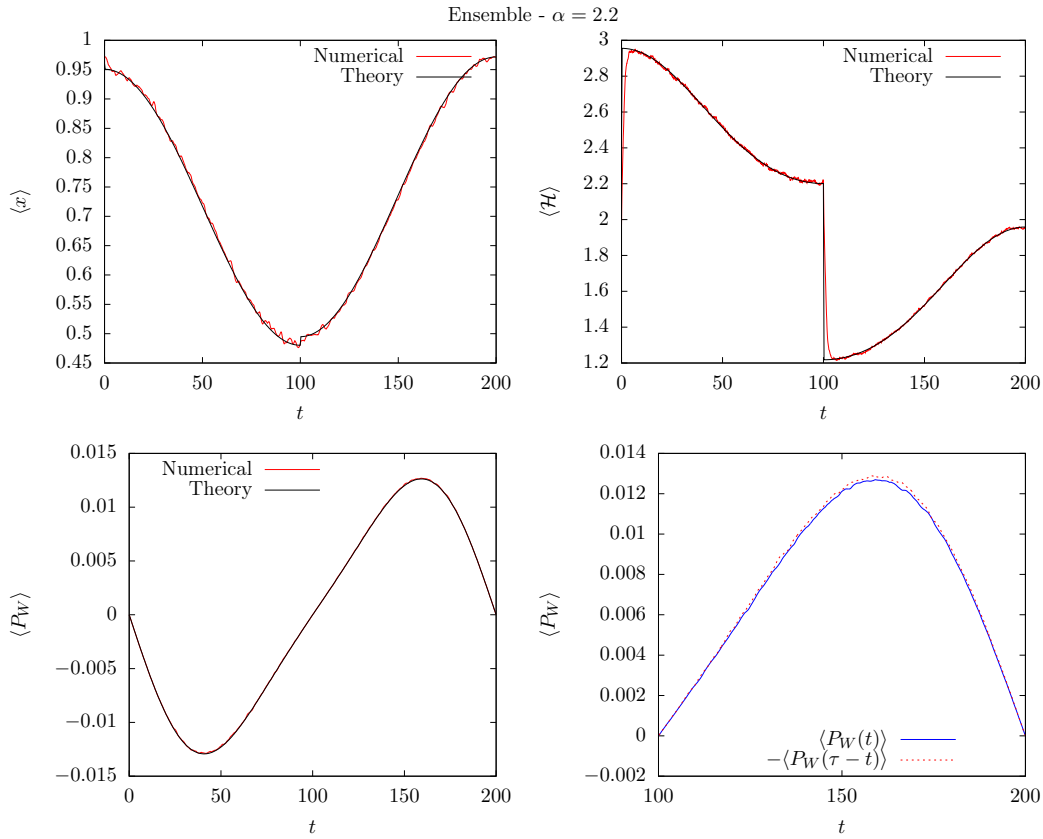


Figure 4.6: The ensemble average of the expected position on the top left, internal energy on the top right, instantaneous power below left and a comparison between of the instantaneous power during the hot phase in red and cold phase in dotted blue. The values used are  $k_\alpha = k_L = m = \gamma = \Delta L = 1$ ,  $L_m = 1.5$ ,  $T_H = 2$ ,  $T_C = 1$  for the exponent  $\alpha = 2.2$ .

While in classical statistical mechanics there is no difference between isentropy and adiabaticity,

$$dQ = TdS, \quad (4-31)$$

however in a realistic scenario the definition of adiabaticity becomes wider. For instance, a process could be done so quickly that there is no time for the system exchange heat with the reservoir, such process would be adiabatical but not isentropic. Since our cycle periods are bounded by a quasi-static restriction, the approach by isentropies much better suited.

The isentropic trajectories are used in the following way: we are interested in going from a point in the phase space of  $L$  and  $T$ , which we can label  $(L_0, T_0)$  to another point very close  $(L_0 + dL, T_0 + dT)$ , where both points have the

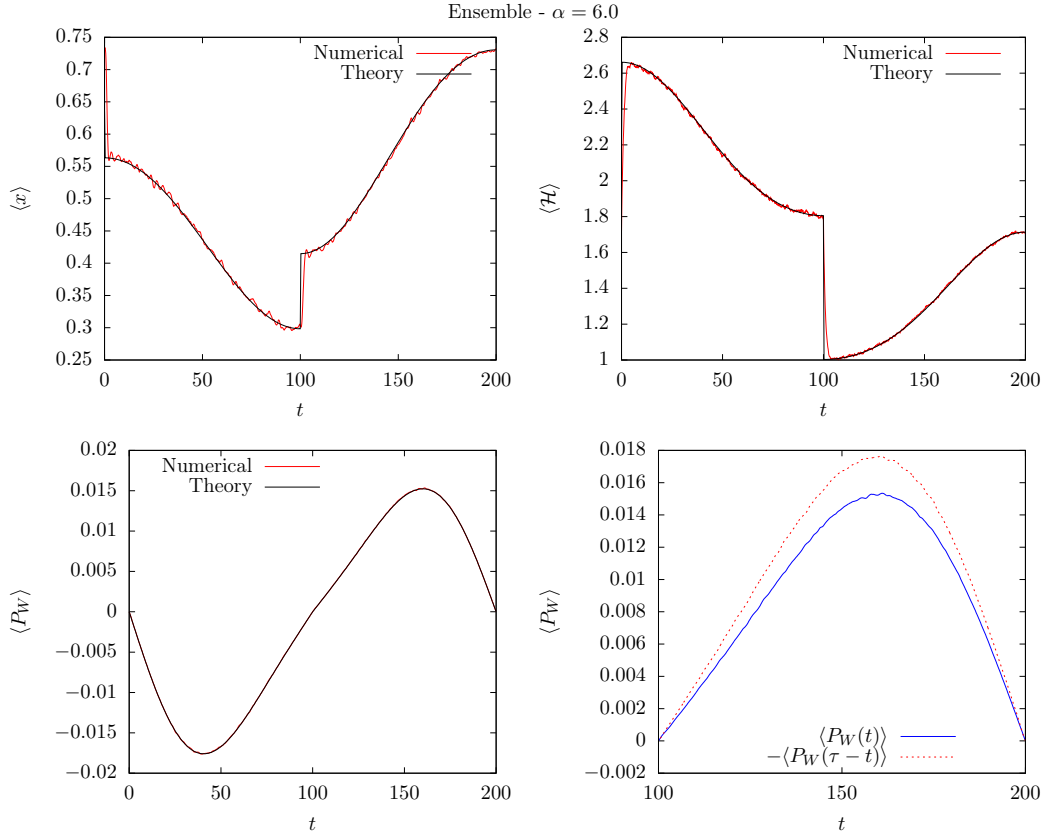


Figure 4.7: The ensemble average of the expected position on the top left, internal energy on the top right, instantaneous power bellow left and a comparisson between the instantaneous power during the hot phase in red and cold phase in dotted blue, the area between curves is the work output. The values used are  $k_\alpha = k_L = m = \gamma = \Delta L1$ ,  $L_m = 1.5$ ,  $T_H = 2$ ,  $T_C = 1$  for the exponent  $\alpha = 6.0$ .

same entropy

$$S(L_0, T_0) = S(L_0 + dL, S_0 + dT), \quad (4-32)$$

so we must obtain, for a given displacement  $dL$  what must be the equivalent displacement  $dT$  for the entropy to remain constant. We have dedicated Appendix D to the derivation of this restriction, the final result is

$$dT = \frac{dL}{T} \frac{\left\langle \frac{\partial \mathcal{H}}{\partial L} \right\rangle - \frac{\partial \langle \mathcal{H} \rangle}{\partial L}}{\frac{\partial \langle \mathcal{H} \rangle}{\partial T}} \Bigg|_{L_0, T_0} = T \frac{\left\langle \mathcal{H} \frac{\partial \mathcal{H}}{\partial L} \right\rangle_C}{\langle \mathcal{H}^2 \rangle_C} \Bigg|_{L_0, T_0} dL, \quad (4-33)$$

the denominator is quite straightforward, it is the definition of heat capacity. In the numerator we have an intuitive result, the first term  $\frac{\partial \langle \mathcal{H} \rangle}{\partial L}$  how much the internal energy changed from the displacement  $dL$ , while the term  $\left\langle \frac{\partial \mathcal{H}}{\partial L} \right\rangle$  represents how much of that energy was in work form, the difference between

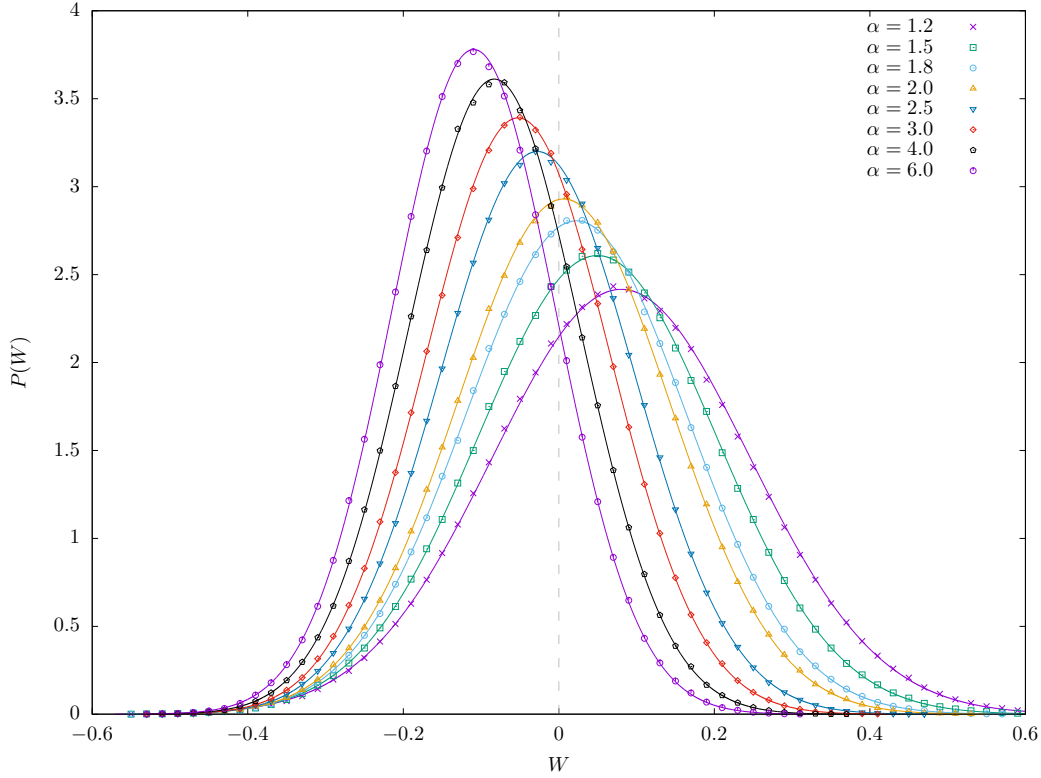


Figure 4.8: Distribution of the work per cycle  $p(W) \times W$  for different values of  $\alpha$  using the step cycle operating between  $T_H = 2$  and  $T_C = 1$ . The cycle period is  $\tau = 200$  or  $\Omega = \pi/100$  and  $m = k_\alpha = k_L = \gamma = \sigma = 1$ . The solid lines are defined by equation 4-25 using the respective  $\mathcal{W}$  and  $\sigma_W$  for each  $\alpha$ . We highlight how the average work shifts from positive for  $\alpha < 2$  to negative  $\alpha > 2$  and exactly in  $\alpha = 2$  the average work is zero.

both terms yields as result how much entropy this exchange generated.

#### 4.6 $\alpha$ -type Isentropy

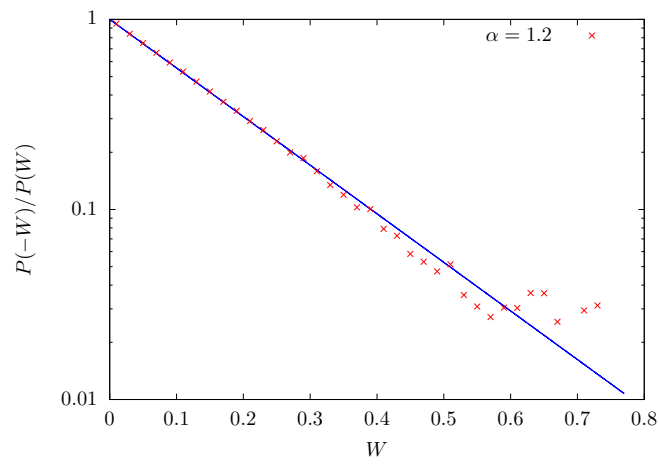
For an ideal gas, the adiabatic process obeys the restriction

$$pV^\Gamma = \text{constant}, \quad (4-34)$$

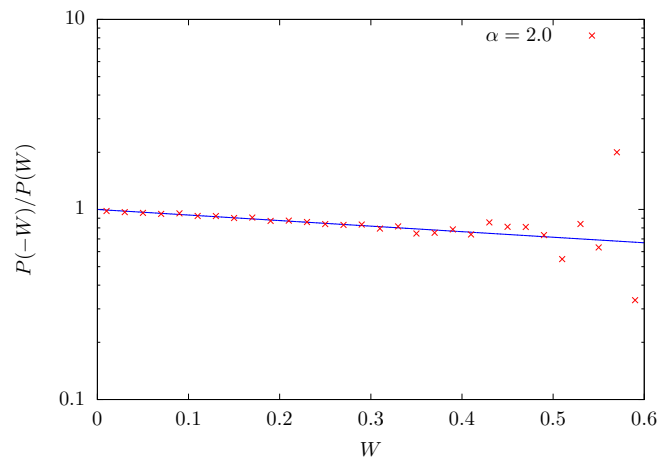
$$TV^{\Gamma-1} = \text{constant}, \quad (4-35)$$

which will be connected to the BP properties (namely its degrees of freedom) by means of  $\Gamma$ , which is the ration between the heat capacity at constant pressure and at constant volume

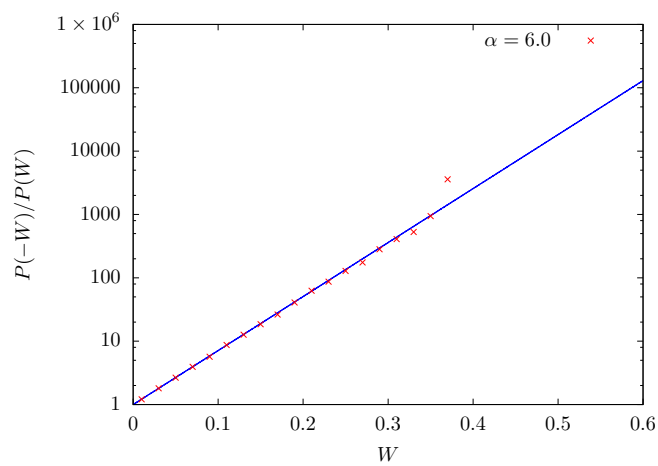
$$\Gamma = \frac{C_p}{C_v}. \quad (4-36)$$



4.9(a):



4.9(b):



4.9(c):

Figure 4.9: The fluctuation relations  $p(-W)/p(W) \times W$  presented in the log-linear scale for the different values of  $\alpha$  presented in figure 4.8. The solid blue lines were obtained using equation 4-25 with the respective values of  $\mathcal{W}$  and  $\sigma_W$ .

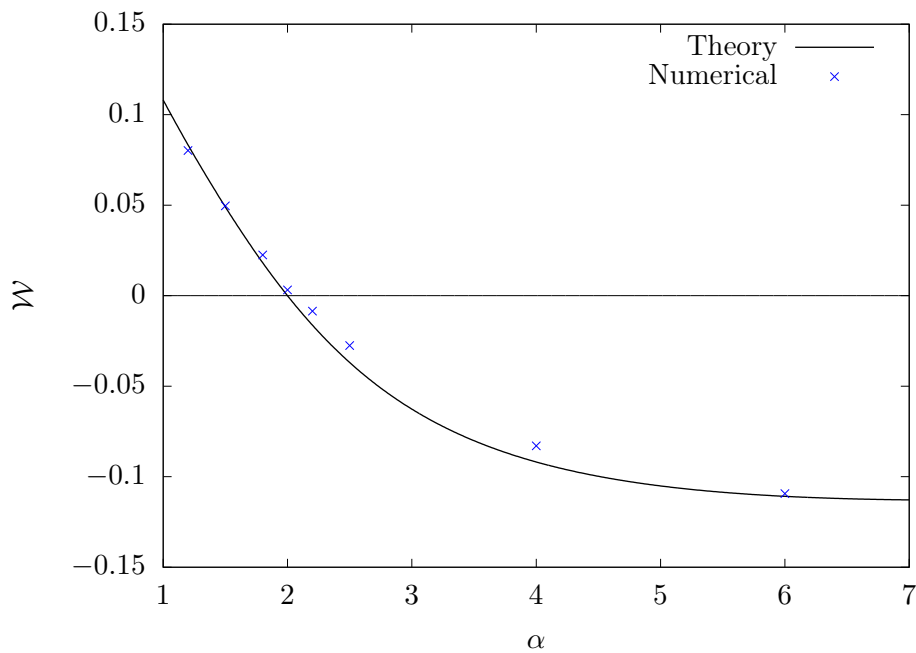


Figure 4.10: Average work performed by the machine on a  $\mathcal{W} \times \alpha$  plot with  $m = 1 = \gamma = k_L = k_\alpha$ . The cycle used was the step cycle with  $L_m = 3/2$ ,  $\Delta L = 1$ ,  $T_C = 1$  and  $T_H = 2$ .

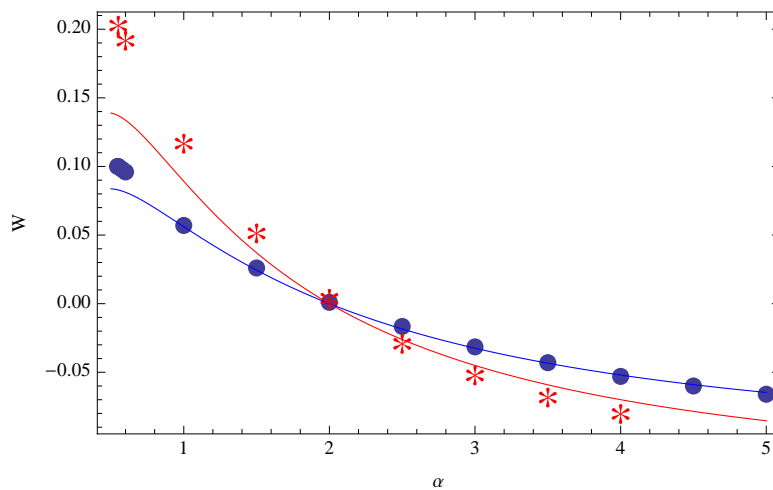


Figure 4.11: Average work performed by the machine on a  $\mathcal{W} \times \alpha$  plot with  $m = \gamma = k_L = k_\alpha = \sigma = 1$ . The cycle used was the elliptical cycle with  $L_m = 3/2$ ,  $\Delta L = 1$ ,  $T_C = 1$  and  $T_H = 2$ . The internal potential of the particle represented in the blue line also contains a quadratic pinning  $V_i(x) = k_\alpha|x/\sigma|^\alpha/\alpha + k_2(x - L)^2/2$ , where  $k_2 = 1$ . The pinning does not affect the qualitative behaviour, only decreases the overall work output. By increasing the cycle period to  $\tau = 1000$ , we observe that the points more disconnected to the curve get closer.

The value of  $\gamma$  is constant as both heat capacities are constant for the ideal gas as a consequence of the quadratic Hamiltonian. Our BP is governed by an  $\alpha$ -type potential will not be constant, and will in fact depend on the nonlinearities.

Let us evaluate the isentropic trajectories for a BP subjected to a quadratic potential. As we stated in Chapter 2, a linear system cannot be used as a machine, but it is possible to evaluate its isentropic process exactly. Starting from the Hamiltonian

$$H(x, p) = \frac{p^2}{2m} + \frac{k_2}{2}x^2 + \frac{k_L}{2}(x - L)^2, \quad (4-37)$$

the force is defined as

$$\frac{\partial H}{\partial L} = -k_L(x - L), \quad (4-38)$$

evaluating

$$\begin{aligned} \left\langle H \frac{\partial H}{\partial L} \right\rangle &= \frac{k_2 k_L L T}{k_2 + k_L} + \frac{k_2^2 k_L^2 L^3}{2(k_2 + k_L)^2} \\ \left\langle \frac{\partial H}{\partial L} \right\rangle &= \frac{k_2 k_L}{k_2 + k_L} L \\ \langle H \rangle &= \frac{k_2 k_L L^2}{2(k_2 + k_L)} L^2 + T \\ \langle H^2 \rangle &= \frac{k_2^2 k_L^2 L^4}{4(k_2 + k_L)^2} L^4 + \frac{k_2 k_L}{k_2 + k_L} L^2 T + 2T^2, \end{aligned}$$

leads to the result that

$$\left\langle H \frac{\partial H}{\partial L} \right\rangle - \langle H \rangle \left\langle \frac{\partial H}{\partial L} \right\rangle = 0. \quad (4-39)$$

Therefore, only if we maintain the temperature constant will the process be isentropic, there is no coupling between the temperature and the displacement in the definition of entropy. Further examples and a more detailed derivation can be found in Appendix D.

For the more general case of the  $\alpha$ -type potential, it becomes quite difficult to obtain analytical expressions for the isentropic processes. For that reason, we will be using mostly numerical calculations of equation 4-33 to obtain the isentropic trajectories.

The external potential applied to the particle is centred at the position  $L$  while the internal potential, in this case the  $\alpha$ -type is centred at the origin. The position of minimal potential represents the point where the external force,

pulling the particle to  $L$  and the internal force, pulling the particle to the origin  $x = 0$  become constant.

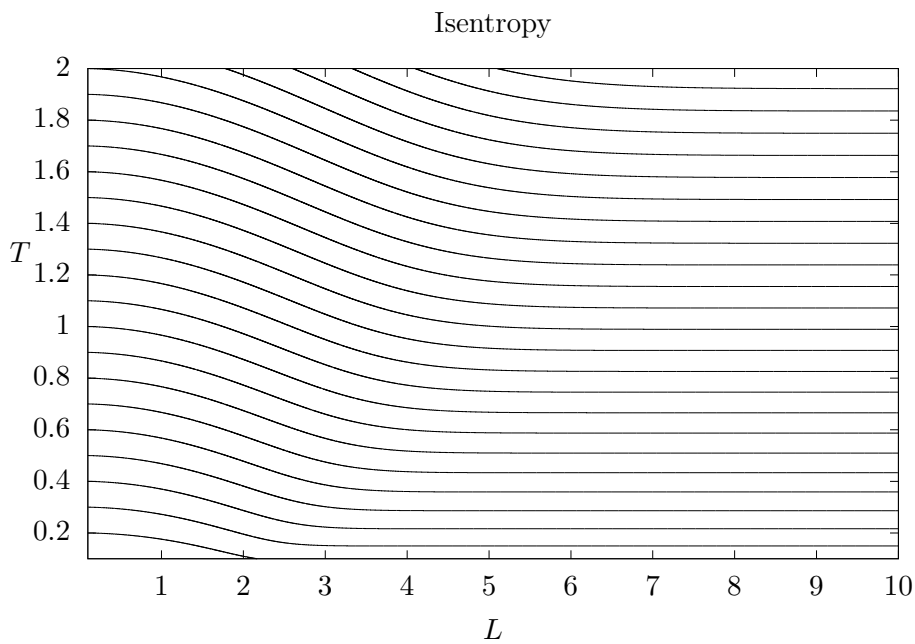
In the sublinear limit,  $\alpha < 2$ , the exponent of the external potential is larger than the internal leading to a stronger interaction. Starting with  $L = 0$  the potential is clearly symmetric, early displacements cause great asymmetry in the direction of  $L$ , thus reducing the internal temperature of the BP. When the displacement  $L$  becomes large enough, the BP effectively “steals” the particle from its internal potential. There is only a small range of values where both internal and external potentials are coupled in the probability function of the BP, as we increase the value of  $L$ , the external potential dominates the internal, reducing the problem to a linear machine. As a consequence, as we show in figure 4.12, the isentropic processes converge on the isotherms for large values of  $L$ .

The superlinear behaviour is different, because the internal exponent  $\alpha$  is larger than the external potential, the displacement  $L$  and temperature  $T$  never decouple. We highlight this effect in figure 4.13, where we show a set of isentropic processes for  $\alpha = 8$ , with an isolated longer process. Unlike the sublinear model, here the internal potential becomes steeper, pulling the particle closer to the origin, so that as we increase the value of  $L$ , so does the internal temperature.

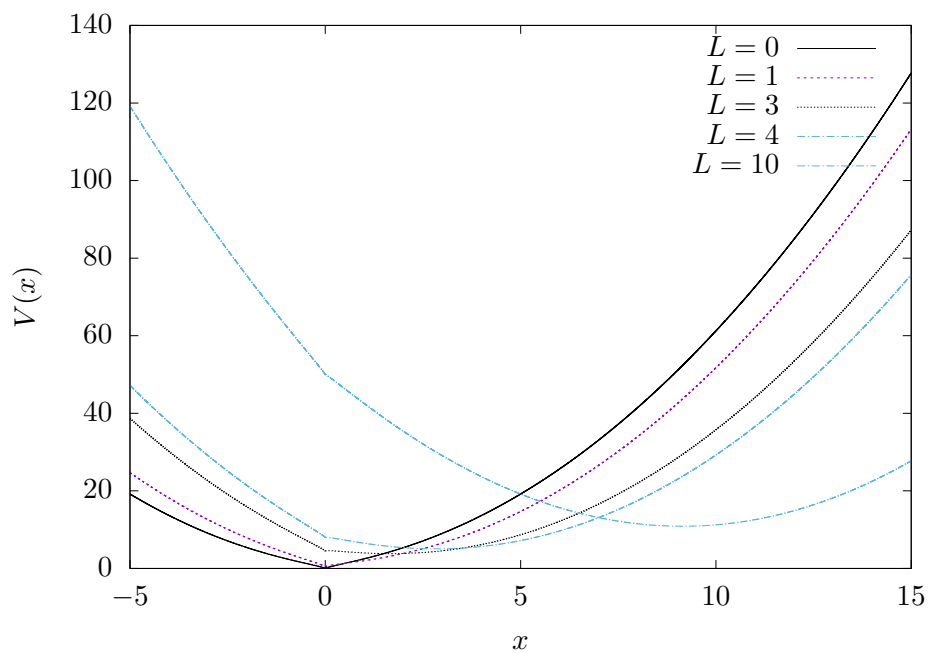
To demonstrate that the isentropic trajectories obtained can be used effectively as adiabatic processes we performed a series of numerical simulations for  $\alpha = 5$ . In a realistic situation it is very difficult to disconnect the particle from the heat bath, however for the numerical simulations it is quite simple to recreate this effect. At the end of each isotherm we simply disconnect the particle from bath as

$$m\ddot{x} + V'(x) = -k_L(x - L) + \eta(t) - m\gamma v \longrightarrow m\ddot{x} + V'(x) = -k_L(x - L) \quad (4.14)$$

The results of these simulations are displayed in 4.14, where we compare the internal temperature of the BP and compare it with the equivalent bath temperature obtained through the isentropic condition. The efficiency obtained was 38%, much closer to the 50% expected in the Carnot limit. For machines with exponents in the sublinear limit ( $\alpha < 2$ ), the temperature gap available for such cases is very small and we could only produce a very limited Carnot cycle configuration.

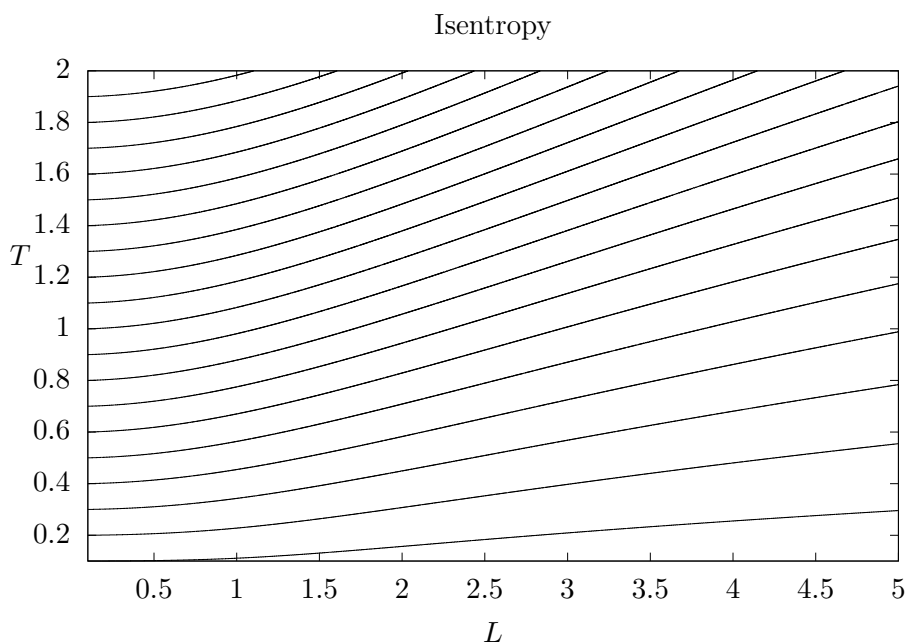


4.12(a):

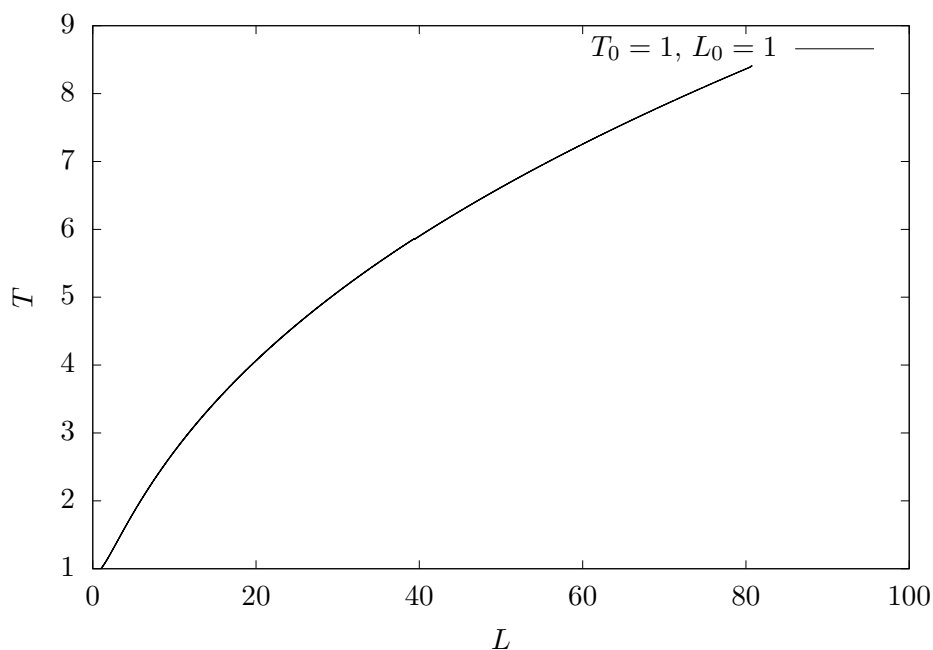


4.12(b):

Figure 4.12: A large set of isentropic processes with sublinear potentials ( $\alpha = 0.75$ ) on the top (a). There is a very brief range of values of displacements where the potential will be asymmetric. Starting with  $L = 0$  the potential is clearly symmetric, early displacements cause great asymmetry but as the displacements increase, the external potential  $V_e$  becomes dominant over the sublinear internal potential effectively decoupling  $L$  and  $S$ . Bottom figure (b) represents the this decoupling effect. The parameters used were  $m = k_L = 1$  and  $k_\alpha = 1.5$ .



4.13(a):



4.13(b):

Figure 4.13: The isentropic trajectories of overlinear potentials ( $\alpha = 8$ ) on the top (a). Early increases in  $L$  will intensify the potential asymmetry and increase its temperature. On the bottom (b), a specific isentropic trajectory demonstrates that, even for very large displacements,  $L$  and  $S$  never decouple. Note that in order to obtain temperature shifts it is necessary employ displacements ten time larger. The parameters used were  $m = k_L = 1$  and  $k_\alpha = 1.5$ .

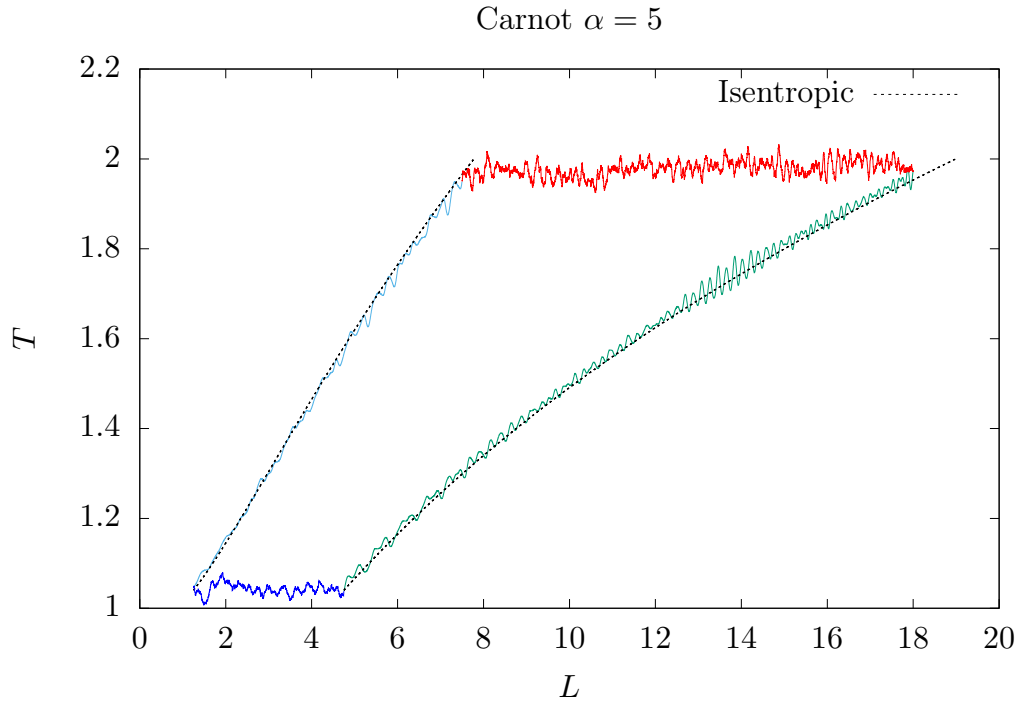


Figure 4.14: Representation of a Carnot cycle for a nonlinear Brownian machine. The dashed lines are the isentropic processes while the solid lines represent the internal temperature of the particle, defined as  $\langle v^2 \rangle / m$ , where the adiabaticity was achieved by removing the contact with the heat sources. The present cycle verifies exactly the isentropic relations proposed on equation 4-33. The parameters used were  $m = \gamma = k_L = \sigma = 1$  and  $k_\alpha = 5$ .

## 4.7

### Final Remarks

We have introduced a new type of internal potential, which we labelled  $\alpha$ -type, in order to better understand the connection between the exponent  $\alpha$  and the work output. The reasoning presented in section 2.2 of Chapter 2 mainly from an intuitive perspective holds true for the  $\alpha$ -type potential. This new potential also encompasses the results obtained in the previous chapters when  $\alpha = 4$ , while also allowing us to probe further the role nonlinearities play in the conversion of heat into work.

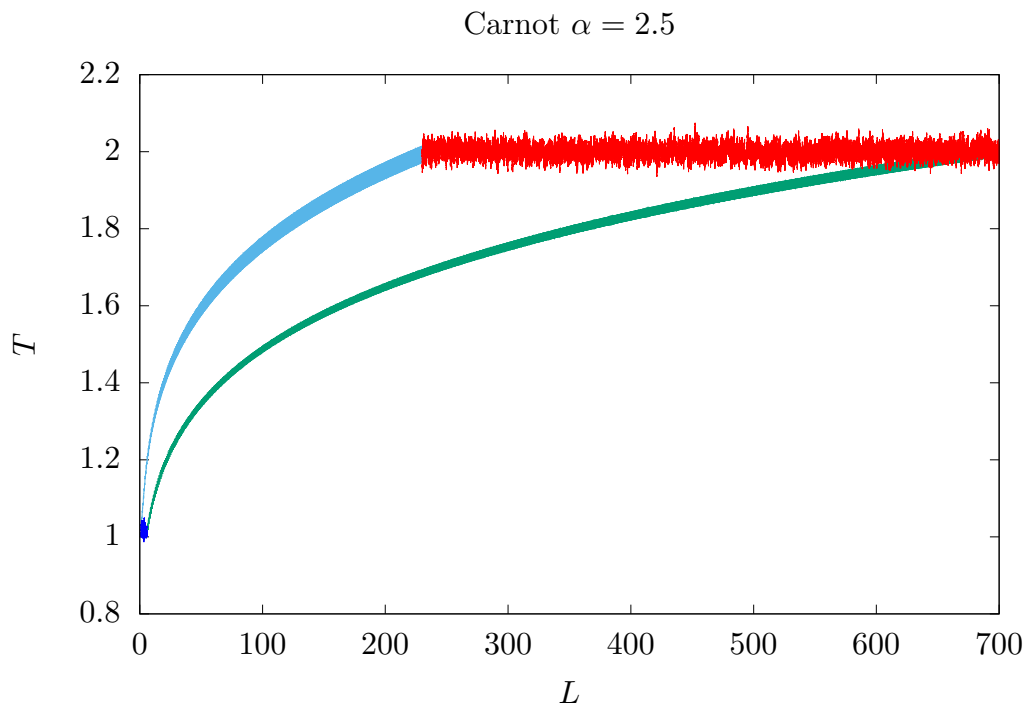


Figure 4.15: Representation of a Carnot cycle for a nonlinear Brownian machine. The solid lines represent the internal temperature of the particle, defined as  $\langle v^2 \rangle / m$ , where the adiabaticity was achieved by removing the contact with the heat sources. Note that in order to obtain a  $\Delta T = 1$ , we had to displace the potential by  $\Delta L \approx 700$ , which severely limits the applicability of the isentropics in experimental situations. The parameters used were  $m = \gamma = k_L = \sigma = 1$  and  $k_\alpha = 2.5$ .

## 5 Final Remarks

### 5.1 What have we done?

We started Chapter 2 mainly focused on providing a complete description of our model. Starting with the Langevin equation (Eq. 2-2) describing the system dynamics, our goal was to provide a clear physical picture of the role every term was meant to represent in describing the dynamics of an actual BP. The impossibility of a machine with quadratic internal potential was explained, together with a very intuitive explanation to the key role of asymmetry to have an efficient machine.

Assuming a small nonlinear correction to a predominantly linear one which is consistent with scenarios where we are expanding in a power series a naturally occurring confining potential, we were able to use perturbation theory to obtain the work and heat output per cycle.

In chapter 3 we dropped the small nonlinear restriction and, by imposing an equilibrium restriction on the cycle period (or equivalently  $\Omega \rightarrow 0$ ) we were able to use the tools of equilibrium statistical mechanics to evaluate the work and heat outputs. Despite managing to increase the value of the work output by almost 100 times, that value was still much lower than the heat intake during the hot phase. The maximum efficiency obtained was of  $\approx 10\%$  while the expected Carnot efficiency was 50%.

Since the key element is that the potential be asymmetric, we decided to extend the definition of our internal potential. Solving the Langevin equation (Eq. 2-2) perturbatively would have been a very challenging task if the interaction was non-analytical, however, within the equilibrium regime the analysis becomes quite simple. In order to investigate the influence different exponents may have on the work output, we define and investigate the  $\alpha$ -type potential  $V_\alpha \propto |x|^\alpha$ . We show that if  $\alpha < 2$ , which we label sub-linear regime the machine behaves like a refrigerator while in the over-linear regime  $\alpha > 2$  it behaves closely to the results obtained in Chapter 3.

Lastly, we create an "effectively" adiabatical process by imposing that the displacements in the potential  $dL$  and temperature  $dT$  are made in

a very specific way to maintain the entropy constant [6, 16, 18, 65]. For massless harmonic systems with modulated frequency the isentropic trajectory is quite straightforward proportional to  $T$ , for our nonlinear systems however, such trajectories strongly depend on the system properties, specially on the exponent  $\alpha$ . In order to effectively change the system temperature by  $\Delta T$  we are forced to deform the potential by a  $\Delta L$  orders of magnitude higher greatly limiting the attainability of isentropic trajectories in the context of nonlinear machines. Despite this drawbacks, for values of  $\alpha > 2$  we were capable of obtaining a very efficient Carnot equivalent.

## 5.2

### What have we learned?

#### System Potential

Our work in chapter 2 started with a small quartic correction to a quadratic potential, and we relaxed the restriction of small nonlinearities in chapter 3 considering a general quartic potential. In the end we attempted to study a wider range of values with the introduction of the  $\alpha$ -type potentials in chapter 4.

After analysing these different types of potentials we can underline the most important characteristic that any potential which could be used as a machine must obey: when we deform it with an external potential *it must become asymmetric*. As we stated in section 2.2 of chapter 2 and latter in section 4.2 of chapter 4, nonlinearities are the means by which a potential becomes asymmetric, a nonlinear potential that remains symmetric could not be used to create a machine.

Most importantly, the tools employed in this work are not restricted to the simple polynomial (or  $\alpha$ -types) we presented here and could be easily extended, at least numerically, to any type of potential. In an experimental situation, if we know the BP's potential with some degree of precision and that by deforming it using some experimental technique available it becomes asymmetric then the fluctuations *will* be guided and the set-up *will* be able to convert heat into work.

#### Cycle Choice

The cycles we have studied extensively are the step and elliptical cycle (chapters 1 to 4), which are suboptimal in terms of efficiency when compared

to the Carnot cycle. In chapter 5 we used isentropic conditions to create an actual Carnot cycle.

In an experimental scenario, the heat bath is generally composed by a large number of particles diluted in some sort of viscous liquid which will surround the BP, such a setting would be consistent with 2-2. The temperature can be introduced by either directly heating the system with a laser [14] or simply vibrating the system with an external white noise generator [16].

As we change the temperature, we can expect the bath particles to require some time  $\tau_B$  to reach the new temperature. In a situation where the particles require a long time when compared to the temporal resolution of our measurements, the step cycle becomes the ideal choice since it only undergoes two changes in the temperature per cycle. If the bath particles are quick to reach the applied temperature, the elliptical cycle or the Carnot cycle become an approachable choice.

The Carnot cycle is plagued by two problems: the isentropic trajectories require a great deal of precision regarding the BP's potential, which may not always be possible, and in order to reach a sensible  $\Delta T$  we may be forced to cause deformations that are too large for a real system. If the Carnot cycle becomes an experimental impossibility, the elliptical cycle becomes the optimal solution.

### 5.3

#### Where can we go from here?

Our work here contemplates many directions. Within the topic of energy harvesters, the addition of nonlinear potentials (usually  $V \propto x^4$ ) is capable of widening the frequency range where the device is efficient. It has been shown that there is an optimal exponent to the potential [52] when investigating integer exponents, we could employ our techniques to the energy harvester attempting to uncover whether a non-integer exponent (the  $\alpha$  type potential) may improve the efficiency even further.

Most of our assumptions involved some kind of equilibrium, or quasi-equilibrium notion (small  $\Omega$ ). The classical theoretical Carnot machine is unachievable in reality since the hypothesis of equilibrium statistics require the cycle period to be immensely large. In realistic scenarios it is common to search for a practical trade-off between maximum power output and efficiency [43, 66–68]. We would like to investigate the behaviour of our BP with a protocol frequency  $\Omega \approx \omega_2$  and attempt to recover the Novikov-Curzon-Albhorn efficiency by maximizing the power.

A very interesting topic would be to consider the repercussions of

introducing a non equilibrium bath, like a Poissonian reservoir. It is known that the interplay between Gaussian-Poisson baths is capable of causing “apparent” violations of the second law of thermodynamics such as the reversion of the law of conduction [58]. We could create a machine employing the same principles which caused the heat flow inversion.

Lastly, but definitely not least, following on the footsteps of other great experimental achievements [12–16,69], we could search for a working substance that, when deformed has its potential become asymmetric allowing us to recreate our results experimentally.

## A Stratonovich Calculus

In chapter 2 we have made several statements regarding the nature of the terms in the equations of motion of our system. All of these were crafted by using an extensive amount of intuition regarding the physical interpretation of these constituent terms, specifically we have labelled  $\eta(t)v(t)$  as the fluctuating heat flow, and because of the stochastic nature of  $\eta(t)$ , we cannot naively assume that the rules of regular differential calculus will always be applicable to such a quantity.

Our aim in this section is to demonstrate that, by considering Stratonovich's prescription to integration, we may continue to use rules of regular differential calculus. Let us start by defining the Wiener function

$$G(t) - G(0) = \int_0^t \eta(t') dt', \quad (\text{A-1})$$

and we'll be very careful with our deductions since in our case, unlike the more general definitions regarding the Wiener process, the temperature in our problem is a function of time:

$$\langle \eta(t) \rangle = 0 \quad ; \quad \langle \eta(t)\eta(t') \rangle = 2m\gamma T(t)\delta(t - t'). \quad (\text{A-2})$$

Taking the differential of the Wiener function  $G(t)$ ,

$$dG_t = G(t + dt) - G(t) = \int_t^{t+dt} \eta(t') dt' \quad (\text{A-3})$$

and even though it is tempting, we cannot naively consider that  $dG_t = \eta(t')dt'$ . We also evaluate that

$$\begin{aligned} \langle dG_t dG_{t'} \rangle &= \int_{t'}^{t'+dt} ds' \int_t^{t+dt} ds \langle \eta(s)\eta(s') \rangle \\ &= \int_{t'}^{t'+dt} ds' \int_t^{t+dt} ds 2m\gamma T(s)\delta(s - s'), \end{aligned} \quad (\text{A-4})$$

so only when  $t = t'$  the previous correlation will be non zero

$$\begin{aligned}\langle dG_t^2 \rangle &= \int_t^{t+dt} ds ds' \langle \eta(s) \eta(s') \rangle \\ &= \int_t^{t+dt} ds ds' 2m\gamma T(s) \delta(s - s') = 2m\gamma \int_t^{t+dt} T(s) ds, \quad (\text{A-5}) \\ &= 2m\gamma T(t) dt.\end{aligned}$$

The equations of motion in chapter 2 can be written as

$$\begin{aligned}\frac{dp}{dt} &= \left\{ -\gamma p - V'(x) - k_L(x - L) \right\} + \eta(t) \\ \frac{dx}{dt} &= \frac{p}{m},\end{aligned} \quad (\text{A-6})$$

evaluating

$$\begin{aligned}dp_t &= \int_t^{t+dt} \frac{dp}{dt} dt' = \left\{ -\gamma p_t - V'(x_t) - k_L(x_t - L_t) \right\} dt + dG_t \\ dp_t &= a(p_t, x_t, L_t) dt + dG_t \quad (\text{A-7}) \\ dx_t &= \frac{p_t}{m} dt\end{aligned}$$

where we have defined  $a(p_t, x_t, L_t) = -\gamma p_t - V'(x_t) - k_L(x_t - L_t)$ , which for simplicity we will abbreviate as  $a_t$ .

We can discretize the motion as

$$\begin{aligned}p_{t+dt} &= p_t + a_t dt + dG_t \\ x_{t+dt} &= x_t + \frac{p_t}{m} dt.\end{aligned} \quad (\text{A-8})$$

Following Stratonovich lemma (which we are representing with a  $\circ$ ) we have that [55]

$$\int_0^t p(t') \eta(t') dt' = \int_0^t p(t') \circ dG_{t'} \quad (\text{A-9})$$

we also have that [55, 56]

$$p(t) \circ dG_t = \frac{p_{t+dt} + p_t}{2} dG_t = \frac{dp_t}{2} dG_t + p_t dG_t, \quad (\text{A-10})$$

from the discretized equation we can conclude that the momenta  $p$  at an instant  $t$  is a function of  $dG_{t'}$  only at times  $t' < t$ , and therefore  $\langle p_t dG_t \rangle = 0$  and for the same reasoning  $\langle a_t dG_t \rangle = 0$ . The remaining term

$$\begin{aligned}\langle p(t) \circ dG_t \rangle &= \frac{1}{2} \langle dp_t dG_t \rangle = \frac{1}{2} \left\{ \langle a_t dG_t \rangle + \langle dG_t^2 \rangle \right\} = \frac{1}{2} \langle dG_t^2 \rangle \\ &= m\gamma T(t).\end{aligned} \quad (\text{A-11})$$

Lastly, since  $v = p/m$  we obtain

$$\langle \eta(t)v(t) \rangle = \gamma T(t). \quad (\text{A-12})$$

## B General Calculations

### B.1 Time Average of a Single Function

The time average of a function  $f$  is defined as

$$\overline{f(t)} = \lim_{\lambda \rightarrow \infty} \frac{1}{\lambda} \int_0^\lambda dt f(t) = \lim_{\lambda \rightarrow \infty} \frac{1}{\lambda} \int_0^\lambda dt \int_0^\infty dt_1 \delta(t - t_1) f(t_1), \quad (\text{B-1})$$

we replace

$$\delta(t) = \lim_{\epsilon \rightarrow 0^+} \int_{-\infty}^{\infty} \frac{dq}{2\pi} e^{(iq+\epsilon)t}, \quad (\text{B-2})$$

$$\begin{aligned} \overline{f(t)} &= \lim_{\lambda \rightarrow \infty} \frac{1}{\lambda} \int_0^\lambda dt f(t) = \lim_{\lambda \rightarrow \infty} \lim_{\epsilon \rightarrow 0^+} \frac{1}{\lambda} \int_0^\lambda dt \int_0^\infty dt_1 \int_{-\infty}^{\infty} \frac{dq}{2\pi} e^{(iq+\epsilon)(t-t_1)} f(t_1) \\ &= \lim_{\lambda \rightarrow \infty} \lim_{\epsilon \rightarrow 0^+} \frac{1}{\lambda} \int_{-\infty}^{\infty} \frac{dq}{2\pi} \int_0^\lambda e^{(iq+\epsilon)t} dt \int_0^\infty e^{-(iq+\epsilon)t_1} f(t_1) dt_1, \end{aligned}$$

now we identify that the last term is the definition of the Laplace Transform, and the middle integration can be easily done:

$$\overline{f(t)} = \lim_{\lambda \rightarrow \infty} \lim_{\epsilon \rightarrow 0^+} \int_{-\infty}^{\infty} \frac{dq}{2\pi} \frac{e^{(iq+\epsilon)\lambda} - 1}{(iq + \epsilon)\lambda} \tilde{f}(iq + \epsilon). \quad (\text{B-3})$$

In order to simplify further we will define the time auxiliary function

$$\tau(x) = \frac{e^{x\lambda} - 1}{x\lambda}, \quad (\text{B-4})$$

allowing us to write

$$\overline{f(t)} = \lim_{\lambda \rightarrow \infty} \lim_{\epsilon \rightarrow 0^+} \int_{-\infty}^{\infty} \frac{dq}{2\pi} \tau(iq + \epsilon) \tilde{f}(iq + \epsilon) \quad (\text{B-5})$$

the result may be extended to the average of the product of two functions (which we will use specifically):

$$\overline{f(t)g(t)} = \lim_{\lambda \rightarrow \infty} \lim_{\epsilon \rightarrow 0^+} \int_{-\infty}^{\infty} \frac{dq_1 dq_2}{(2\pi)^2} \frac{e^{(iq_1+iq_2+2\epsilon)\lambda} - 1}{(iq_1 + iq_2 + 2\epsilon)\lambda} \tilde{f}(iq_1 + \epsilon) \tilde{g}(iq_2 + \epsilon) \quad (\text{B-6})$$

or of several functions

$$\overline{\prod_{j=1}^n f_j(t)} = \lim_{\lambda \rightarrow \infty} \lim_{\epsilon \rightarrow 0^+} \int_{-\infty}^{\infty} \frac{\prod_{j=1}^n dq_j}{(2\pi)^n} \frac{e^{\sum_{j=1}^n (iq_j + \epsilon)\lambda} - 1}{\sum_{j=1}^n (iq_j + \epsilon)\lambda} \prod_{j=1}^n \tilde{f}_j(iq_j + \epsilon). \quad (\text{B-7})$$

## B.2

### Broken Time Averages

In order to correctly obtain the absorbed heat  $Q_H$  we must evaluate the time average of  $Q(t)$  only during the hot phase (and equivalently during the cold phase to obtain  $Q_C$ ). So we will also obtain the time average on broken intervals of period  $\theta$  as shown in figure B.1:

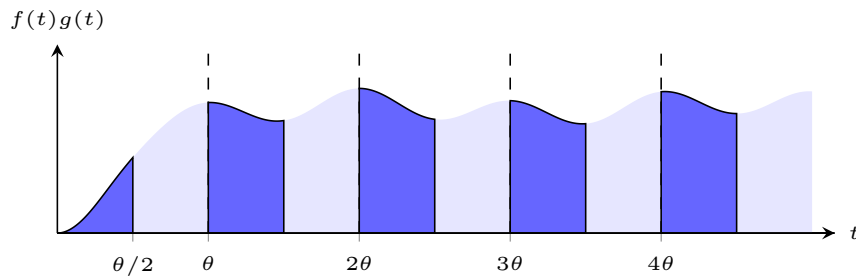


Figure B.1: This is a visual representation of the broken averages. The dark blue represents the early time average and the light blue represents the late time average.

$$\begin{aligned} \overline{f(t)} &= \overline{f(t)}^{\text{late}} + \overline{f(t)}^{\text{early}} = \\ &= \lim_{n \rightarrow \infty} \sum_{m=0}^n \frac{1}{n\theta} \left\{ \int_{m\theta}^{(m+1/2)\theta} f(t) dt + \int_{(m+1/2)\theta}^{(m+1)\theta} f(t) dt \right\}. \quad (\text{B-8}) \end{aligned}$$

The early average:

$$\begin{aligned} \overline{f(t)}^{\text{early}} &= \lim_{n \rightarrow \infty} \sum_{m=0}^n \frac{1}{n\theta} \int_{m\theta}^{(m+1/2)\theta} f(t) dt = \\ &= \lim_{n \rightarrow \infty} \lim_{\epsilon \rightarrow 0} \sum_{m=0}^n \int_{-\infty}^{\infty} \frac{dq}{2\pi} \frac{1}{n\theta} \int_{m\theta}^{(m+1/2)\theta} e^{(iq+\epsilon)t} dt \tilde{f}(iq + \epsilon) \\ &= \lim_{n \rightarrow \infty} \lim_{\epsilon \rightarrow 0} \int_{-\infty}^{\infty} \frac{dq}{2\pi} \frac{1}{n\theta} \sum_{m=0}^n e^{(iq+\epsilon)\theta m} \left[ \frac{e^{(iq+\epsilon)\theta/2} - 1}{(iq + \epsilon)} \right] \tilde{f}(iq + \epsilon), \end{aligned}$$

with the geometric sum being:

$$\sum_{m=0}^n e^{(iq+\epsilon)\theta m} = \frac{e^{(iq+\epsilon)\theta n} - 1}{e^{(iq+\epsilon)\theta} - 1} = \frac{e^{(iq+\epsilon)\theta n} - 1}{(e^{(iq+\epsilon)\theta/2} - 1)(e^{(iq+\epsilon)\theta/2} + 1)}. \quad (\text{B-9})$$

Replacing the previous result we obtain the final expression:

$$\overline{f(t)}^{\text{early}} = \lim_{n \rightarrow \infty} \lim_{\epsilon \rightarrow 0} \int_{-\infty}^{\infty} \frac{dq}{2\pi} \frac{e^{(iq+\epsilon)n\theta} - 1}{n\theta(iq+\epsilon)(e^{(iq+\epsilon)\theta/2} + 1)} \tilde{f}(iq+\epsilon). \quad (\text{B-10})$$

In order to simplify the result even further we will define the early time average function:

$$\tau_E(x) = \frac{e^x - 1}{n\theta(e^{x/2} + 1)x}, \quad (\text{B-11})$$

making

$$\overline{f(t)}^{\text{early}} = \lim_{n \rightarrow \infty} \lim_{\epsilon \rightarrow 0} \int_{-\infty}^{\infty} \frac{dq}{2\pi} \tau_E(iq+\epsilon) \tilde{f}(iq+\epsilon). \quad (\text{B-12})$$

For the late average

$$\begin{aligned} \overline{f(t)}^{\text{late}} &= \lim_{n \rightarrow \infty} \sum_{m=0}^n \frac{1}{n\theta} \int_{(m+1/2)\theta}^{(m+1)\theta} f(t) dt = \\ &= \lim_{n \rightarrow \infty} \lim_{\epsilon \rightarrow 0} \sum_{m=0}^n \int_{-\infty}^{\infty} \frac{dq}{2\pi} \frac{1}{n\theta} \int_{(m+1/2)\theta}^{(m+1)\theta} e^{(iq+\epsilon)t} dt \tilde{f}(iq+\epsilon) \\ &= \lim_{n \rightarrow \infty} \lim_{\epsilon \rightarrow 0} \int_{-\infty}^{\infty} \frac{dq}{2\pi} \frac{1}{n\theta} \sum_{m=0}^n e^{(iq+\epsilon)\theta m} \left[ \frac{e^{(iq+\epsilon)\theta/2} - 1}{(iq+\epsilon)} \right] e^{(iq+\epsilon)\theta/2} \tilde{f}(iq+\epsilon), \end{aligned}$$

and using the geometric sum result

$$\overline{f(t)}^{\text{late}} = \lim_{n \rightarrow \infty} \lim_{\epsilon \rightarrow 0} \int_{-\infty}^{\infty} \frac{dq}{2\pi} \frac{(e^{(iq+\epsilon)n\theta} - 1)e^{(iq+\epsilon)\theta/2}}{n\theta(iq+\epsilon)(e^{(iq+\epsilon)\theta/2} + 1)} \tilde{f}(iq+\epsilon). \quad (\text{B-13})$$

we can also define the late time average function as

$$\tau_L(x) = \frac{(e^{xN} - 1)e^{x\theta/2}}{n\theta(e^{x/2} + 1)x} \quad (\text{B-14})$$

which allows us to rewrite

$$\overline{f(t)}^{\text{late}} = \lim_{n \rightarrow \infty} \lim_{\epsilon \rightarrow 0} \int_{-\infty}^{\infty} \frac{dq}{2\pi} \tau_L(iq+\epsilon) \tilde{f}(iq+\epsilon). \quad (\text{B-15})$$

### B.3

#### An Illustrative Example

Before evaluating the example, we will take this opportunity to illustrate the most important (and convenient) propriety of the auxiliary time functions

introduced, namely  $\tau$ ,  $\tau_E$  and  $\tau_L$ . Starting with the simpler complete time average, if we take the limit

$$\lim_{x \rightarrow 0} \tau(ix) = \lim_{x \rightarrow 0} \frac{e^{ix\lambda} - 1}{ix\lambda} = 1, \quad (\text{B-16})$$

we can see that the result does not depend on  $\lambda$ . If we consider  $x \neq 0$  (with  $x$  being real) then

$$\tau(ix) \leq \frac{1}{x\lambda} \quad (\text{B-17})$$

so if we take the limit when  $\lambda$  goes to infinity we have

$$\lim_{\lambda \rightarrow \infty} \tau(ix) = 0. \quad (\text{B-18})$$

For the early and late functions we have a similar result with the only difference being how many points the function isn't null:

$$\lim_{x \rightarrow 0} \tau_E(ix) = \frac{1}{2} \quad (\text{B-19})$$

$$\lim_{x \rightarrow 0} \tau_L(ix) = \frac{1}{2} \quad (\text{B-20})$$

$$\lim_{x \rightarrow (2n+1)\Omega} \tau_E(ix) = -\frac{i}{(2n+1)\pi} \quad (\text{B-21})$$

$$\lim_{x \rightarrow (2n+1)\Omega} \tau_L(ix) = +\frac{i}{(2n+1)\pi}, \quad (\text{B-22})$$

where we have defined  $\Omega = 2\pi/\theta$ . For any other value of  $x$  we have that

$$\lim_{\lambda \rightarrow \infty} \tau_E(ix) = 0 \quad (\text{B-23})$$

$$\lim_{\lambda \rightarrow \infty} \tau_L(ix) = 0. \quad (\text{B-24})$$

These last results are very useful; in order to evaluate the time average as defined in B-5, B-12 and B-15 we will be usually using Jordan's Lemma to integrate on a semi-circle in the complex plane. Since there are no poles contained in the auxiliary functions, the only poles that will account for Cauchy residue integration will be associated with  $\tilde{f}$ .

The auxiliary functions have the key role to filter the transient averages from the secular averages. We can see this in principle in action with our example:

$$\overline{\cos^2(\Omega t)} = \lim_{\lambda \rightarrow \infty} \lim_{\epsilon \rightarrow 0} \int_{-\infty}^{\infty} \frac{dq}{2\pi} \tau(iq + \epsilon) \frac{(iq + \epsilon)^2 + 2\Omega^2}{(iq + \epsilon)((iq + \epsilon)^2 + 4\Omega^2)}, \quad (\text{B-25})$$

to solve this naively we would need to evaluate the residue over  $q = i\epsilon$ ,

$q = \pm 2\Omega + i\epsilon$ , but we can simplify our calculations because, as we discovered before, only the first pole ( $q = i\epsilon$ ) will yield a non-zero result in the auxiliary term, so we can ignore the rest to obtain that

$$\overline{\cos^2(\Omega t)} = \tau(0) \left( \frac{-i}{2} \right) = \frac{1}{2}. \quad (\text{B-26})$$

## C Useful Laplace Transforms

Here we focus on obtaining some Transforms that will be used in chapter 2.

### C.1 Laplace Transform of $x^3(t)$

For the model presented in chapter 2, we will obtain the expression for

$$\begin{aligned}
 \mathcal{L}\{x^3(t)\}(s) &= \int_0^{\infty} x^3(t)e^{-st} dt = \\
 &= \int_0^{\infty} e^{-st} \delta(t-t_1)\delta(t-t_2)\delta(t-t_3)x(t_1)x(t_2)x(t_3) dt dt_1 dt_2 dt_3 \\
 &= \lim_{\epsilon \rightarrow 0^+} \int_{-\infty}^{\infty} \frac{dq_1 dq_2 dq_3}{(2\pi)^3} \int_0^{\infty} dt dt_1 dt_2 dt_3 e^{-st} e^{(iq_1+\epsilon)(t-t_1)} e^{(iq_2+\epsilon)(t-t_2)} \times \\
 &\times e^{(iq_3+\epsilon)(t-t_3)} x(t_1)x(t_2)x(t_3) = \\
 &= \lim_{\epsilon \rightarrow 0^+} \int_{-\infty}^{\infty} \frac{dq_1 dq_2 dq_3}{(2\pi)^3} \int_0^{\infty} dt e^{-(s+iq_1+iq_2+iq_3+3\epsilon)t} \int_0^{\infty} e^{-(iq_1+\epsilon)t_1} x(t_1) dt_1 \times \\
 &\times \int_0^{\infty} e^{-(iq_2+\epsilon)t_2} x(t_2) dt_2 \int_0^{\infty} e^{-(iq_3+\epsilon)t_3} x(t_3) dt_3 \\
 \mathcal{L}\{x^3(t)\}(s) &= \lim_{\epsilon \rightarrow 0^+} \int_{-\infty}^{\infty} \frac{dq_1 dq_2 dq_3}{(2\pi)^3} \frac{\tilde{x}(iq_1+\epsilon)\tilde{x}(iq_2+\epsilon)\tilde{x}(iq_3+\epsilon)}{s-iq_1-iq_2-iq_3-3\epsilon}, \quad (C-1)
 \end{aligned}$$

since the derivation of the previous relation was quite straightforward, its easy to see that in fact

$$\lim_{\lambda \rightarrow \infty} \mathcal{L}\{x^n(t)\}(s) = \lim_{\epsilon \rightarrow 0^+} \int_{-\infty}^{\infty} \frac{\prod_{j=1}^n dq_j}{(2\pi)^n} \frac{\prod_{j=1}^n \tilde{x}(iq_j+\epsilon)}{s-\sum_{j=1}^n (iq_j+\epsilon)} \quad (C-2)$$

### C.2 Correlation with Time-Dependent Temperature

We obtain the Laplace transform of the noise correlation when the temperature is a function of time. Starting with the correlation

$$\langle \eta(t_1)\eta(t_2) \rangle = 2m\gamma T(t_1)\delta(t_1-t_2), \quad (C-3)$$

and the Laplace transform is written as

$$\langle \tilde{\eta}(s_1)\tilde{\eta}(s_2) \rangle = \int_0^\infty \langle \eta(t_1)\eta(t_2) \rangle e^{-s_1 t_1 - s_2 t_2} dt_1 dt_2. \quad (\text{C-4})$$

Integrating first in  $t_2$

$$\begin{aligned} \langle \tilde{\eta}(s_1)\tilde{\eta}(s_2) \rangle &= \int_0^\infty dt_1 \int_0^\infty dt_2 2m\gamma T(t_1) \delta(t_1 - t_2) e^{-s_1 t_1 - s_2 t_2} \\ &= \int_0^\infty dt_1 2m\gamma T(t_1) e^{-t_1(s_1 + s_2)} \\ \langle \tilde{\eta}(s_1)\tilde{\eta}(s_2) \rangle &= 2m\gamma \frac{\tilde{T}(s_1 + s_2)}{s_1 + s_2} \end{aligned} \quad (\text{C-5})$$

] Where  $\tilde{T}$  is the Laplace transform of the temperature.

### C.3

#### Laplace Transform of the Temperature

For the elliptical cycle, the Laplace transform of  $T(t)$  is quite straightforward

$$T(t) = T_m + \frac{\Delta T}{2} \sin(\Omega t) \quad \longrightarrow \quad \tilde{T}(s) = \frac{T_m}{s} + \frac{\Delta T}{2} \frac{\Omega}{s^2 + \Omega^2}. \quad (\text{C-6})$$

The transform of the step cycle temperature is not as straightforward, we present the calculations here

$$\begin{aligned} \int_0^\infty e^{-st} T(t) dt &= \sum_{n=0}^\infty \int_{n\theta}^{(n+1/2)\theta} T_H e^{-st} dt + \int_{(n+1/2)\theta}^{(n+1)\theta} T_C e^{-st} dt \\ &= \sum_{n=0}^\infty \frac{T_H}{s} e^{-sn\theta} (1 - e^{-s\theta/2}) + \frac{T_C e^{-s\theta/2}}{s} e^{-sn\theta} (1 - e^{-s\theta/2}) \\ &= \left\{ \sum_{n=0}^\infty e^{-sn\theta} \right\} \left\{ \frac{T_H + T_C e^{-s\theta/2}}{s} \right\} (1 - e^{-s\theta/2}) \\ &= \frac{1}{1 - e^{-s\theta}} \left\{ \frac{T_H + T_C e^{-s\theta/2}}{s} \right\} (1 - e^{-s\theta/2}) \\ \tilde{T}(s) &= \frac{T_H + T_C e^{-s\theta/2}}{s[1 + e^{-s\theta/2}]}. \end{aligned} \quad (\text{C-7})$$

## D Isentropic Process Derivation

Here we present the complete calculations necessary to obtain  $dS = 0$ , or in an expanded form

$$dS(L, T) = \frac{\partial S}{\partial L} dL + \frac{\partial S}{\partial T} dT = \frac{\partial S}{\partial L} dL - \frac{1}{T^2} \frac{\partial S}{\partial \beta} dT = 0. \quad (\text{D-1})$$

Expanding the entropy we obtain

$$\begin{aligned} S(L, T) &= - \int d\Gamma \left\{ \ln \frac{e^{-\beta\mathcal{H}(\Gamma)}}{Z(L, T)} \right\} \frac{e^{-\beta\mathcal{H}(\Gamma)}}{Z(L, T)} \\ &= \int d\Gamma \left\{ \beta\mathcal{H}(\Gamma) + \ln Z(L, T) \right\} \frac{e^{-\beta\mathcal{H}(\Gamma)}}{Z(L, T)} \\ &= \beta \int d\Gamma \mathcal{H}(\Gamma) \frac{e^{-\beta\mathcal{H}(\Gamma)}}{Z(L, T)} + \ln Z(L, T) \int d\Gamma \frac{e^{-\beta\mathcal{H}(\Gamma)}}{Z(L, T)} = \\ &= \int d\Gamma \beta\mathcal{H}(\Gamma) \frac{e^{-\beta\mathcal{H}(\Gamma)}}{Z(L, T)} + \ln Z(L, T). \end{aligned} \quad (\text{D-2})$$

We will perform our calculations using the previous explicit result for the entropy, however we can clearly identify the Maxwell relation  $S = F/T - E/T$ . Let us derive some useful expressions beforehand

$$\begin{aligned} \frac{\partial}{\partial L} \ln Z &= \frac{1}{Z} \frac{\partial Z}{\partial L} = \frac{1}{Z} \int d\Gamma' \frac{\partial}{\partial L} e^{-\beta\mathcal{H}(\Gamma')} = -\frac{\beta}{Z} \int d\Gamma' \frac{\partial \mathcal{H}}{\partial L} e^{-\beta\mathcal{H}(\Gamma')} = -\beta \left\langle \frac{\partial \mathcal{H}}{\partial L} \right\rangle \\ \frac{\partial}{\partial \beta} \ln Z &= \frac{1}{Z} \frac{\partial Z}{\partial \beta} = \frac{1}{Z} \int d\Gamma' \frac{\partial}{\partial \beta} e^{-\beta\mathcal{H}(\Gamma')} = -\frac{1}{Z} \int d\Gamma' \mathcal{H} e^{-\beta\mathcal{H}(\Gamma')} = -\langle \mathcal{H} \rangle \\ \frac{\partial}{\partial L} \frac{1}{Z} &= -\frac{1}{Z^2} \frac{\partial Z}{\partial L} = -\frac{1}{Z^2} \int d\Gamma' \frac{\partial}{\partial L} e^{-\beta\mathcal{H}(\Gamma')} = \frac{\beta}{Z^2} \int d\Gamma' \frac{\partial \mathcal{H}}{\partial L} e^{-\beta\mathcal{H}(\Gamma')} = \frac{\beta}{Z} \left\langle \frac{\partial \mathcal{H}}{\partial L} \right\rangle \\ \frac{\partial}{\partial \beta} \frac{1}{Z} &= -\frac{1}{Z^2} \frac{\partial Z}{\partial \beta} = -\frac{1}{Z^2} \int d\Gamma' \frac{\partial}{\partial \beta} e^{-\beta\mathcal{H}(\Gamma')} = \frac{1}{Z^2} \int d\Gamma' \mathcal{H} e^{-\beta\mathcal{H}(\Gamma')} = \frac{1}{Z} \langle \mathcal{H} \rangle \end{aligned}$$

Using these results we can write

$$\begin{aligned}
\frac{\partial S}{\partial L} &= \int d\Gamma \left\{ \beta \frac{\partial \mathcal{H}}{\partial L} \frac{e^{-\beta \mathcal{H}(\Gamma)}}{Z} + \beta \mathcal{H} \frac{\partial}{\partial L} \frac{e^{-\beta \mathcal{H}(\Gamma)}}{Z} \right\} + \frac{\partial}{\partial L} \ln Z \\
&= \beta \left\langle \frac{\partial \mathcal{H}}{\partial L} \right\rangle + \int d\Gamma \left\{ \beta \mathcal{H} \frac{\partial}{\partial L} \frac{e^{-\beta \mathcal{H}(\Gamma)}}{Z} \right\} - \beta \left\langle \frac{\partial \mathcal{H}}{\partial L} \right\rangle = \int d\Gamma \left\{ \beta \mathcal{H} \frac{\partial}{\partial L} \frac{e^{-\beta \mathcal{H}(\Gamma)}}{Z} \right\} \\
&= -\beta^2 \int d\Gamma \mathcal{H} \frac{\partial \mathcal{H}}{\partial L} \frac{e^{-\beta \mathcal{H}(\Gamma)}}{Z} + \beta \int d\Gamma \mathcal{H} e^{-\beta \mathcal{H}(\Gamma)} \frac{\partial}{\partial L} \frac{1}{Z} 0 \\
&= -\beta^2 \left\langle \mathcal{H} \frac{\partial \mathcal{H}}{\partial L} \right\rangle + \beta \int d\Gamma \mathcal{H} e^{-\beta \mathcal{H}(\Gamma)} \frac{\beta}{Z} \left\langle \frac{\partial \mathcal{H}}{\partial L} \right\rangle \\
\frac{\partial S}{\partial L} &= -\beta^2 \left\langle \mathcal{H} \frac{\partial \mathcal{H}}{\partial L} \right\rangle + \beta^2 \langle \mathcal{H} \rangle \left\langle \frac{\partial \mathcal{H}}{\partial L} \right\rangle, \tag{D-3}
\end{aligned}$$

and

$$\begin{aligned}
\frac{\partial S}{\partial \beta} &= \frac{\partial}{\partial \beta} \int d\Gamma \beta \mathcal{H}(\Gamma) \frac{e^{-\beta \mathcal{H}(\Gamma)}}{Z(L, T)} + \frac{\partial}{\partial \beta} \ln Z(L, T) \\
&= \int d\Gamma \mathcal{H} \frac{e^{-\beta \mathcal{H}(\Gamma)}}{Z} + \int d\Gamma \beta \mathcal{H} \frac{\partial}{\partial \beta} \frac{e^{-\beta \mathcal{H}(\Gamma)}}{Z} - \langle \mathcal{H} \rangle = \langle \mathcal{H} \rangle + \int d\Gamma \beta \mathcal{H} \frac{\partial}{\partial \beta} \frac{e^{-\beta \mathcal{H}(\Gamma)}}{Z} - \langle \mathcal{H} \rangle \\
&= - \int d\Gamma \beta \mathcal{H}^2 \frac{e^{-\beta \mathcal{H}}}{Z} + \int d\Gamma \beta \mathcal{H} e^{-\beta \mathcal{H}(\Gamma)} \frac{\partial}{\partial \beta} \frac{1}{Z} = -\beta \langle \mathcal{H}^2 \rangle + \int d\Gamma \beta \mathcal{H} \frac{e^{-\beta \mathcal{H}(\Gamma)}}{Z} \langle \mathcal{H} \rangle \\
\frac{\partial S}{\partial \beta} &= \beta \langle \mathcal{H} \rangle^2 - \beta \langle \mathcal{H}^2 \rangle. \tag{D-4}
\end{aligned}$$

Replacing our findings in the iso-entropic restriction we obtain the definitive version of the restriction

$$\begin{aligned}
dS &= 0 \longrightarrow -\beta^2 \left\{ \left\langle \mathcal{H} \frac{\partial \mathcal{H}}{\partial L} \right\rangle - \langle \mathcal{H} \rangle \left\langle \frac{\partial \mathcal{H}}{\partial L} \right\rangle \right\} dL + \beta \left\{ \langle \mathcal{H}^2 \rangle - \langle \mathcal{H} \rangle^2 \right\} dT = 0 \\
dT &= T \frac{\left\langle \mathcal{H} \frac{\partial \mathcal{H}}{\partial L} \right\rangle - \langle \mathcal{H} \rangle \left\langle \frac{\partial \mathcal{H}}{\partial L} \right\rangle}{\langle \mathcal{H}^2 \rangle - \langle \mathcal{H} \rangle^2} dL = T \frac{\left\langle \mathcal{H} \frac{\partial \mathcal{H}}{\partial L} \right\rangle_c}{\langle \mathcal{H}^2 \rangle_c} dL. \tag{D-5}
\end{aligned}$$

In other words, assume that we start from a point in the phase space  $(L_0, T_0)$  to the point  $(L_1, T_1) \rightarrow (L_0 + dL, T_0 + dT)$ , by choosing a small enough  $dL$  we can obtain  $dT$  using the previous equation as:

$$dT = T_0 \frac{\left\langle H \frac{\partial H}{\partial L} \right\rangle - \langle H \rangle \left\langle \frac{\partial H}{\partial L} \right\rangle}{\langle H^2 \rangle - \langle H \rangle^2} \Bigg|_{L_0, T_0} dL. \tag{D-6}$$

## D.1

### Interpreting the result

Let us define the *work capacity* of our system as

$$\frac{\partial \langle \mathcal{H} \rangle}{\partial L} = \left\langle \frac{\partial \mathcal{H}}{\partial L} \right\rangle - \frac{1}{T} \left\langle \mathcal{H} \frac{\partial \mathcal{H}}{\partial L} \right\rangle_c, \quad (\text{D-7})$$

in other words, the work capacity represents the rate in which the internal energy changes by displacing the value of  $L$  without distinguishing whether that energy is in the form of work or heat. We may write

$$\left\langle \mathcal{H} \frac{\partial \mathcal{H}}{\partial L} \right\rangle_c = -T \left\{ \left\langle \frac{\partial \mathcal{H}}{\partial L} \right\rangle - \frac{\partial \langle \mathcal{H} \rangle}{\partial L} \right\}, \quad (\text{D-8})$$

which allows us to interpret the left hand side of the previous equation is proportional to the heat rate, since we subtracted the work rate from the complete energy change, caused by a displacement in  $L$ .

The isentropic restriction is therefore expressed quite intuitively as: the heat change in the system resulting from a displacement  $dL$  must be the opposite of the resulting from a temperature displacement  $dT$ , if that is true, then the system can be seen as isolated.

## D.2

### Examples

#### Modulated Frequency - Overdamped

If the damping constant is much larger than the mass, the equations of motion become [6]

$$\gamma \dot{x} + k(t)x = \eta(t). \quad (\text{D-9})$$

The Hamiltonian of this system is

$$H(x) = \frac{k(t)}{2} x^2, \quad (\text{D-10})$$

unlike in the previous example where the length  $L$  was the protocol parameter, in this case we the stiffness of the harmonic potential  $k(t)$ . We can write the power output

$$\frac{\partial H}{\partial k} = \frac{x^2}{2} = \frac{H}{k}, \quad (\text{D-11})$$

so that the isentropic restriction becomes

$$\left\langle H \frac{\partial H}{\partial L} \right\rangle - \langle H \rangle \left\langle \frac{\partial H}{\partial L} \right\rangle = \frac{1}{k} \{ \langle H^2 \rangle - \langle H \rangle^2 \}, \quad (\text{D-12})$$

which leads us to

$$dT = \frac{T}{k} \frac{\langle H^2 \rangle - \langle H \rangle^2}{\langle H^2 \rangle - \langle H \rangle^2} dL \longrightarrow \frac{dT}{T} = \frac{dk}{k} \longrightarrow \frac{dT}{dk} = \frac{T}{k} \longrightarrow T = \alpha k. \quad (\text{D-13})$$

which is in accordance with the literature [6]. We have outlined this result in Chapter 1, having the temperature proportional to the stiffness will not only ensure that the entropy is unchanged, but it also will make the probability density remain constant

$$\rho(x) \propto e^{-\frac{k}{2T}x^2} = e^{-\frac{1}{2\alpha}x^2}. \quad (\text{D-14})$$

### Modulated Frequency - Underdamped

In the underdamped limit the particle mass is large enough when compared to the dissipation, the equations of motion are

$$m\ddot{x} + \gamma\dot{x} + k(t)x = \eta(t), \quad (\text{D-15})$$

with Hamiltonian

$$H(x, p) = \frac{p^2}{2m} + \frac{k(t)}{2}x^2. \quad (\text{D-16})$$

The power output can be written as

$$\frac{\partial H}{\partial k} = \frac{H - \frac{p^2}{2m}}{k}, \quad (\text{D-17})$$

which we use to derive that

$$\left\langle H \frac{\partial H}{\partial L} \right\rangle - \langle H \rangle \left\langle \frac{\partial H}{\partial L} \right\rangle = \frac{T^2}{k} - \frac{T^2}{2k} = \frac{T^2}{2k}. \quad (\text{D-18})$$

leading to the isentropic condition

$$\frac{\left\langle H \frac{\partial H}{\partial k} \right\rangle - \langle H \rangle \left\langle \frac{\partial H}{\partial k} \right\rangle}{\langle H^2 \rangle - \langle H \rangle^2} = \frac{1}{2k}.$$

Therefore, the isentropic process for an underdamped system is

$$dT = \frac{T}{2k} dk \longrightarrow \frac{dT}{T} = \frac{dk}{2k} \rightarrow \ln T = \frac{1}{2} \ln k + C \rightarrow T = \alpha k^{1/2}, \quad (\text{D-19})$$

which is also in accordance with the literature available literature [16]. The difference can be understood from the probability function

$$\rho(x, p) \propto e^{-\frac{p^2}{2mT} - \frac{k}{2T} x^2}, \quad (\text{D-20})$$

in the massless case,  $k$  and  $T$  must only compensate each other, but in the massive case we must take into account the entropy change caused by the momenta  $p$ , which is why  $k$  must increase as  $T^2$  to compensate that effect.

## Bibliography

- [1] BUSTAMANTE, C.; LIPHARDT, J. ; RITORT, F. **Physics Today**. The nonequilibrium thermodynamics of small systems, journal, v.58, n.7, p. 43–48, 2005.
- [2] KOLOMEISKY, A. B.; FISHER, M. E. **Annual Review of Physical Chemistry**. Molecular Motors: A Theorist's Perspective, journal, v.58, n.1, p. 675–695, 2007.
- [3] HÄNGGI, P.; MARCHESONI, F. ; NORI, F. **Annalen der Physik**. Brownian motors, journal, v.14, n.1-3, p. 51–70, feb 2005.
- [4] LUO, X. G.; LIU, N. ; HE, J. Z. **Physical Review E**. Optimum analysis of a Brownian refrigerator, journal, v.87, n.2, p. 022139, feb 2013.
- [5] GHOSH, P. K.; RAY, D. S. **Physical Review E - Statistical, Nonlinear, and Soft Matter Physics**. Stochastic energetics of quantum transport, journal, v.73, n.3, p. 1–9, 2006.
- [6] RANA, S.; PAL, P. S.; SAHA, A. ; JAYANNAVAR, A. M. **Physical Review E - Statistical, Nonlinear, and Soft Matter Physics**. Single-particle stochastic heat engine, journal, v.90, n.4, p. 1–12, 2014.
- [7] PARK, J. M.; CHUN, H. M. ; NOH, J. D. **Physical Review E**. Efficiency at maximum power and efficiency fluctuations in a linear Brownian heat-engine model, journal, v.94, n.1, p. 1–9, 2016.
- [8] ASFAW, M. **Physical Review E - Statistical, Nonlinear, and Soft Matter Physics**. Thermodynamic feature of a Brownian heat engine operating between two heat baths, journal, v.89, n.1, p. 1–10, 2014.
- [9] BRANDNER, K.; SAITO, K. ; SEIFERT, U. **Physical Review X**. Thermodynamics of micro- and nano-systems driven by periodic temperature variations, journal, v.5, n.3, p. 1–16, 2015.
- [10] LEE, J. S.; PARK, H. **Scientific Reports**. Carnot efficiency is reachable in an irreversible process, journal, v.7, n.1, p. 10725, dec 2017.

- [11] TOYABE, S.; OKAMOTO, T.; WATANABE-NAKAYAMA, T.; TAKE-TANI, H.; KUDO, S. ; MUNHEYUKI, E. **Physical Review Letters**. Nonequilibrium Energetics of a Single F1-ATPase Molecule, journal, v.104, n.19, p. 198103, may 2010.
- [12] KOSKI, J. V.; KUTVONEN, A.; KHAYMOVICH, I. M.; ALA-NISSILA, T. ; PEKOLA, J. P. **Physical Review Letters**. On-Chip Maxwell's Demon as an Information-Powered Refrigerator, journal, v.115, n.26, p. 260602, dec 2015.
- [13] ARGUN, A.; SONI, J.; DABELOW, L.; BO, S.; PESCE, G.; EICHHORN, R. ; VOLPE, G. **Physical Review E**. Experimental realization of a minimal microscopic heat engine, journal, v.96, n.5, p. 1–8, 2017.
- [14] BLICKLE, V.; BECHINGER, C. **Nature Physics**. Realization of a micrometre-sized stochastic heat engine, journal, v.8, n.2, p. 143–146, 2011.
- [15] ROSSNAGEL, J.; DAWKINS, S. T.; TOLAZZI, K. N.; ABAH, O.; LUTZ, E.; SCHMIDT-KALER, F. ; SINGER, K. **Science**. A single-atom heat engine, journal, v.352, n.6283, p. 325–330, 2016.
- [16] MARTÍNEZ, I. A.; ROLDÁN, É.; DINIS, L.; PETROV, D.; PARRONDO, J. M. R. ; RICA, R. A. **Nature Physics**. Brownian Carnot engine, journal, n.October, p. 1–6, 2015.
- [17] GELBWASER-KLIMOVSKY, D.; ALICKI, R. ; KURIZKI, G. **Physical Review E - Statistical, Nonlinear, and Soft Matter Physics**. Minimal universal quantum heat machine, journal, v.87, n.1, p. 1–9, 2013.
- [18] AGARWAL, G. S.; CHATURVEDI, S. **Physical Review E - Statistical, Nonlinear, and Soft Matter Physics**. Quantum dynamical framework for Brownian heat engines, journal, v.88, n.1, p. 1–12, 2013.
- [19] BRUNNER, N.; HUBER, M.; LINDEN, N.; POPESCU, S.; SILVA, R. ; SKRZYPCZYK, P. **Physical Review E - Statistical, Nonlinear, and Soft Matter Physics**. Entanglement enhances cooling in microscopic quantum refrigerators, journal, v.89, n.3, p. 1–6, 2014.
- [20] ROULET, A.; NIMMRICHTER, S.; ARRAZOLA, J. M.; SEAH, S. ; SCARANI, V. **Physical Review E**. Autonomous rotor heat engine, journal, v.95, n.6, p. 062131, jun 2017.
- [21] STRASBERG, P.; CERRILLO, J.; SCHALLER, G. ; BRANDES, T. **Physical Review E - Statistical, Nonlinear, and Soft Matter**

- Physics.** Thermodynamics of stochastic Turing machines, journal, v.92, n.4, 2015.
- [22] BRUNNER, N.; LINDEN, N.; POPESCU, S. ; SKRZYPCZYK, P. **Physical Review E - Statistical, Nonlinear, and Soft Matter Physics.** Virtual qubits, virtual temperatures, and the foundations of thermodynamics, journal, v.85, n.5, p. 1–14, 2012.
- [23] TÜRKPENÇE, D.; MÜSTECAPLIOĞLU, Ö. E. **Physical Review E.** Quantum fuel with multilevel atomic coherence for ultrahigh specific work in a photonic Carnot engine, journal, v.93, n.1, p. 012145, jan 2016.
- [24] AGARWALLA, B. K.; JIANG, J.-H. ; SEGAL, D. **Physical Review B.** Quantum efficiency bound for continuous heat engines coupled to noncanonical reservoirs, journal, v.96, n.10, p. 104304, sep 2017.
- [25] QUAN, H. T. **Physical Review E.** Quantum thermodynamic cycles and quantum heat engines. II., journal, v.79, n.4, p. 041129, apr 2009.
- [26] GHOSH, P.; SHIT, A.; CHATTOPADHYAY, S. ; CHAUDHURI, J. R. **Physical Review E - Statistical, Nonlinear, and Soft Matter Physics.** Realization of a Brownian engine to study transport phenomena: A semiclassical approach, journal, v.81, n.6, p. 1–10, 2010.
- [27] ZHOU, Y.; SEGAL, D. **Physical Review E.** Minimal model of a heat engine: Information theory approach, journal, v.82, n.1, p. 011120, jul 2010.
- [28] BORGA, F.; BEKELE, M.; TATEK, Y. B. ; TSIGE, M. **Physical Review E - Statistical, Nonlinear, and Soft Matter Physics.** Efficiency, power, and period at two optimum operations of a thermoelectric single-level quantum dot, journal, v.86, n.3, p. 1–4, 2012.
- [29] XIAO, G.; GONG, J. **Physical Review E - Statistical, Nonlinear, and Soft Matter Physics.** Construction and optimization of a quantum analog of the Carnot cycle, journal, v.92, n.1, p. 1–5, 2015.
- [30] GARDAS, B.; DEFFNER, S. **Physical Review E - Statistical, Nonlinear, and Soft Matter Physics.** Thermodynamic universality of quantum Carnot engines, journal, v.92, n.4, p. 1–6, 2015.
- [31] DOYEUX, P.; LEGGIO, B.; MESSINA, R. ; ANTEZZA, M. **Physical Review E.** Quantum thermal machine acting on a many-body quantum system: Role of correlations in thermodynamic tasks, journal, v.93, n.2, p. 1–13, 2016.

- [32] MAN, Z. X.; XIA, Y. J. **Physical Review E**. Smallest quantum thermal machine: The effect of strong coupling and distributed thermal tasks, journal, v.96, n.1, p. 1–9, 2017.
- [33] TERÇAS, H.; RIBEIRO, S.; PEZZUTTO, M. ; OMAR, Y. **Physical Review E**. Quantum thermal machines driven by vacuum forces, journal, v.95, n.2, p. 1–8, 2017.
- [34] HUMPHREY, T. E.; NEWBURY, R.; TAYLOR, R. P. ; LINKE, H. **Physical Review Letters**. Reversible Quantum Brownian Heat Engines for Electrons, journal, v.89, n.11, p. 9–12, 2002.
- [35] NOVIKOV, I. I. **The Soviet Journal of Atomic Energy**. Efficiency of an atomic power generating installation, journal, v.3, n.11, p. 1269–1272, 1957.
- [36] CURZON, F. L.; AHLBORN, B. **American Journal of Physics**. Efficiency of a Carnot engine at maximum power output, journal, v.43, n.1, p. 22–24, jan 1975.
- [37] ABREU, D.; SEIFERT, U. **Physical Review Letters**. Thermodynamics of Genuine Nonequilibrium States under Feedback Control, journal, v.108, n.3, p. 030601, jan 2012.
- [38] CAO, Y.; GONG, Z. ; QUAN, H. T. **Physical Review E**. Thermodynamics of information processing based on enzyme kinetics: An exactly solvable model of an information pump, journal, v.91, n.6, p. 062117, 2015.
- [39] BATALHÃO, T. B.; SOUZA, A. M.; MAZZOLA, L.; AUCCAISE, R.; SARTHOUR, R. S.; OLIVEIRA, I. S.; GOOLD, J.; DE CHIARA, G.; PATERNOSTRO, M. ; SERRA, R. M. **Physical Review Letters**. Experimental reconstruction of work distribution and study of fluctuation relations in a closed quantum system, journal, v.113, n.14, p. 1–5, 2014.
- [40] CAMATI, P. A.; PETERSON, J. P.; BATALHÃO, T. B.; MICADEI, K.; SOUZA, A. M.; SARTHOUR, R. S.; OLIVEIRA, I. S. ; SERRA, R. M. **Physical Review Letters**. Experimental Rectification of Entropy Production by Maxwell’s Demon in a Quantum System, journal, v.117, n.24, p. 1–6, 2016.
- [41] BAUER, M.; ABREU, D. ; SEIFERT, U. **Journal of Physics A: Mathematical and Theoretical**. Efficiency of a Brownian information machine, journal, v.45, n.16, p. 162001, apr 2012.

- [42] HONDOU, T.; SEKIMOTO, K. **Physical Review E**. Unattainability of Carnot efficiency in the Brownian heat engine, journal, v.62, n.5, p. 6021–6025, nov 2000.
- [43] SHIRAISHI, N.; SAITO, K. ; TASAKI, H. **Physical Review Letters**. Universal Trade-Off Relation between Power and Efficiency for Heat Engines, journal, v.117, n.19, p. 1–6, 2016.
- [44] BENENTI, G.; SAITO, K. ; CASATI, G. **Physical Review Letters**. Thermodynamic bounds on efficiency for systems with broken time-reversal symmetry, journal, v.106, n.23, p. 1–4, 2011.
- [45] ALLAHVERDYAN, A. E.; HOVHANNISYAN, K. V.; MELKIKH, A. V. ; GEVORKIAN, S. G. **Physical Review Letters**. Carnot cycle at finite power: Attainability of maximal efficiency, journal, v.111, n.5, p. 1–5, 2013.
- [46] MOREAU, M.; GAVEAU, B. ; SCHULMAN, L. S. **Physical Review E - Statistical, Nonlinear, and Soft Matter Physics**. Efficiency of a thermodynamic motor at maximum power, journal, v.85, n.2, p. 1–9, 2012.
- [47] JIMÉNEZ DE CISNEROS, B.; HERNÁNDEZ, A. C. **Physical Review Letters**. Collective working regimes for coupled heat engines, journal, v.98, n.13, p. 1–4, 2007.
- [48] MANN, B.; SIMS, N. **Journal of Sound and Vibration**. Energy harvesting from the nonlinear oscillations of magnetic levitation, journal, v.319, n.1-2, p. 515–530, jan 2009.
- [49] LEE, C.; STAMP, D.; KAPANIA, N. R. ; MUR-MIRANDA, J. O. **Energy**. Harvesting Vibration Energy Using Nonlinear Oscillations of an Electromagnetic Inductor, journal, v.7683, n.2010, p. 76830Y–76830Y–12, 2010.
- [50] MANN, B. P.; OWENS, B. A. **Journal of Sound and Vibration**. Investigations of a nonlinear energy harvester with a bistable potential well, journal, v.329, n.9, p. 1215–1226, 2010.
- [51] GAMMAITONI, L.; NERI, I. ; VOCCA, H. **Applied Physics Letters**. Nonlinear oscillators for vibration energy harvesting, journal, v.94, n.16, p. 164102, apr 2009.
- [52] ROSSELLO, J. I. P.; WIO, H. S.; DEZA, R. R. ; HANGGI, P. Enhancing energy harvesting by coupling monostable oscillators, journal, 2016.

- [53] DEFAVERI, L. A.; MORGADO, W. A. ; QUEIRÓS, S. M. **Physical Review E**. Power output for a nonlinear Brownian machine, journal, v.96, n.5, p. 1–8, 2017.
- [54] SEKIMOTO, K. 17 Langevin Equation and Thermodynamics, journal, n.130, p. 17–27, 1998.
- [55] SEKIMOTO, K. **Stochastic Energetics**, volume 799 of **Lecture Notes in Physics**. Berlin, Heidelberg: Springer Berlin Heidelberg, 2010.
- [56] KAMPEN, N. G. V. **Stochastic Processes in Physics and Chemistry**. 3. ed., Elsevier, 2007.
- [57] CÂNDIDO, M. M.; MORGADO, W. A. ; DUARTE QUEIRÓS, S. M. **Brazilian Journal of Physics**. Eliminating the Cuspidal Temperature Profile of a Non-equilibrium Chain, journal, v.47, n.3, p. 366–375, jun 2017.
- [58] CÂNDIDO, M. M.; MORGADO, W. A. M. ; DUARTE QUEIRÓS, S. M. **Physical Review E**. Macroscopic violation of the law of heat conduction, journal, v.96, n.3, p. 032143, sep 2017.
- [59] MORGADO, W. A. M.; QUEIRÓS, S. M. D. **Physical Review E**. Thermostatistics of small nonlinear systems: Poissonian athermal bath, journal, v.93, n.1, p. 012121, jan 2016.
- [60] HONEYCUTT, R. L. Stochastic Runge-Kutta algorithms. I. White noise, journal, v.45, n.2, p. 600–603, 1992.
- [61] HONEYCUTT, R. L. **Physical Review A**. Stochastic Runge-Kutta algorithms. II. Colored noise, journal, v.45, n.2, p. 604–610, 1992.
- [62] FERMI, E.; PASTA, J. ; ULAM, S. **Studies of nonlinear problems**, 1955.
- [63] KUMAR, S.; KUMAR, R. ; JANKE, W. **Physical Review E**. Periodically driven DNA: Theory and simulation, journal, v.93, n.1, p. 010402, jan 2016.
- [64] WANG, Y.; TU, Z. C. **Physical Review E**. Efficiency at maximum power output of linear irreversible Carnot-like heat engines, journal, v.85, n.1, p. 011127, jan 2012.
- [65] TU, Z. C. **Physical Review E - Statistical, Nonlinear, and Soft Matter Physics**. Stochastic heat engine with the consideration of inertial effects and shortcuts to adiabaticity, journal, v.89, n.5, p. 1–9, 2014.

- [66] ZHANG, Y.; HUANG, C.; LIN, G. ; CHEN, J. **Physical Review E**. Universality of efficiency at unified trade-off optimization, journal, v.93, n.3, p. 1–4, 2016.
- [67] TAJIMA, H.; HAYASHI, M. **Physical Review E**. Finite-size effect on optimal efficiency of heat engines, journal, v.96, n.1, 2017.
- [68] GAVEAU, B.; MOREAU, M. ; SCHULMAN, L. S. **Physical Review Letters**. Stochastic thermodynamics and sustainable efficiency in work production, journal, v.105, n.6, p. 1–4, 2010.
- [69] HERNANDEZ, J. V. **Science**. A Reversible Synthetic Rotary Molecular Motor, journal, v.306, n.5701, p. 1532–1537, nov 2004.